Testing and Advancement of a Variable Stiffness Transverse Plane Adapter for Use in a Lower Limb Prosthesis

Corey Pew

A dissertation

submitted in partial fulfillment of the

requirements for the degree of

Doctor of Philosophy

University of Washington

2017

Reading Committee:

Glenn Klute, Chair

Gador Canton

Santosh Devasia

Nate Sniadecki

Program Authorized to Offer Degree:

Mechanical Engineering

Corey Pew

University of Washington

Abstract

Testing and Advancement of a Variable Stiffness Transverse Plane Adapter for Use in a Lower Limb Prosthesis

Corey Pew

Chair of the Supervisory Committee:

Glenn Klute, Ph.D.

Affiliate Professor

Department of Mechanical Engineering

Background

The goal of a lower limb prosthesis is to restore the abilities of the intact limb for an individual with lower limb amputation. Daily ambulation includes many maneuvers such as turning, and twisting, which require a component of transverse plane mobility. It has been shown that the inclusion of a transverse plane adapter could reduce peak torsional loads on the residual limb and may alleviate soft tissue damage, increase comfort, and improve mobility level for a lower limb amputee. However, currently available transverse plane adaptors only allow for a single stiffness setting and do not allow for variation to accommodate the maneuvers of everyday ambulation. The specific aims of this research were to determine the transverse plane stiffness that minimizes the transverse plane moment applied to the residual limb of lower limb amputees during different ambulatory activities and identify a user's preferred transverse plane stiffness during different ambulatory activities at different speeds. Three tasks were performed to achieve these aims. First, proof of concept human subject performance tests were conducted using the first-

generation prototype (VSTA I). Next, a second-generation prototype (VSTA II) was developed using more refined design criteria gleaned from the testing of the VSTA I. Third, the VSTA II was used to perform preference testing with human subjects during different ambulatory activities at varying walking speeds.

First Generation VSTA Design (VSTA I)

Design of the VSTA I focused primarily on existing transverse rotation adapter devices and the capabilities of other prototypes in recent literature. The VSTA I is a device that allows for variable stiffness in transverse plane about its central axis. Variation of the VSTA I is accomplished by an electric motor adjusting the position of a lever arm via an ACME lead screw. The change in position of the lever arm in relation to a central torsion spring effectively varies the mechanical advantage by modifying the lever arm length. This allows for infinitely variable stiffness between 0.10 Nm/° and fully locked.

VSTA I Mechanical Testing

Mechanical bench testing was performed on the VSTA I via a servo-hydraulic material test machine. The VSTA I was run through its full range of motion (+/- 30°) at both 0.5 °/s and 60°/s at four static stiffness settings: 0.10, 0.33, 0.64, and 1.17 Nm/°. It was found that the VSTA I was not direction or rate dependent and was capable of stiffness variation between 0.12-0.91 Nm/°, with a rotational range of ±30°.

VSTA I Human Subject Testing

The first generation VSTA (VSTA I) was used to completed pilot testing on human subject individuals with lower limb amputation. These tests conducted participants through simulated

activities of daily living that focused on turning and twisting maneuvers. These included straight walking, 90° turns (spin and step), 180° turns, standing reach, and the L-Test of Functional Mobility. Testing was performed at three constant settings of the VSTA I (compliant: 0.30 Nm/°, intermediate: 0.57 Nm/°, stiff: 0.91 Nm/°). Evaluation of the testing focused primarily on peak transverse plane moments during each maneuver. It was hypothesized that reduced transverse plane loading on the residual limb relates to decreased transverse plane stiffness. Additionally, the self-selected walking speed and L-Test time of each subject was used as an indicator of mobility. Results indicated that activities requiring high levels of transverse plane motion (90° spin and 180° turns) had significantly reduced peak transverse plane moments at the socket when walking with the compliant transverse plane stiffness as compared to the stiff setting. Additionally, use of the VSTA resulted in no measurable loss of mobility at self-selected walking speeds between the three settings. These preliminary results indicate that a transverse rotation adapter with variable stiffness capability could be useful for a lower limb amputee to help reduce stresses at the socket-limb interface. Testing of the VSTA I also resulted in an updated set of design requirements. It was found that the VSTA I was too heavy, causing fatigue, and too tall, restricting subject population. It also lacked an onboard controller, and suffered from internal deflections that limited its stiffness capabilities.

Second Generation VSTA Design (VSTA II)

Given the lessons learned during the testing of the VSTA I, a new and improved VSTA II has been designed. The VSTA II features a 42% reduction in height and 51% reduction in mass compared to the VSTA I with an intended finite stiffness variability from 0.30 Nm/° to 1.25 Nm/°, in five 0.25 Nm/° increments. Stiffness variation is enabled by five independent spring subunits that can be combined in parallel to create different, linear, stiffness settings. It also features an

onboard controller that can control the stiffness states, and record rotational displacement and stiffness setting during use.

VSTA II Mechanical Testing

Mechanical bench testing performed on the VSTA II mirrored that of the VSTA I. Deflection testing performed on a servo-hydraulic material test machine through its full range of motion (+/- 30°) at both 0.5 °/s and 60°/s. Additionally, tests were performed to determine the VSTA II's ability to modulate stiffness in real time and determine power consumption during operation. The VSTA II was found to be capable of five discrete stiffness settings (0.31, 0.56, 0.83, 1.08, 1.29 Nm/°) with ±30° of motion in addition to fully locked operation. Stiffness settings were found to be independent of rotation rate and direction. Stiffness selection performed via small locking mechanisms operated by electro-mechanical solenoids can vary the stiffness of the VSTA II in 0.029 ± 0.008 seconds while the device is unloaded during the swing phase of gait. Lastly, the 2200 mAh battery was found to last 105 minutes under full electrical load.

Turn Intent Prediction

Daily use of the VSTA would require an autonomous control algorithm to determine optimal stiffness for a given activities and modulate the device accordingly via the onboard controller. Ideally, IMU signals from the shank of the lower limb prosthesis could be used to identify upcoming changes in activity with adequate time to modulate stiffness before the foot is loaded during a turn (changes in VSTA stiffness performed under no load during swing). Three classifiers were trained and tested: support vector machine (SVM), K nearest neighbors (KNN), and a bagged decision tree ensemble (Ensemble). Training for an individual gave superior results over training on a pooled set of five individuals. Coupled with a simple control scheme, the SVM,

KNN, and Ensemble classifiers could attain 96%, 93%, and 91% accuracy (no significant difference), respectively, predicting an upcoming turn 400 ± 70 ms prior to the heel strike of the turn. However, classification of straight walking transition steps varied between classifiers at 85%, 82%, 97% (Ensemble significantly different, $p = 0.002$), respectively. The Ensemble model produced the best result overall, however, depending the priority of identifying turning vs transition steps and processor requirements, the SVM or KNN might still be considered.

VSTA II Human Subject Testing

Testing to determine ideal settings for control of the VSTA II consisted of paired preference testing at varying activity and walking speed combinations. Subjects performed walking trials for three separate activities (straight walking, prosthesis inside turning, prosthesis outside turning), at their self-selected walking speed and at speeds 20% faster and slower than self-selected. At each activity-speed combination subjects compared stiffness settings and indicated their preference for one of three settings (Compliant: A (0.31 Nm/deg), Moderate: B (0.83 Nm/deg), Stiff: C (1.29 Nm/deg). Results indicated correlation between increased peak transverse plane moment with increasing walking speed when turning, but not when walking straight. However, contrary to the outcome of previous findings, no significant relation was found between peak transverse plane moment and the stiffness of the VSTA II. Lastly, results indicated no significant trend for stiffness preference between speeds or activities, while subjects did qualitatively prefer lower stiffness when turning vs straight walking. Findings may indicate that no global ideal stiffness settings may be available given activity and speeds variations, but that VSTA II settings may have to be tailored to individual users.

Conclusions

Testing with the VSTA I and VSTA II prototypes identified that reduced transverse plane stiffness in the shank of a lower limb prosthesis can significantly reduce peak loading on the residual limb. Moreover, that transverse plane stiffness could be reduced beyond what is available in current, single stiffness, transverse rotation adapters. Reductions in stiffness also have no effect on the user's mobility when walking at their self-selected speed. Initial attempts were made to determine a global control scheme that could indicate when and to what level stiffness should be adjusted, however, no overall trend could be found. It was determined that reduced transverse plane stiffness produces the most significant reductions in limb loading when turning compared to straight walking. Additionally, walking speed played a significant role in transverse plane limb loading such that both factors should be considered when determining the optimal transverse plane stiffness for a given activity and speed combination. Overall a control scheme that optimizes when and to what level to adjust transverse plane stiffness should be customized to an individual's specific needs and preferences.

Table of Contents

List of Figures

List of Tables

1 Background

Loss of a lower limb is an event that has serious implications to an individual's life and well-being. Approximately 2 million people were living with an amputation, with 185,000 additional amputations performed per year in the United States [1], [2]. Improvements on prosthetic technologies, therefore, can influence a large population. Development of new prosthetic technologies often focuses on straight walking, with attention to movements in the sagittal plane. This research tends to overlook complex maneuvers like turning, twisting, and pivoting that require movement in the transverse plane [3], [4]. As early as 1977, Lamoureux and Radcliff recommended the inclusion of a torsion device in lower limb prostheses to improve movement when turning, and during daily activity [5]. The inclusion of a device that allows movement in the transverse plane could reduce peak torsional loads on the residual limb to alleviate soft tissue damage, increase comfort, and improve mobility level for an individual with lower limb amputation.

1.1 Soft Tissue Stress

Many modern prostheses use a socket to couple the residual limb to the mechanical replacement parts. The soft tissues of the residual limb are then responsible for transmitting the loads of ambulation between the prosthesis and skeletal system. This can results in chronic dermal maladies for amputees such as abrasions, cysts, and ulcers [6]. While endoskeleton style prostheses will always present these issues, the inclusion of a transverse rotation adapter (TRA) has been shown to help decrease peak rotational moments that exacerbate these problems [5], [7], [8]. Reduction in soft tissue stresses and skin ailments could lead to a greater level of comfort for the amputee.

1.2Mobility

When replacing the lost limb with a prosthesis, the intention is to restore the individual to the greatest activity level possible. Complex maneuvers with transverse plane motion such as turning account for a significant portion of daily steps [9]. Transverse rotation adapters can reduce step width during straight walking in the laboratory, which may indicate greater stability [10], [11]. Additionally, a study by Su et al. allowed patients to acclimate for two weeks in their homes with a commercial TRA after which a survey assed their use of the adapter, indicating that the addition of a TRA was useful when turning and negotiating uneven terrain [10]. Torsion adapters can furthermore reduce metabolic cost during straight walking, and marginally increase activity level [12], [13]. Improvements in mobility and activity can lead to amputees being more independent, healthier, and less likely to need external support services over the course of their lives.

1.3Variable Stiffness Torsion

Current TRAs allow for single stiffness settings, only adjustable by a prosthetist, and unable to adapt to the varying activities of daily living [14]. Additionally, it has been shown that the stiffness of joints, such as the ankle, have variable stiffness capabilities that change based on gait dynamics [15], [16]. These two ideas are the basis for the conclusion that a device capable of variable stiffness in the transverse plane would be of benefit to amputees. A variable stiffness transverse plane adaptor (VSTA) was designed, prototyped, and mechanically tested [17]. The

VSTA is a device added into the pylon of lower limb prostheses, and its stiffness is electromechanically variable to meet the needs of the user.

Testing of the VSTA in human subject's trials aims to determine if the device could reduce loading on the residual limb with no impediment to mobility. It is hypothesized that use of the VSTA at lower stiffness settings will reduce the peak values of transverse plane moments in the lower limb when performing turning and reaching maneuvers similar to everyday activities. Additionally, the use of the VSTA at those lower stiffness settings will not impede the function and mobility of the user when performing walking tasks that involve such maneuvers, as evaluated by their self-selected walking speed and the clinical L-Test of Functional Mobility [18]. Testing of the VSTA will additionally identify any shortcomings in the design. These shortcomings will drive the design of a new prototype, the VSTA II. Construction of the VSTA II and its evaluation both mechanically and with human subject's trials, will further investigate the advantages of variable stiffness in the transverse plane. Human subjects testing with the VSTA II will primarily determine possible optimal settings for given activities to develop guidelines for a future autonomous control system. To avoid confusion between the original VSTA and the VSTA II, the first generation VSTA will be referred to as the VSTA I, and the second generation as VSTA II.

2 VSTA I Review

This chapter will provide a complete overview of the VSTA I, beginning with a brief introduction. The VSTA I (Figure 1) is a device that allows for variable stiffness in torsion about its central axis [19]. Variation of the VSTA I is accomplished, ideally under no load conditions, by the electric motor moving the spring carrier via an ACME lead screw. The change in position of the spring carrier effectively varies the mechanical advantage of the upper housing over the

torsion spring by modifying the lever arm length. The VSTA I capabilities and specifications determined by mechanical validation testing are outlined in Table 1 [17]. The following subsections will review the design criteria, design mechanical testing, and controller testing previously done on the VSTA I.

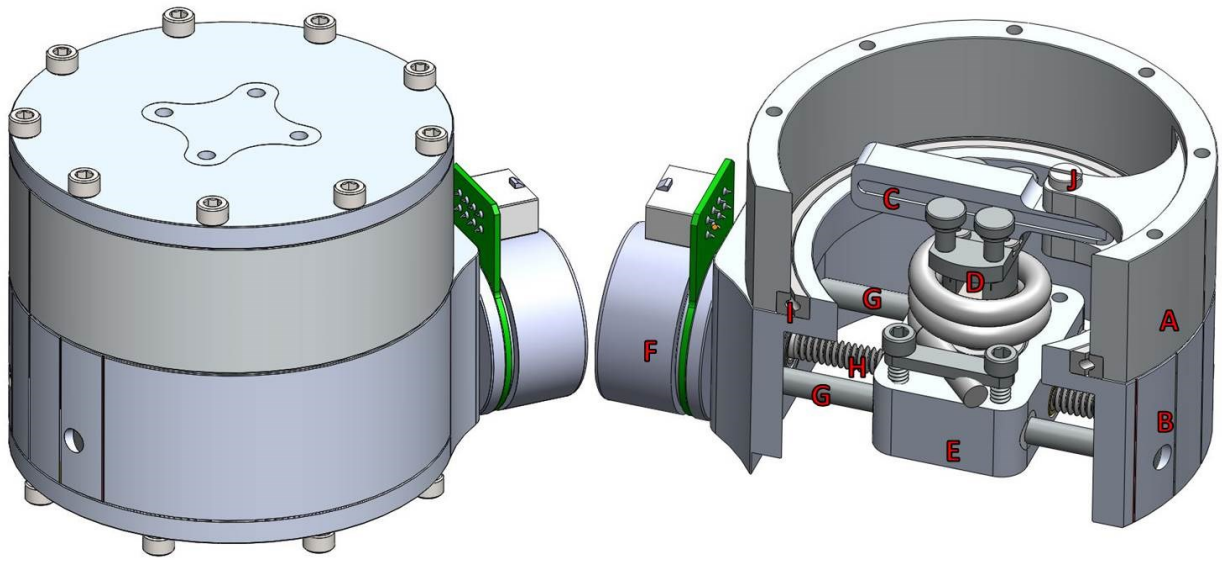

Figure 1: Variable stiffness torsion device. A) Upper Housing, B) Lower Housing, C) Lever Arm, D) Carriage, E) Spring Carrier, F) Electric Motor, G) Guide Rail (2x), H) ACME Lead Screw, I) Main Bearing

Table 1: VSTA I Specifications

Motion Range	Stiffness Range	Mass	Size
±30°	0.10-∞ Nm/°	1.27 Kg	89 mm tall x 111 mm Dia

The VSTA is symmetric for either direction of travel, and provides for a locked condition when the axis of rotation of the Slider and that of the Lever Arm pivot are aligned, Figure 2.

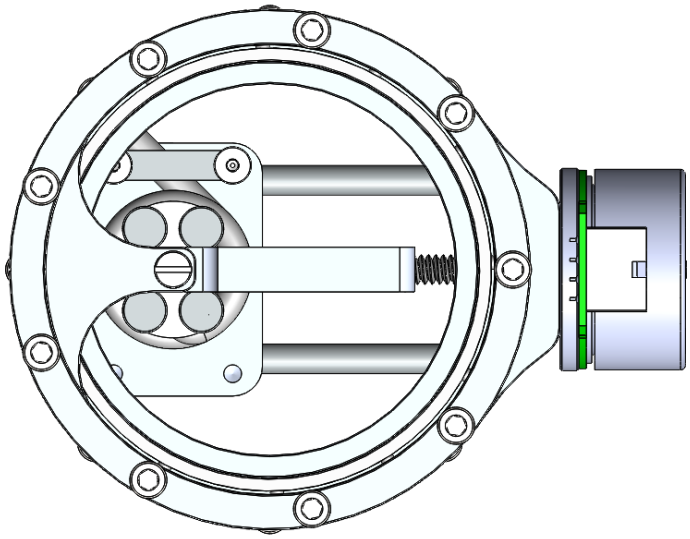

Figure 2: VSTA in “Locked” Position

2.1 VSTA I Design Criteria

Criteria were established to guide the design and modeling of the VSTA I. These criteria were split into two groups: structural and functional. An initial dimensional goal was set based on the 76-mm diameter of a standard prosthetic adaptor plate like those seen in Figure 3. This represents an ideal diameter that will integrate seamlessly into existing hardware.

Figure 3: Attachment Plates for Lower Limb Prosthesis

The VSTA I installs into the pylon of an existing lower limb prosthesis, Figure 4. The length of a pylon is variable, depending on variables such as residual limb length, patient height, and the hardware the patient is utilizing (foot and, if applicable, knee). Because of this, the VSTA I height must be kept to a minimum to fit into existing pylon space. Static load structural requirements, Table 2, were the next design criteria considered and were the main consideration for the outer housings. Structural requirements were derived mostly from the ISO 10328:2006 Prosthetics--Structural testing of lower-limb prostheses—Requirements and test methods, as well as a theoretical bending load [20]. A crouching scenario (Figure 5) determined the worst case bending scenario with anthropometry values set by a 50^{th} percentile male with the maximum load set by the ISO 10328:2006 standard. This scenario involved in a 254-mm lever arm with 65 kg of load at the end resulting in a 163 Nm bending load on the outer housings. It is most optimal to have the device as close to the knee as possible as this will decrease the moment of inertia for the limb during swing, and have less influence on the swing dynamics of the limb while walking. These structural standards represented near worst case static scenarios that would most likely not be encountered by the VSTA I, but gave a good starting point for design and analysis.

Figure 4: VSTA I Placement

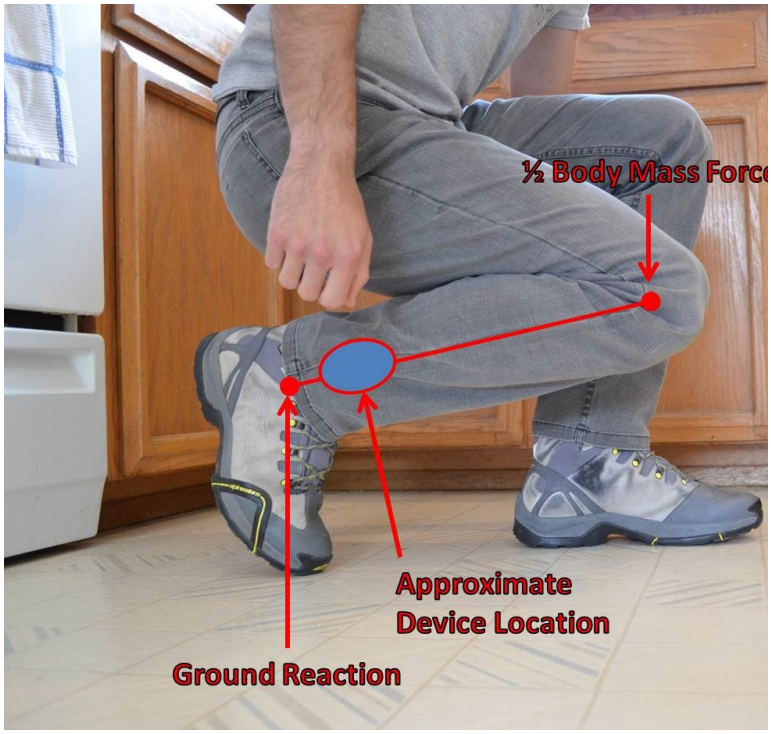

Figure 5: Maximum Bending Condition

The functional requirements (Table 3) of the design concern its ability to perform the tasks necessary to be a successful variable stiffness torsion adaptor. These were derived primarily from background research of existing torsion adaptors on the market, prototype devices, and the capabilities of the intact human ankle. The main criteria for these were stiffness capabilities, range

of motion, and device mass and size. It has been shown that the human ankle is capable of a maximum torque of 11-12 Nm around 15-20° of internal rotation, and a maximum rotation of 26° [14], [21]. Maximum device mass was set to 3.97 kg, as it has been indicated that this mass can be added to a lower limb prosthesis with no significant effect on self-selected walking speed of the amputee [22]. Using the information gathered, the VSTA I's 1:1 spring rate was targeted at 0.6 Nm/° and a range of +/- 30°.

Table 2: Structural Requirements for a Lower Limb Prosthetic Device

Load Condition	**Max Load**	**Reference**
Compression	287 lbs	ISO 10328, A100, Condition I
Torsion	575 lb-in	ISO 10328, A100, Condition I
Bending	1440 lb-in	Theoretical Static Worst Case

Table 3: Functional requirements for a torsion adaptor

Device Basis	Torsion Range	Spring Rate	Device Mass	Device Size	Reference
Existing Device	+/- 20°	0.23 Nm/°	No Data	No Data	Lamoureux, 1977
Existing Device	±30°	0.5, 0.6, 0.7 Nm/°	379 g	No Data	Flick, 2005
Series Elastic Actuator Prototype	360°	Variable	3.175 kg	No Data	Lagoda, 2010
AwAS-II Prototype	+/- 17°	Variable	1.1 kg	0.18mx0.14m	Jafari, 2013
Planetary Gear Prototype	360°	Variable	No Data	45x61x41mm	B.S. Kim, 2007
Intact Ankle	+/- 20°	0.8 Nm/°	Not Applicable	Not Applicable	Flick, 2005; Glaister, 2009

2.2 VSTA I Spring Design Considerations

The rate for the ideal torsion spring was set at 0.6 Nm/° to match the mid-range adjustment of the existing device described by Flick et al. [14]. When the Slider is set to the center of travel along the lever arm, the VSTA I has a 1:1 mechanical advantage over the spring. This means the mid-range value of the VSTA I would also be 0.6 Nm/°, adjustable in either direction. A commercial torsion spring of this rate was not found so one was designed specifically for this application using design equations found in [23]. The design requirements initially assumed for the spring are a rate of 0.6 Nm/°, 90° deflection, fitting within the confines of the VSTA I. Because the VSTA I could be designed around the spring to some degree, the actual dimensions were variable, but some minimum and maximum values were used to estimate the spring. Assumptions were a supporting rod diameter of 15.9 mm, mean coil diameter of 25.4 mm (D), a minimum of three active coils (N), and a maximum deflection of 90° (F), and Music Wire with an Elastic Modulus (E) of 196500 MPa. At 90° of deflection, the spring would be at 54 Nm of torque (T). The wire diameter was determined from in equation [1].

$$d = \sqrt[4]{\frac{4000TND}{EF}} = \sqrt[4]{\frac{4000 * 54\ \text{Nm} * 3\ \text{coils} * 0.0254\ \text{m}}{196500e6 * 90°}} = 0.0055\ \text{meters} \quad [1]$$

$$= 5.5\ \text{mm}$$

Also, the minimum diameter of the spring when under load should be considered to verify that the support rod is not too large:

$$\text{Loaded ID} = \frac{ND_{free}}{N + \frac{F}{360}} = \frac{3\ \text{coils} * 0.00254\ \text{m}}{3\ \text{coils} + \frac{90}{360}} = 0.023\ \text{m} = 23.4\ \text{mm} \quad [2]$$

These calculations show that the support rod is feasible, and might possibly be larger, or the mean diameter of the spring could be decreased if necessary giving more clearance for the

bearing (Figure 8-A). Generally, the calculations indicate that a spring could be made to meet the requirements of the VSTA I. However, after consulting spring manufacturers it was found that a maximum wire diameter (d_w) of 5.26 mm (0.00524 m in equations [3] and [4]), 3.8 active spring coils (N), and a mean coil diameter (D_m) of 31.8 mm (0.0318 m in equations [3] and [4]) the highest spring rate that could be manufactured to fit was 0.33 Nm/°. This number was determined by rearranging equation [1]:

$$\text{Spring Rate } \left(\frac{\text{Nm}}{^\circ}\right) = \frac{d_w^4 * E}{4000 * N * D_m} \quad [3]$$

Music wire has a maximum yield stress of 1758 MPa. A calculation of the stress in the wire:

$$\sigma = \frac{d_w * E * \theta}{392 * N * D_m} \quad [4]$$

While one spring manufacturer indicated that this spring would be capable of deflections up to 90°, equation [4] indicates that the max stress in the spring will be reached at a deflection (θ) of 71°. This meant that for the VSTA I to maintain a full range of +/- 30° the carrier cannot be moved infinitely between the minimum stiffness and infinitely stiff. The maximum stiffness was updated to 1.17 Nm/° due to increased spring stress during counter-clockwise rotation. This result will be discussed later during the bench testing sections, and 1.17 Nm/° will be taken as the maximum from this point on for the VSTA I. The infinitely stiff, locked position does not depend on deformation of the spring and so can still be used, but should only be activated when the VSTA I is not under load.

2.3 VSTA I Mathematical Modeling and Motor Selection

The mathematical model is based on the geometric interactions of components in the VSTA I with the stiffness depending primarily on the length of the lever arm. Because the rotational axes of the spring and the VSTA I housings only align at the 1:1 ratio, as the housing rotates the actual lever arm length changes. The lever arm length is measured from the lever arm pivot to the spring center. With the VSTA I at zero deflection, the spring offset is equal to the lever arm length. As the VSTA I rotates, the lever arm length will change as the lever arm pivot is moved relative to the spring center. This change in lever arm length is more drastic the farther the spring offset is from the VSTA I center (Figure 6).

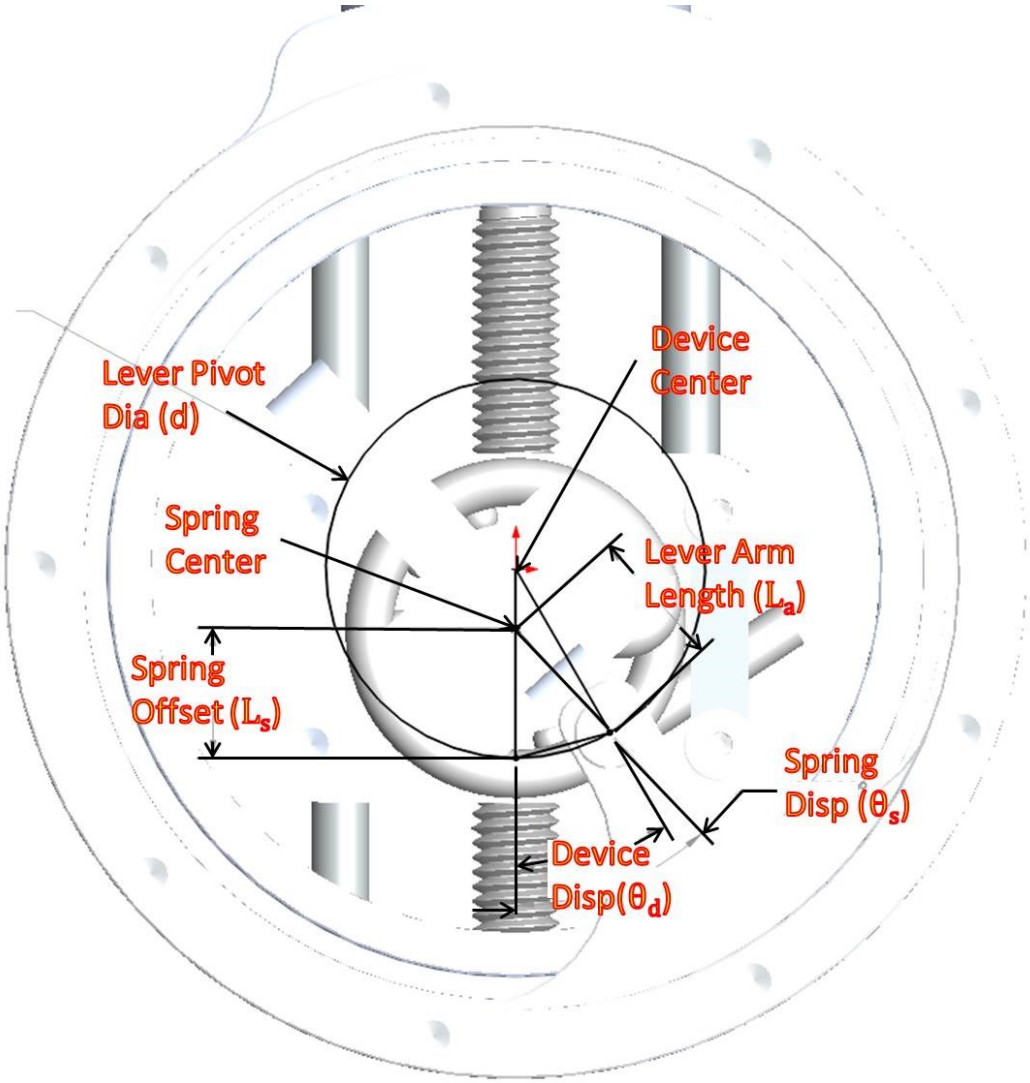

Figure 6: Geometric layout of VSTA I. This top view shows how the geometric relations between the lever arm and the spring center offset change as the VSTA I is deflected. In the depicted orientation, the spring offset is closer to the lever pivot than the device center. As the lever pivot sweeps along its diameter, the lever arm will effectively lengthen.

Using the length and angular relations between the components, the length of the lever arm (L_a) can be found based on the distance the spring center is offset from the locked position (L_s), the rotational displacement of the housings (θ_d), and the diameter of the lever pivot pin circle (d) in the upper housing:

$$L_a = \sqrt{\left(d\sin\left(\frac{\theta_d}{2}\right)\right)^2 + {L_s}^2 - 2d\sin\left(\frac{\theta_d}{2}\right)L_s\cos\left(\frac{180-\theta_d}{2}\right)} \quad [5]$$

Using the length of the lever arm and the displacement of the VSTA I, the displacement of the torsion spring (θ_s) can then be determined:

$$\theta_s = \sin^{-1}\left(d\sin\left(\frac{\theta_d}{2}\right)\frac{\sin\left(\frac{180-\theta_d}{2}\right)}{L_a}\right) \quad [6]$$

Knowing the displacement of the spring and the 0.33 Nm/° designed spring rate, the torque in the spring (τ_s) can be calculated and related to the resulting VSTA I torque (τ_d):

$$\tau_d = \frac{d\tau_s}{2L_a\cos(\theta_s - \theta_d)} \quad [7]$$

Modeling of the device torque, τ_d, for any fixed carrier position, L_s, through the displacement range of the VSTA I (± 30°), was achieved utilizing equations [5]-[7]. Figure 7 shows the predicted torque curves for the VSTA I for several discrete settings of the lever arm position. The VSTA I has a relatively linear torque response through the range of motion. As the stiffness of the VSTA I is increased the torque curve gradually becomes less linear because of the lengthening of the lever arm during operation.

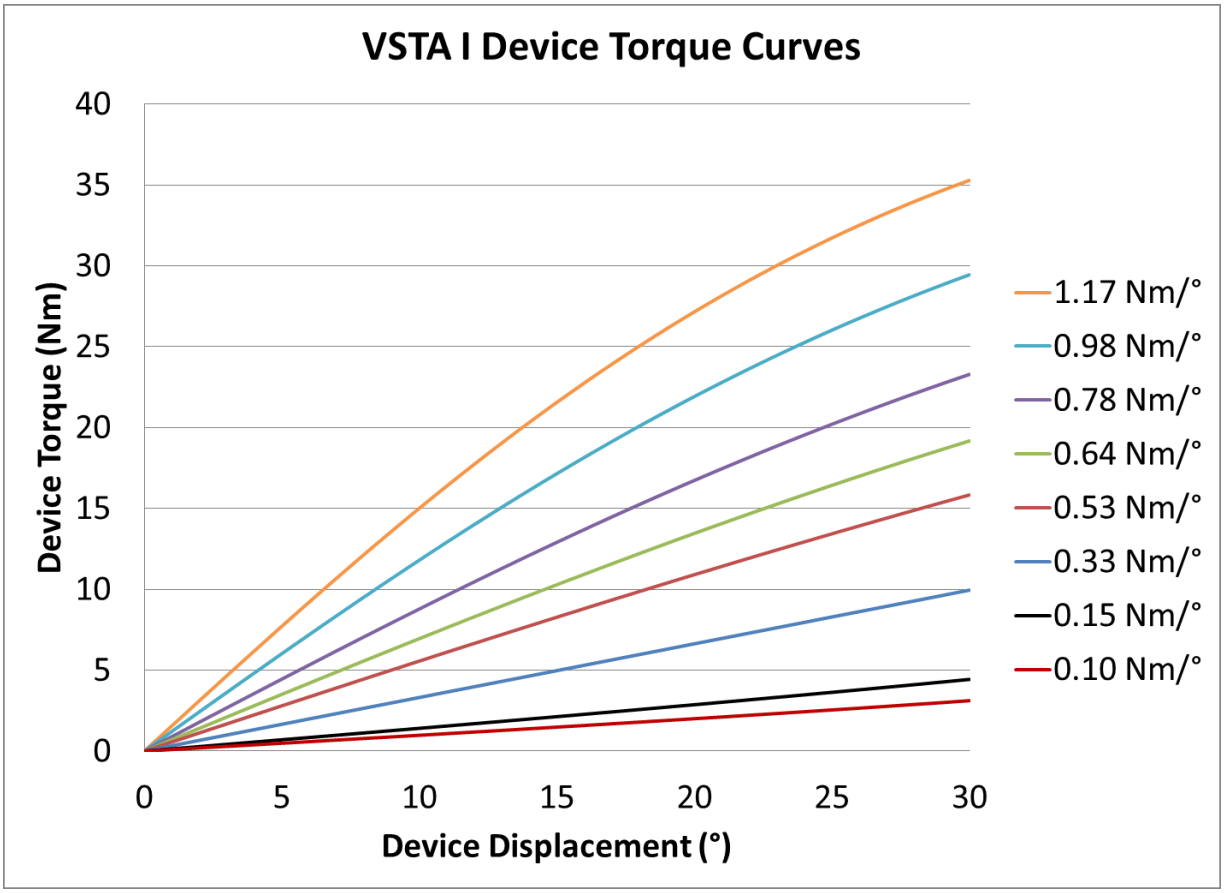

Figure 7: Modeled torque curves for the VSTA I at eight different static settings between the maximum and minimum stiffness.

An electric motor is used to position the spring carrier and set the stiffness of the VSTA I. Ideally, the motor should have the capability to change stiffness even at peak deflection, and so a calculation was performed to determine the necessary torque requirements. The force needed to push the carrier to the maximum torque condition (1.17 Nm/°) was calculated as the component of the forces parallel to the rails that guide the carrier:

$$F_c = \frac{\tau_d}{d}\sin(\theta_d) \qquad [8]$$

The previously calculated linear force on the carrier can determine the peak electric motor torque. This is derived from the spring displacement (θ_d), the mean thread diameter (d_m), the lead

of the acme screw (L), and the coefficient of friction (f) between the steel screw and the brass bushing taken as 0.16 for greased steel on brass [24]:

$$\tau_m = \frac{F_c d_m}{2} \frac{f\pi d_m - L}{\pi d_m - fL} \quad [9]$$

The resulting peak motor torque was calculated at 180 Nmm. Using this information, a Maxon EC 45 Flat Motor (PN 397172, Maxon Motor AG, Switzerland) was selected as it had a nominal torque capacity of 130 Nmm and a stall torque of 820 Nmm.

Motor speed for stiffness changes was also evaluated. Stiffness changes during initial testing will be done between trials or in the swing phase of gait when torsional load is zero. Swing phase times are variable between 0.19-0.25 seconds for adults [25]. Performance testing of the motor and control system are presented later.

2.4 VSTA I Mechanical Bench Testing

To test the physical capabilities of the VSTA I a servo-hydraulic material test machine (MTS) (Model 858 Bionix™; MTS System Corporation, Eden Prairie, MN) was used. The VSTA I was setup on the MTS as it would be connected in the pylon of a prosthesis, using pyramid adaptors, Figure 8.

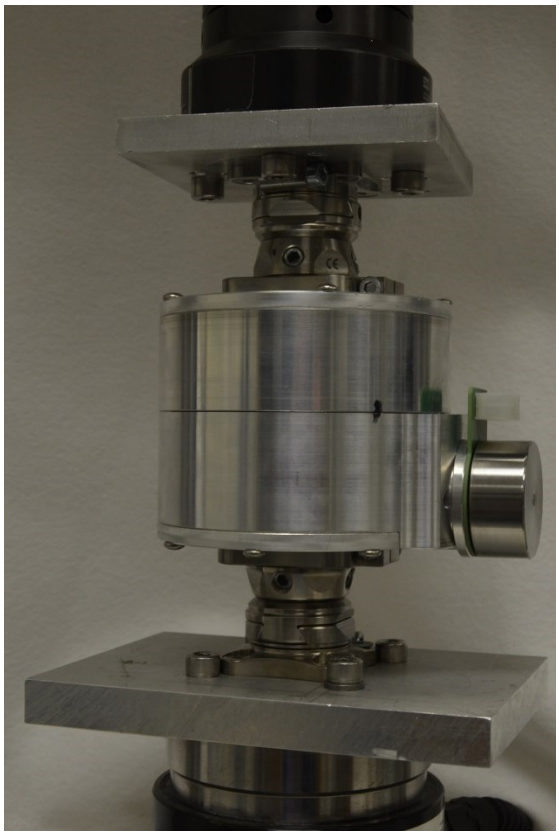

Figure 8: VSTA I fixture on MTS for torsional bench testing.

The VSTA I was run through its full range of motion (+/- 30°) at both 0.5 °/s and 60°/s similar to testing performed by Flick et al. [14]. Testing on the VSTA I was done at four static stiffness setting: 0.10, 0.33, 0.64, and 1.17 Nm/°. These settings represent the minimum and maximum stiffness capable by the VSTA I. The stiffness of 0.64 Nm/° represents a mean value of other devices currently on the market, and the 0.33 Nm/° represents the 1:1 (spring deflection : device deflection) ratio of the VSTA I which was useful to evaluate any effects the VSTA I might have over the torsional spring alone. After testing was complete, the VSTA I was evaluated with no spring using the same test procedure to characterize friction.

2.4.1 VSTA I Mechanical Bench Testing Results

Testing was separated into the four categories of direction and load rate (CW, CCW, 0.5°/s, and 60°/s). Data from each set of trials was then compared to the predicted model. Each condition

was a combination of speed and direction denoted in the figures as clockwise (CW), counter-clockwise (CCW), 0.5 °/s, and 60 °/s. The settings for the stiffness of the VSTA I are noted by both by the modeled stiffness and the distance of the slider from the spring pivot (Spring Offset, Figure 6). The farther the slider is from the pivot, the lower the stiffness of the VSTA I. The relationship between the VSTA I stiffness and the position of slider is shown in Table 4.

Table 4: Correlation between VSTA I stiffness and position of slider in relation to lever arm pivot.

Stiffness (Nm/°)	**Offset from Pivot (mm)**
0.10	38.10
0.33	20.64
0.64	14.17
1.17	9.53

Data from the following four charts shows results from the individual stiffness settings for the VSTA I. Each condition was run for three trials which were found to have less than 1% variation between trials, with a maximum of 3.5% variation between trials at the 1.17 Nm/° setting (Figure 9), the cause of which is discussed later. Because of the consistency between the three trials, data at each of the four conditions consists of the combined data from the three trials at each condition. Figure 9 depicts VSTA I testing at the highest stiffness setting of 1.17 Nm/°.

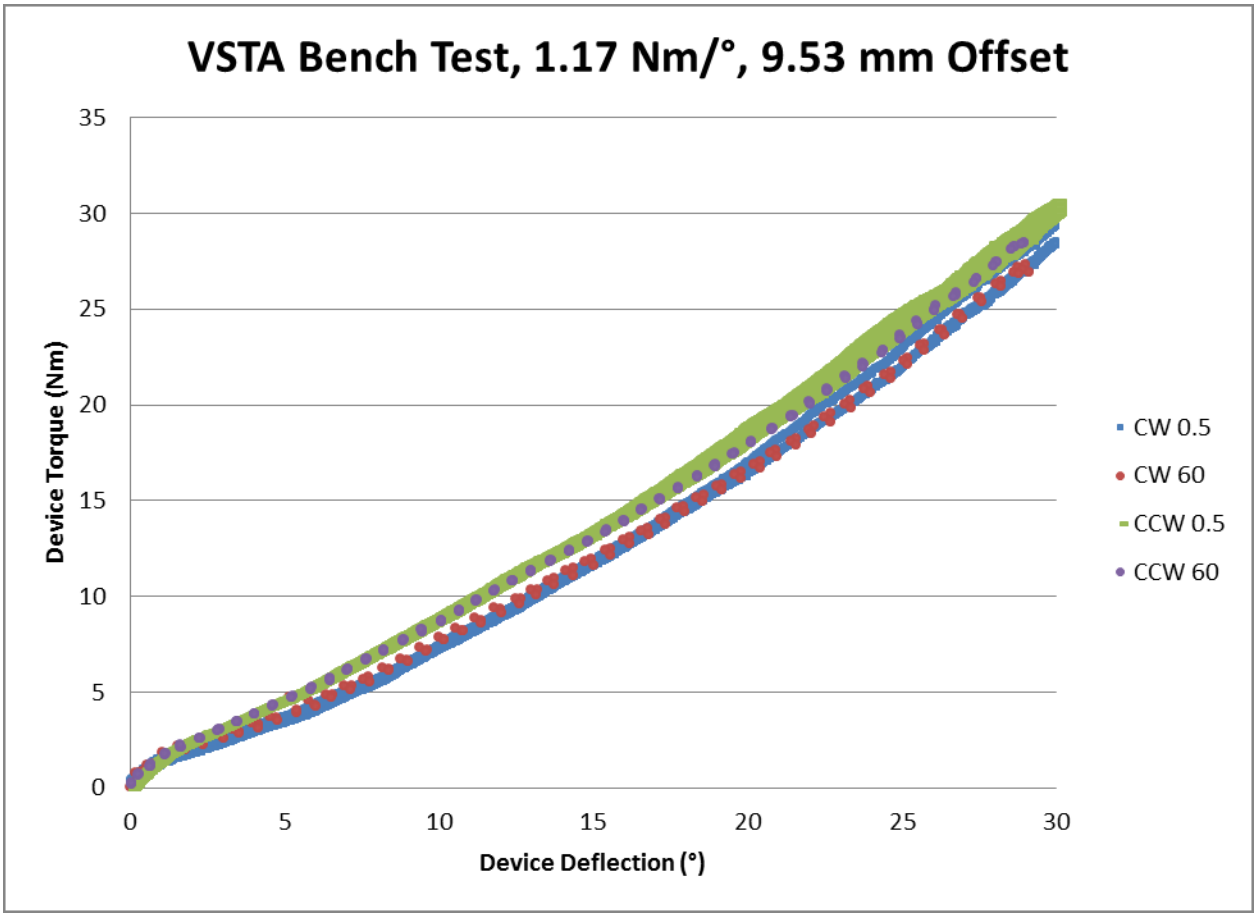

Figure 9: VSTA I test at 1.17 Nm/°, 9.53 mm offset from pivot.

Data from the 0.64 Nm/° setting is seen to be linear and have excellent consistency between conditions, Figure 10.

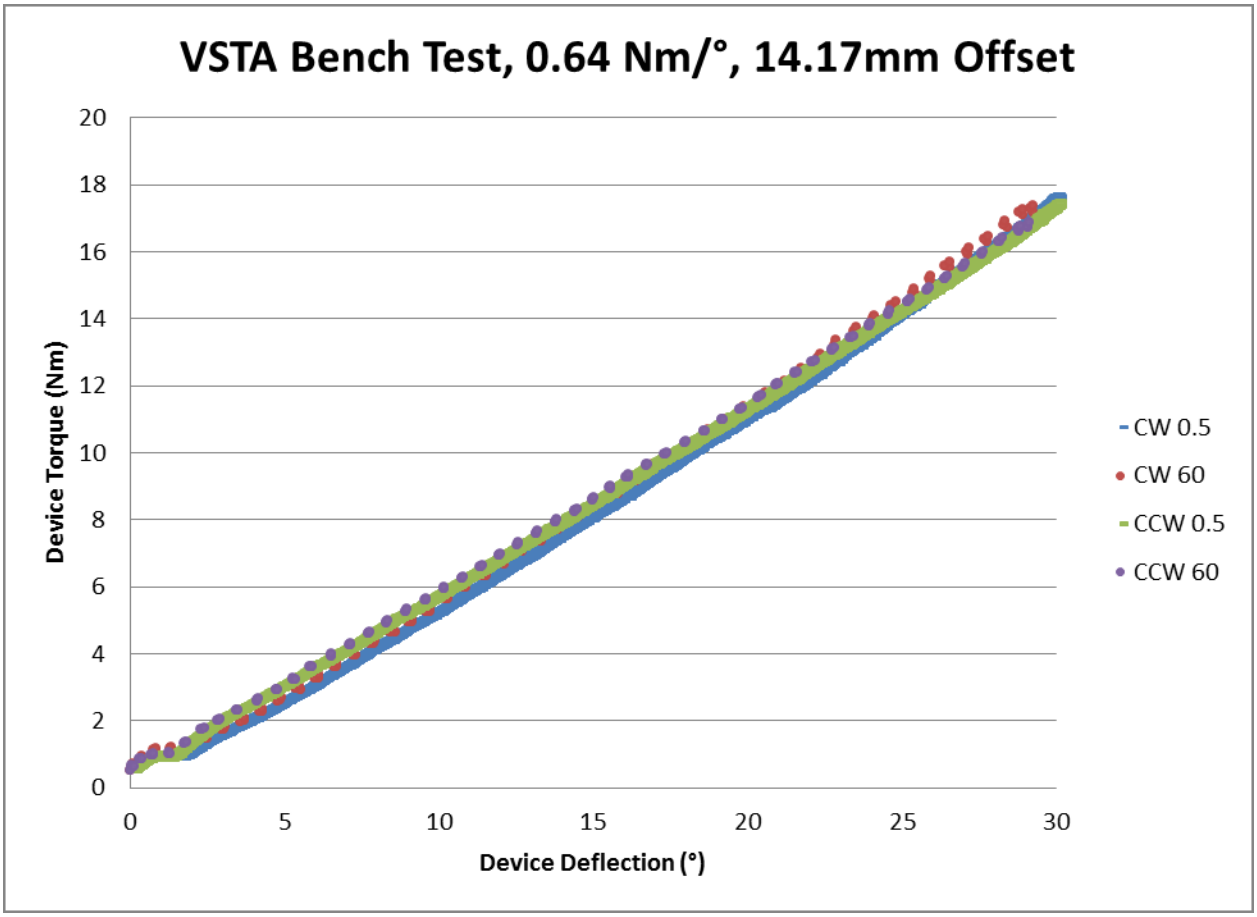

Figure 10: VSTA I test at 0.64 Nm/°, 14.17 mm offset from pivot.

Results from the 0.33 Nm/° VSTA I setting are also linear and consistent, Figure 11. The 0.33 Nm/° setting represents the 1:1 setting of the VSTA I which is reflected in the rate of the VSTA I equaling the rate of the internal torsion spring.

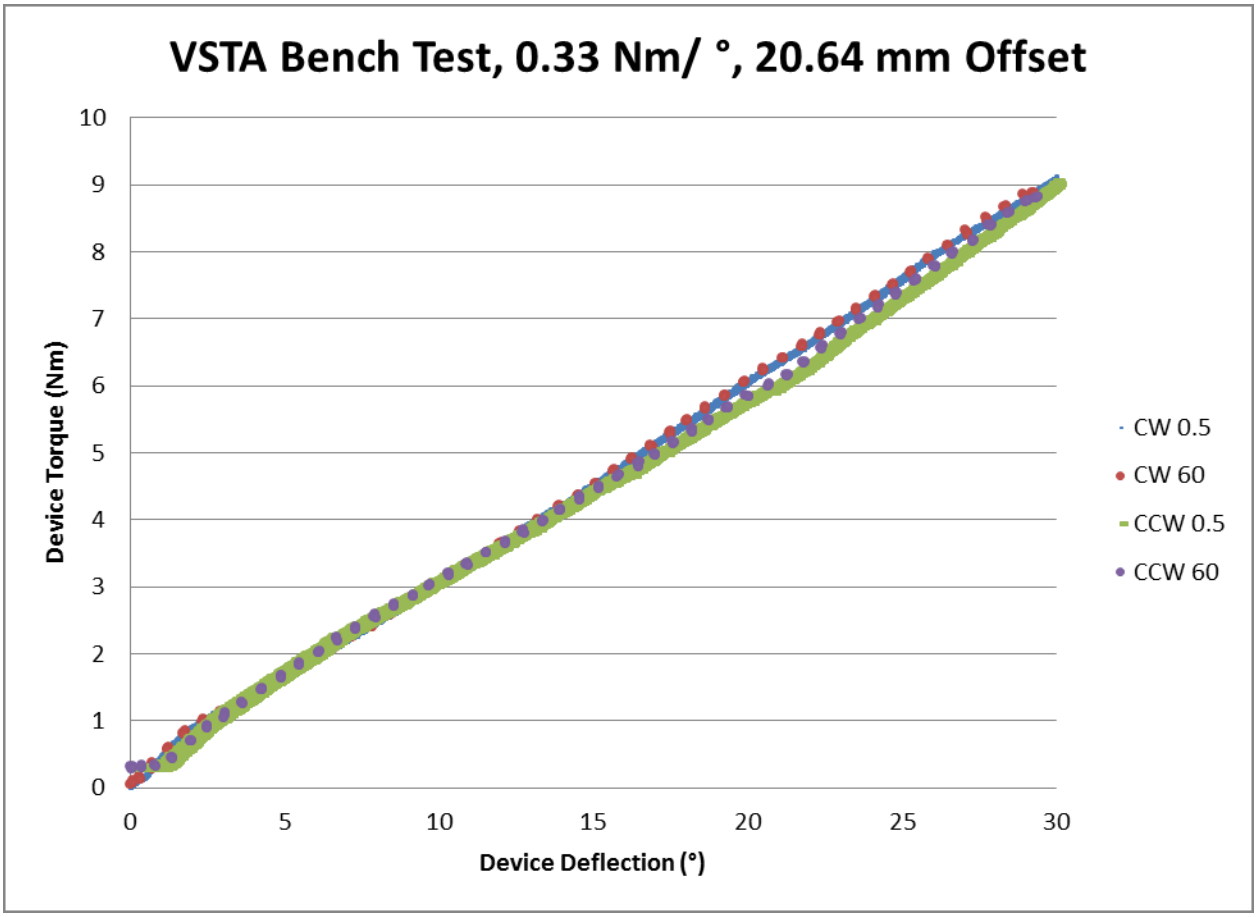

Figure 11: VSTA I test at 0.33 Nm/°, 20.64 mm offset from pivot.

Data from the lightest setting available to the VSTA I is also highly linear and consistent, Figure 12.

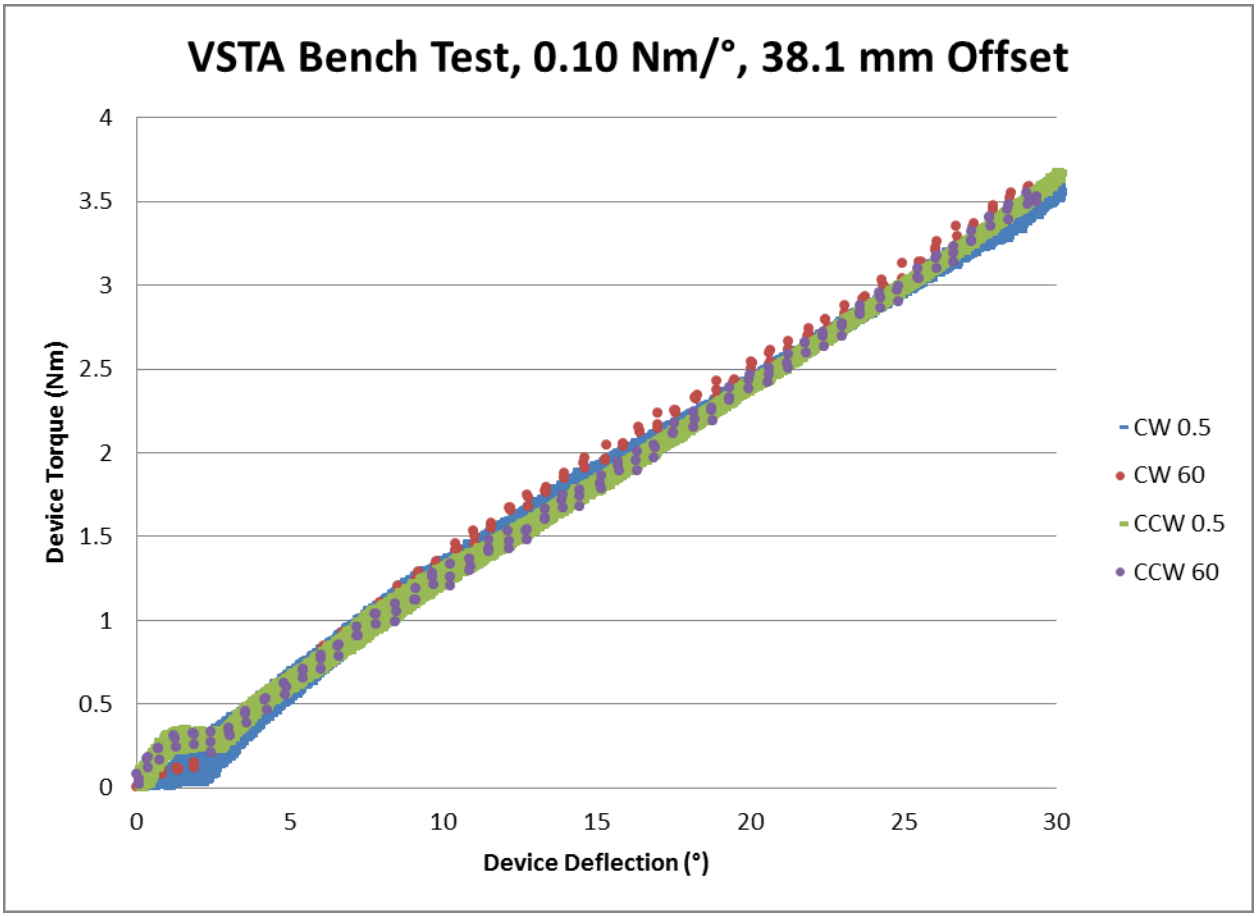

Figure 12: VSTA I test at 0.10 Nm/°, 38.1 mm offset from pivot.

Comparison values for each of the four preceding graphs are compiled in Table 5. This information is important when evaluating if direction or displacement rate play a role in the performance of the VSTA I. The table shows comparisons of the VSTA I rate, between tested conditions, which was determined for each condition via a linear fit trend line forced through the origin. It can be seen in the table that generally the direction and speed of deflection does not greatly influence the measured rate of the VSTA I. One exception was for the 1.17 Nm/° setting, which is discussed later.

Table 5: Comparison of VSTA I performance at each stiffness setting

	Comparison	Percent Difference (%)			
		CW: 0.5 vs 60	**CW 0.5 vs CCW 0.5**	**CCW: 0.5 vs 60**	**CW 60 vs CCW 60**
VSTA Rate (Nm/°)	1.17	0.35%	7.99%	0.81%	9.15%
	0.64	-1.33%	0.95%	0.35%	0.02%
	0.33	-0.11%	0.72%	0.23%	0.60%
	0.1	-0.34%	0.02%	0.07%	0.43%

Using the results at the individual stiffness settings, a comparison could be made between the actual VSTA I performance and the model predictions, Figure 13. In the figure, the data from the four separate conditions (CW, CCW, 0.5 °/s, and 60 °/s) are combined as a single data set. Each data set is then given a linear fit, forced through the origin, to determine the actual spring rate achieved by the VSTA I. This value, along with the goodness of the fit, are shown adjacent to each data set in Figure 13. It can be seen in the figure that at the lower stiffness settings, the VSTA I results match well to the model prediction. However, at the highest stiffness level, there is a significant deviation between the VSTA I actual performance and the model. A summary of the data presented in Figure 13 along with an analysis of how it compares to the model are given in Table 6. The data in the table tabulates how much the VSTA I actual varies from the model, as well as showing how well the linear trend line fit the data. The percentage of deviation is calculated by determining the difference in rate between the model and actual and representing that deviation as a percentage of the total stiffness range of the VSTA I. It can be seen for the lower three stiffness values that the VSTA I differed by less than 10% from the model prediction, the large deviation of the 1.17 Nm/° setting is discussed later. The linear fit numbers show the R^2 values of the linear

trend lines to the data. This indicates that the linear fit is an excellent approximation of the actual data, and that the response of the VSTA I can be taken as linear.

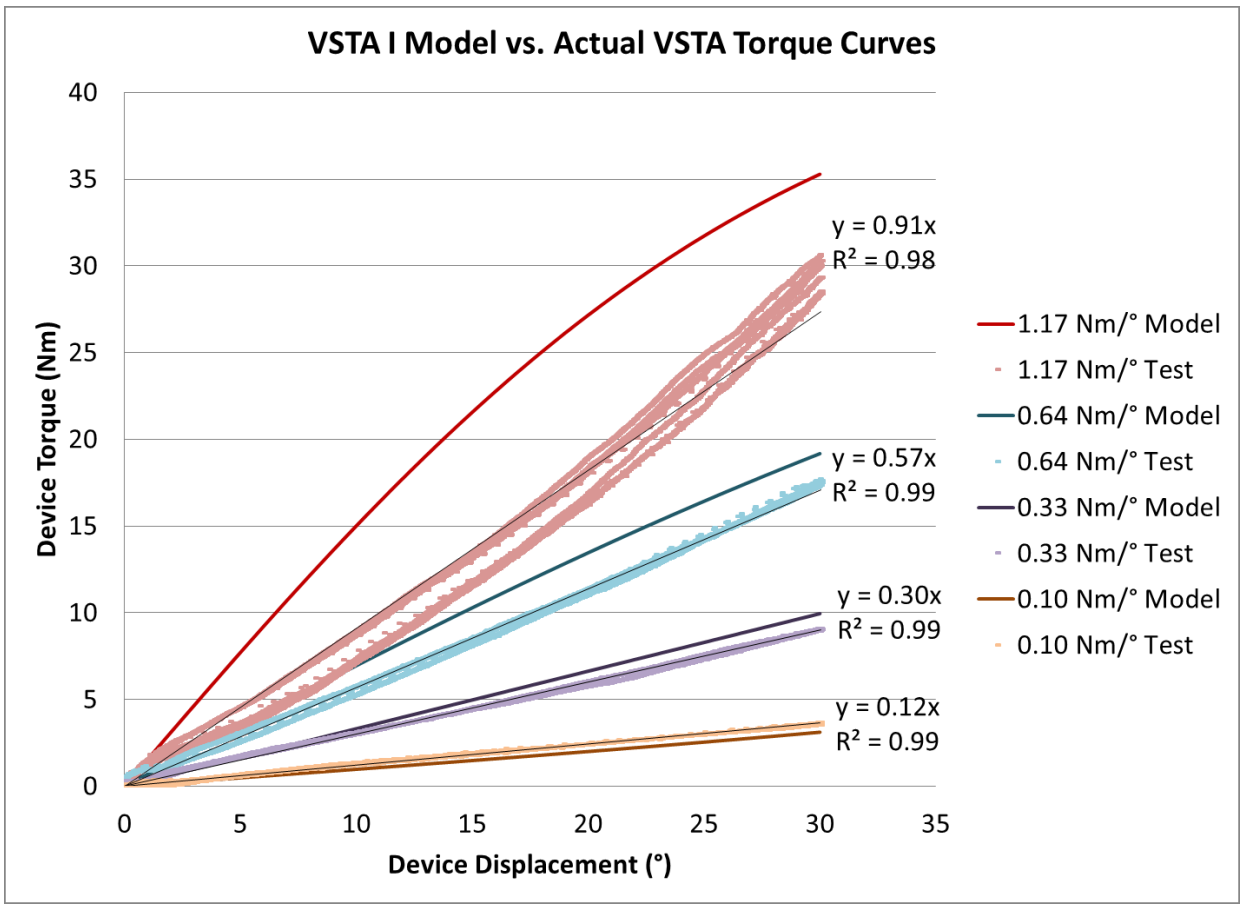

Figure 13: VSTA I Performance as compared to VSTA Model

Table 6: Analysis of VSTA I data in comparison to model predictions.

Modeled Stiffness (Nm/°)	VSTA I Stiffness (Nm/°)	Deviation from Model as Percentage of Full Stiffness Range	Line Fit R^2 (Linearity of Results)
1.17	0.91	24%	0.978
0.64	0.57	7%	0.997
0.33	0.3	3%	0.997
0.10	0.12	2%	0.996

Lastly, the VSTA I was run through the same set of tests as previous, but with no spring installed, to quantify any friction in the system. It was found that the frictional effects of the VSTA I with no spring were less than 0.25 Nm, and deemed inconsequential.

Using the data gathered, a plot of the VSTA I stiffness was made in relation to the Spring Carrier position relative to the Lever Pivot, Figure 14. This plot is interesting as it shows the sensitivity of the position of the spring carrier in relation to the desired stiffness. The plot also shows the deviation of the actual results from the model at higher stiffness values. Figure 14 uses a power curve to establish the relation between the spring position and the stiffness. The curve will later be used to establish a control model for the motor on the VSTA I to command the position of the spring to obtain a specific stiffness.

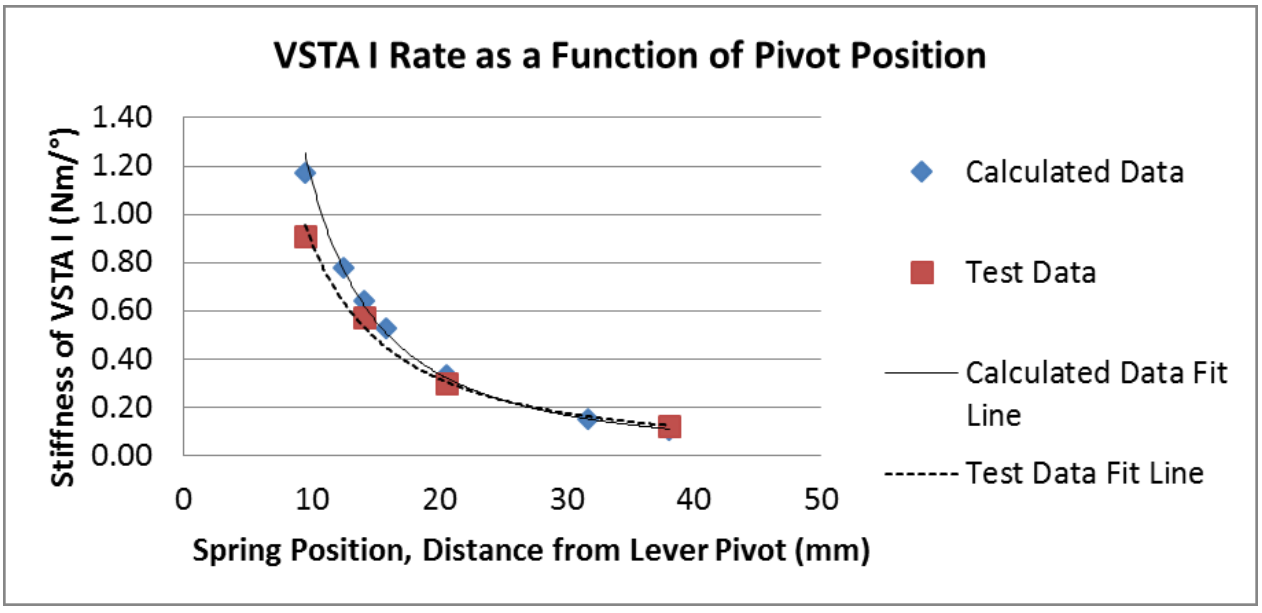

Figure 14: VSTA I Stiffness as a function of Spring Carrier position in relation to the lever Arm Pivot

The final physical attributes, as compared to the initial design goals, can be found in Table 7. It can be seen in the table that the stiffness range of the VSTA I is slightly reduced from

the model predictions, but still maintains a maximum stiffness greater than devices currently on the market. The mass of the VSTA I is also slightly larger than the computer model predicted.

Table 7: Comparison of initial design and final specifications of the VSTA I

	Motion Range	Stiffness Range	Mass (No Adapters)	Size
Initial Design	±30°	0.10-∞ Nm/°	1.27 Kg	89 mm tall x 111 mm Dia
Final Implementation	±30°	0.12-0.91 Nm/°	1.56 Kg	89 mm tall x 111 mm Dia

2.4.2 VSTA I Mechanical Bench Testing Analysis

The VSTA I test results exhibited negligible difference in performance between the 0.5 and 60 °/s speeds and the clockwise and counter-clockwise directions, so all data was grouped together. There was an exception for the 1.17 Nm/° data which varied up to 9% between clockwise and counter clockwise due to internal deflection which is discussed later. The grouped results of the VSTA I test were fit using a least squares optimization to determine the effective stiffness of the VSTA I at the individual settings. The actual tested stiffness of the VSTA I was then compared to those modeled (see Table 6). The goodness of the linear fit of the test data is indicated by the accompanying R^2 values.

It was found that at the lower stiffness settings, the model and VSTA I experimental results matched closely, with deviation from the model less than 10% of the full scale VSTA I stiffness span. However, at the 1.17 Nm/° setting, there was a large deviation from the model, as well as less consistency in the repeatability of the VSTA I. An investigation into the inconsistency found that at the higher stiffness setting, the VSTA I experienced significant internal deflection of the spring carrier along the guide rails. This was a result of the higher forces on the top of the spring

post from the lever arm, and the large moment arm that this induces over the bottom of the carrier at the guide rails, Figure 15.

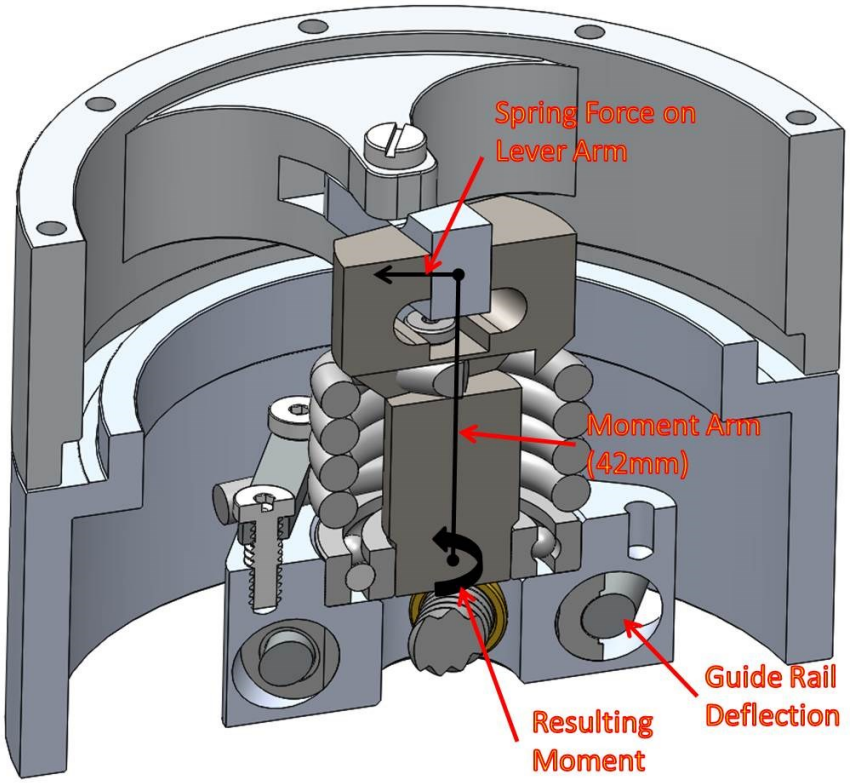

Figure 15: Illustration of forces resulting in large internal deflections at high stiffness settings.

This deflection is a design issue that could be resolved by working to reduce the length of the moment arm and relocating the spring, or by supporting both ends of the spring carrier. This deviation is only an issue at the highest stiffness settings and while it is not congruent with the model, the response of the VSTA I is still linear, and predictable given the test data. Another consideration is that the peak torque for a turning amputee has been recorded to peak around 11.8 Nm, which would be approximately 12° of deflection at the 1.17 Nm/°, less than half the functional range of the VSTA I, minimizing the internal deflection [14].

The VSTA I is infinitely variable within its stiffness limitations; however, the resolution to achieve the stiffness values in relation to the carrier position is non-linear. Figure 14 shows how the stiffness of the VSTA I can be varied through that range by positioning the Spring Carrier, with the trend of the VSTA I accurately fit by a power curve (R^2=0.998). This indicates that for active control of the VSTA I, a controller could be easily programmed with the curve to accurately assign stiffness profiles to motor positions. A discussion of these results follows.

2.4.3 VSTA I Bench Testing Discussion

Results from the bench testing show that the VSTA I was a viable device to demonstrate whether variable transverse plane stiffness would be of benefit to individuals with lower limb amputation. Bench testing methods were modeled to conform with Flick et al. [14] and so comparisons to the single stiffness devices tested can be made. It was found that the VSTA I was not rate dependent, performing equally well at 0.5 °/s and 60 °/s. The VSTA I was capable of stiffness variation between 0.12-0.91 Nm/°, with a movement range of ±30°. This exceeds the capabilities of the single stiffness devices tested by Flick et al., which generally peaked around 0.7 Nm/° [14]. The maximum stiffness range of the VSTA I corresponds to a maximum torque capability of 27 Nm, also in excess to the capabilities of the intact human ankle. At the maximum stiffness setting of 0.91 Nm/° and a deflection of 15°, the torque in the VSTA I would be 13.65 Nm, comparable to the 11-12 Nm maximum at 15-20° found in the intact human ankle [14], [21]. Lastly, testing of the VSTA I at its 1:1 (spring deflection : device deflection) ratio demonstrated that it does little to modify the dynamic response of the internal spring, resulting in a predicable linear response from the VSTA I. The VSTA I is a prototype, and as such has limitations. The current VSTA I prototype is limited to stiffness changes under no load (swing phase), precluding the ability to create custom torque curves by actively adjusting the pivot position while under load.

This also limits the VSTA I to operation as a state machine, with single stiffness settings applied to single tasks such as turning, pivoting, or walking. Another limitation of the current VSTA I layout is its inability for infinite ratio variation between the minimum and completely stiff values. Lastly, Figure 14 shows a significant reduction in position resolution as the stiffness increases. This means that as the stiffness increases, the position controller must become increasingly more accurate to hit a specific stiffness value. This curve could be modified in the future by developing a spring with a higher stiffness value, effectively skewing the trend to the right, and providing more resolution at the higher stiffness levels. These shortfalls will be addressed in future iterations of the VSTA I to achieve the maximum utility, with no risk of damage due to over stress of the spring, and reducing internal deflections.

2.5 VSTA I Control System Testing

A simple control system for the VSTA I was developed and tested. As previously discussed the VSTA I will be used as a state machine, such that single stiffness settings correspond to individual tasks. This type of operation only requires simple position step commands for a controller. To perform this operation, a proportional-integral-derivative (PID) controller was used to modulate the position of the motor to achieve changes in the spring carrier position resulting in a change to VSTA I stiffness.

2.5.1 Controller Testing Methods

A Maxon controller, EPOS 24/5 (PN 275512 Maxon Motor AG, Switzerland), and control software, EPOS Studio (2.0, Revision 2), were used to perform the stiffness selection task. The EPOS 24/5, limited to 24 volts and 5 amps maximum, allowed for direct control of the motor via an RS232 to USB computer connection, while the EPOS studio uses a PID control scheme for step position control. The position of the EC 45 motor was monitored via the three internal Hall effect

sensors. While using Hall effect sensors for motor position is less ideal than an encoder, or linear potentiometer on the carrier, the motor manufacturer indicates that it is sufficient for motors with greater than four pole pairs. The EC 45 has eight pole pairs.

The control employed by the EPOS Studio utilizes parallel PID control (Figure 16) with a sample rate of one kHz, however, recording was limited to 512-bits that was then divided between the channels due to the serial sampling of the software. Three of the four channels were 32-bit, and one was 16-bit, which only allowed for 72 samples over the 2 second period, resulting in a 36 Hz sample rate.

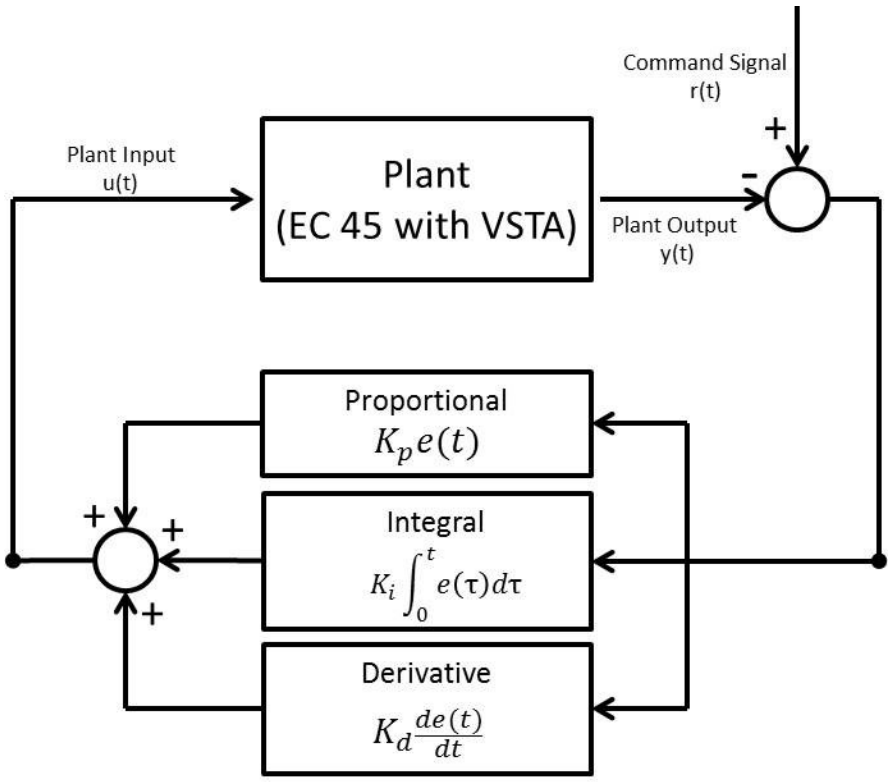

Figure 16: PID Control Diagram

While the EPOS Studio software comes pre-loaded with suggested gains, it was found that these gains resulted in an unstable system. Specifically, when commanding a step input, the controller would command a ramp at too high a rate, causing a motor fault state. Preliminary tests

revealed that the 24-volt supply, coupled with large step input commands, resulted in excessively high current requirements. It was found through trial and error that 16 volts was the maximum supply that could be reliably provided without tripping an excess current fault. Additionally, efforts to use the EPOS Studio auto tune function alone to optimize gain settings did not produce a sufficiently fast response with limited overshoot and oscillation without exceeding motor fault limits. Due to these factors, the PID gains were set manually after utilizing the auto tune function to set base values.

The tests run on the control system of the VSTA I were done with Kp, Ki, and Kd set at 10,000, 75, and 20,000, with a supply of 16 volts. These values for the PID gains, while not optimal, could get a fast response at the lower supply voltage while minimizing overshoot and ringing. This process resulted in Kp and Kd values much greater than expected. The Kd value might normally be kept at a far lower value to minimize interference from signals with rapidly changing values with respect to time, such as noise. However, for this case, it was found that increasing the Kd value did not have any detrimental effects, proving useful in minimizing overshoot and nearly eliminating oscillations.

Tests were run for eight step inputs to the VSTA I of varying size (38.1, 28.57, 20.64, 14.17, 11.11, 9.53, 6.47, 4.64 mm). This was done to best characterize response the system would have to different stiffness requirements. Ranges included the full stiffness range of the device from fully locked to the minimum stiffness position, as well as all the ranges between the five previously tested stiffness positions. Each trial recorded the actual motor position, position command, average actual motor speed, and average actual motor current. The first two variables were chosen to help evaluate if the VSTA I was positioning accurately, and how quickly it could make the position change, the second two were used to evaluate how the controller was conducting the step change.

Response curves were evaluated for the following characteristics: 1) rise time, 2) percent overshoot, 3) settling time, and 4) steady state error. Rise Time is calculated as the time between 5% and 90% of the steady state value. Percent Over Shoot is the percent of the steady state value that the curve achieves at its maximum. Settle Time is set from the step command until the curve settles to within 5% of the steady state value. Steady State Error is the difference between the command and the final steady state value of the response curve. For the purposes of this project the Settle Time and Steady Stat Error are the most important values as this indicates how quickly and accurately the controller could set the stiffness of the VSTA I.

2.5.2 VSTA I Controller Testing Results

Results were recorded for each of the eight step tasks. Figure 17 shows an example of the VSTA I control response for a given step input. Only one full graph is shown as all additional tests exhibited the same information relative to the size of the step command.

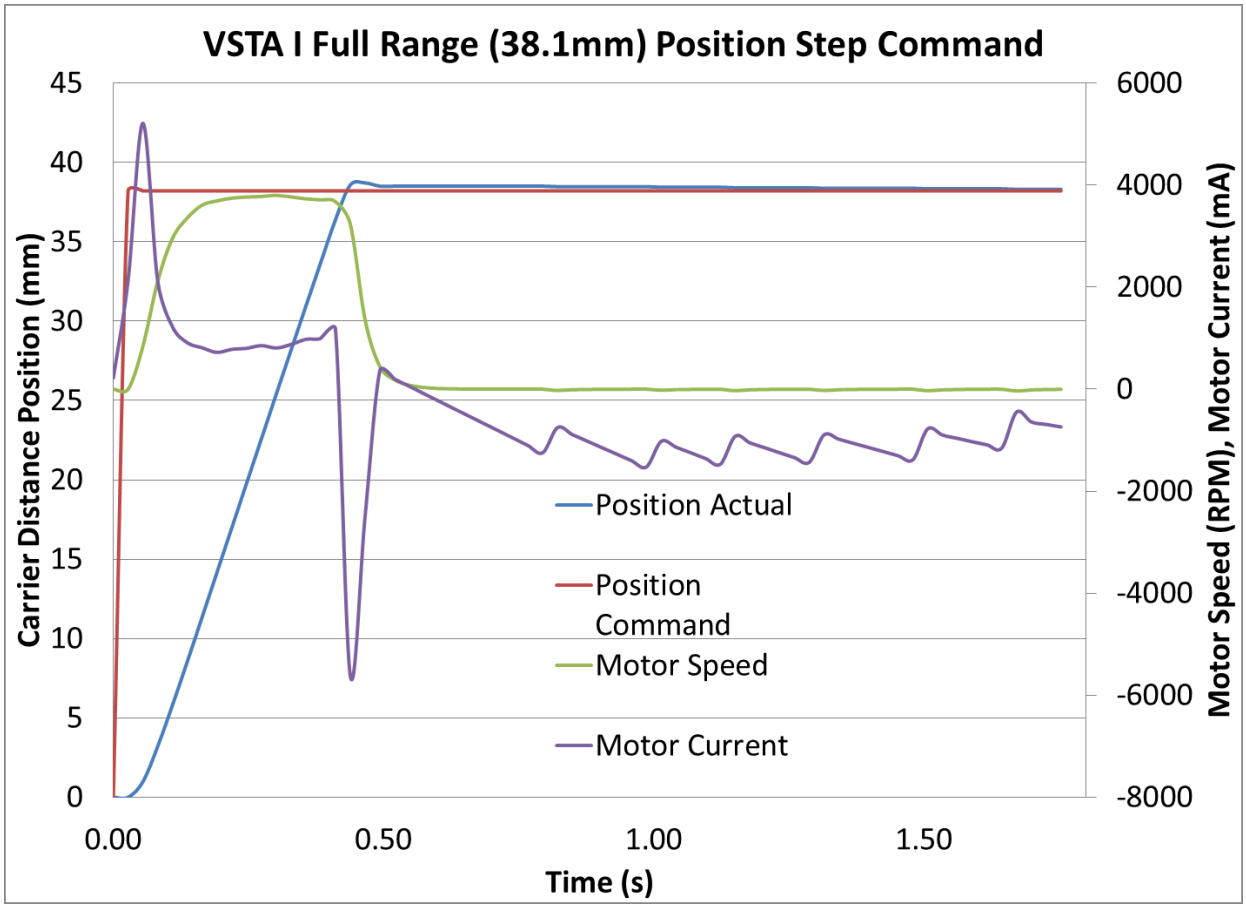

Figure 17: Recorded control response of the VSTA I during a sweep of the full motion range (38.1mm, Full lock to 0.12 Nm/°)

The system responds quickly to step input and achieves the commanded position with an overshoot of 1.06%, a single oscillation, setting in 0.47 s at maximum, Figure 17. This is a factor of the high Kd gain that was described previously. It can also be seen that the motor current quickly reaches the five-amp limit that forced the reduction of the input voltage from 24 volts to 16 volts. Motor speed can also be seen to be very stable during the transition, reaching a peak of around 4000 rpm in 0.30 s. A simplified model calculation relating the motor power (current times voltage) and the mechanical power (torque times angular speed of the motor) shows that at the 3778 rpm, 5.2 amps, 16 volts, the motor is producing 210 Nmm of torque. Referencing the datasheet for the EC 45 [26], this is congruent with the maximum speed, current, and torque conditions. However, if the motor was allowed to run at the full 24 volts more power would be

available for the step command. Torque could be increased, helping to decrease the time required to make the position movement, and will be addressed later in the results and discussion.

The results for six of the eight individual step command, and system responses are shown in Figure 18. Two of the results, as well as the velocity, and current data were left off the chart to enhance readability.

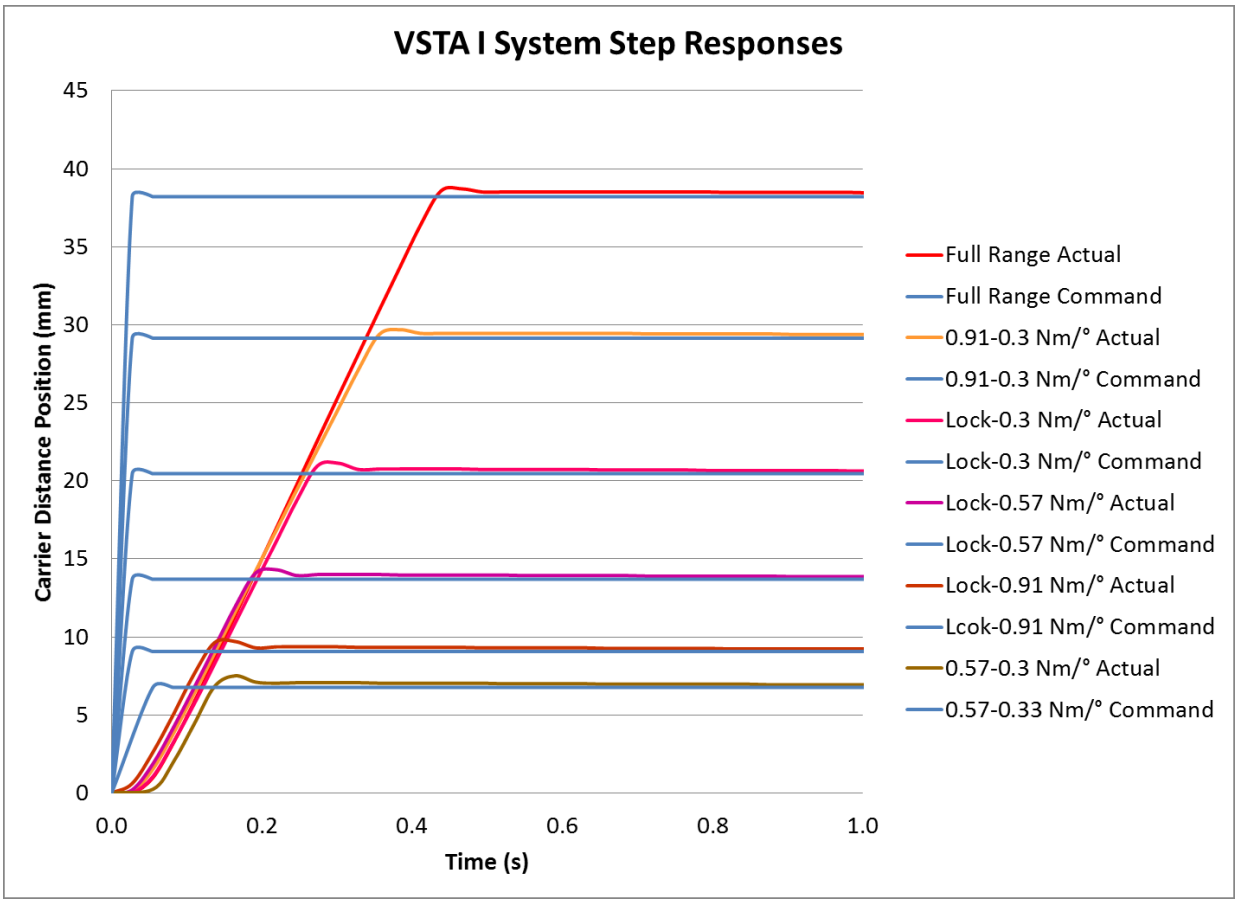

Figure 18: Step input responses for VSTA I position commands of varying lengths

At a maximum, the VSTA I took 0.47 seconds to move from fully locked to the minimum stiffness position for 0.12 Nm/°. The steady state error was found to be very low at 0.03-0.1 mm, a value that is of no consequence to the system. The 0.47 second time is the largest concern, as the target time was to be less than 0.25 seconds to fit within the swing phase of the average human

gait [25].The step response was very consistent for the varying step sizes. Each with similar rise rate, little overshoot, negligible oscillation, and little to no steady state error. Data for these tests is compiled in Table 8.

Table 8: VSTA I Controller Step Response Data

Test	Distance Traveled (mm)	Rise Time (s)	Percent Over Shoot (%)	Settle Time (s)	Steady State Error (mm)
Full Range	38.1	0.33	1.06%	0.47	0.1
0.91-0.1 Nm/°	28.57	0.22	1.05%	0.38	0.1
Lock-0.3 Nm/°	20.64	0.2	2.97%	0.33	0.07
Lock-0.57 Nm/°	14.17	0.15	3.93%	0.25	0.07
Lock-0.91 Nm/°	9.53	0.11	6.30%	0.19	0.07
0.91-0.3 Nm/°	11.11	0.11	6.78%	0.19	0.07
0.57-0.3 Nm/°	6.47	0.08	9.90%	0.16	0.07
0.91-0.57 Nm/°	4.64	0.08	10.14%	0.16	0.03

One way to improve this is to modify the controller to allow for the full 24-volt supply to the motor. Further tests were performed in which the motor was supplied with 24 volts and run through the full range of 38.1 mm and the half range of 20.6 mm. For these tests the motor was deactivated into fault mode before the step could be completed. It was found that for the full range, 24-volt attempt; it took 0.34 s from the step command until commanded position was passed. If the motor could be controlled like the 16-volt trial, which took 0.05 s to settle to the set position from the time it initially overshot the command, it is estimated that the VSTA I is capable of 0.39 s for a full range stiffness variation. A 24-volt attempt was also performed for the half range step,

which took 0.18 s to initially overshoot the command. Using a similar extrapolation, it is assumed the VSTA I can attain 0.23 s for this step size at full power. These values are more in line with the requirements of the VSTA I, and would allow more capability in future testing.

2.5.3 VSTA I Controller Testing Discussion

Testing of the controller and motor of the VSTA I was completed for a step input response congruent with use of the VSTA I as a state machine. The VSTA had acceptable response for position accuracy, and could move relatively quickly. Initially, the results indicate that the VSTA I step response will not be fast enough, even if it is run at the full 24 volts. However, at the time there was not enough data to indicate what stiffness values might be required for varying activities, and so no estimation can be made to predict if the full range step command will ever be necessary. Additionally, it should be noted that the full range of the VSTA I stiffness capability might not even be usable as it is able to attain stiffness values as low as 0.12 Nm/°, well below the minimums of devices currently on the market, which only go as low as 0.5 Nm/° [14]. Using this fact conservatively, allowing that the VSTA I might have useful range as low as the median value of 0.3 Nm/° up to completely stiff, the VSTA I should have the capability to sweep the range in 0.23 seconds, meeting the original goal. Another consideration is that changes in stiffness that do not originate, or end in the completely stiff position will have considerable less distance to travel. Referencing Table 8, even with the 16-volt supply, the VSTA I could sweep the usable range from 0.91-0.3 Nm/° in 0.19 seconds, well within the 0.25 second goal. Additionally, the step command that was required during this project was a worst-case scenario for the VSTA I. Continued testing might show that a gentler sloping command might allow for more smooth transitions at higher voltage supplies, while only adding small amounts of time to the predicted responses.

Another consideration for enhancing the performance of the VSTA I would be to optimize the PID gains of the control system, or devise a more efficient control system completely. This could be done by starting with a system model. Generally, an electric motor system can be characterized by:

$$J\ddot{\theta} + b\dot{\theta} = Ki \quad [10]$$

$$L\frac{di}{dt} + Ri = V - K\dot{\theta} \quad [11]$$

Equations [10] and [11] can be formatted into a state space or frequency domain model which would then allow for offline optimization, and possibly a faster system. However, at this time there is not enough data on the system to accurately complete the model. While the moment of inertia (J) of the motor and armature constant (k) are known from the manufacturer, the additional component for J from the components of the VSTA I would have to be measured, as would the damping coefficient 'b' composed of the friction forces between the VSTA I components.

The VSTA I controller is used to achieve step changes in position of the spring carrier, and so it must be noted that this does not linearly correlate to the stiffness settings of the VSTA I. The relationship between carrier position and VSTA I stiffness was found to be related by:

$$\text{Stiffness} = 30.35x^{-1.519} \quad [12]$$

Where the distance 'x' in equation [12) is measured from the completely stiff position and fit the measured data with an R^2 value of 0.9976. As previously discussed, the useful range of the VSTA I is in a relatively small portion of its overall range. While this was presented as a possible drawback of the VSTA I's ability to resolve different stiffness in the useful range, it is a benefit to allowing fast stiffness variations by reducing the size of step changes. To fully implement control

of the VSTA I, a position sensor would be required to indicate VSTA I deflection, which could then be related to torque in the joint. This information would be crucial for understanding VSTA I performance and operation when being used in future human testing. While the addition of this sensor is critical to successful field testing of the VSTA I, it was negated for this level of the project as measurements of deflection were otherwise accounted for in the lab via the use of the MTS machine, and the infrared camera system for later human subject trials.

2.5.4 Controller Testing Conclusions

This section presented a PID control scheme to allow for step position changes, congruent with the use of the VSTA I as a state machine. It was shown that the VSTA I PID controller could accurately attain any position in the range required by the VSTA I. The controller did lack the speed necessary to sufficiently meet the initial goal of 0.25 seconds for a full range sweep. However, it was estimated that if the controller could have been run at the full 24-volt supply, and the actual usable range of the VSTA I was considered, the controller settling time was more than sufficient to make changes to the stiffness during the swing phase of the average amputee's gait.

2.6 Suggestions for VSTA I Improvements Post Mechanical Testing

The VSTA I's functionality was shown to be acceptable, but as noted previously, some issues were found during initial mechanical testing. As illustrated in Figure 15, the internal function of the VSTA I should be revised to reduce deflection of the internal components. Another limitation of the VSTA I is the inability to vary the stiffness infinitely between the minimum and completely stiff. This feature was limited by the maximum spring stress encountered at higher stiffness settings. This could be avoided by designing and sourcing a spring with a higher rate. A higher spring rate would limit the deflection required to reach higher stiffness settings, and reduce spring stress. A third possible improvement to the VSTA I would be individual springs for

clockwise and counterclockwise motion. During mechanical testing, it was found that deflecting the single spring against the wind direction resulted in higher spring stress, while having the same overall linear stiffness, had a noticeably different load profile than deflection with the coil wind. These modifications, while ideal, would need to be balanced against increases in size and mass that might result from increasing spring size, or adding additional components. Lastly, while the controller was deemed adequate, it was implemented with desktop computing equipment. Future iterations of the VSTA I should include an onboard controller to allow both mobility within the lab, and testing outside of the lab setting.

3 VSTA I Human Subjects Testing

3.1 VSTA I Human Subjects Testing: Methods

Testing of the VSTA I in human subject's trials aims to determine if the device could reduce loading on the residual limb with no impediment to mobility. I hypothesize that use of the VSTA I at lower stiffness settings will reduce the peak values of transverse plane moments in the lower limb when performing turning and reaching maneuvers that occur in everyday activities. Additionally, the use of the VSTA I at those lower stiffness settings will not impede mobility of the user when performing walking tasks that involve such maneuvers, as evaluated by their self-selected walking speed and the clinical L-Test of Functional Mobility [18]. Five healthy transtibial amputees (**Error! Reference source not found.**) gave informed consent to participate in an I nstitutional Review Board (IRB) protocol designed to evaluate the kinematic and kinetic responses of amputees walking with the VSTA I at various stiffness settings through activities designed to target turning and twisting found in daily activities. Gait kinematics and kinetics were collected using a 12-camera Vicon system (Vicon, Centennial, CO), modified Plug-in-Gait model with 65

reflective markers, 8 in-ground force plates (AMTI, Watertown, MA), and an iPecs (College Park, Warren, MI) 6-axis load cell installed to the distal end of the VSTA I.

Table 9: Participant characteristics. "VSTA I Setting Order" indicates the order in which each participant tested the stiffness levels; A: Compliant (0.30 Nm/°), B: Intermediate (0.57 Nm/°), C: Stiff (0.91 Nm/°)

Subject	Gender	Age	Weight (kg)	Amputation Side	Amputation Etiology	VSTA Setting Order
A01	Male	35	64	Left	Traumatic	ACB
A02	Male	47	85	Left	Traumatic	BAC
A03	Male	66	93	Right	Traumatic	CAB
A04	Male	47	98	Right	Traumatic	BCA
A05	Male	69	93	Left	Traumatic	CBA

Subjects were fit with the VSTA I by a certified prosthetist. The VSTA I and iPecs were attached to their as-prescribed socket and liner with a Vari-Flex low profile foot to accommodate the added height of the VSTA I assembly (Figure 19).

Figure 19: VSTA I setup on VSTA A02 subject with distal installation of iPecs sensor

Subjects then performed a 20-meter hallway walk test with the VSTA I in the locked condition to establish self-selected walking speed (SSWS). The subjects were then brought back into the lab and fit with form fitting clothes and reflective markers to allow for in-lab motion capture testing. Five individual tests were performed to test both turning and twisting ability and mobility: Straight Walking, 90° Turns, 180° Turns, Standing Reach, and the L-Test of Functional Mobility. Testing was performed at three constant settings of the VSTA I (A: 0.30 Nm/°, B: 0.57 Nm/°, C: 0.91 Nm/°). Before each test, and after all stiffness adjustments, subjects acclimated to the changes until they felt comfortable, before data recording commenced. Each of the five types

of testing were performed at a single stiffness setting, the VSTA I was then adjusted to the next stiffness and the tests run again at the new setting.

3.1.1 Straight Walking

Subjects walked across the lab in a straight line for 7 meters, crossing five individual force plates with each walk. Walking speed was monitored with light gates and the subjects were instructed to adjust their walking pace if they varied more than ±10% of their previously determined SSWS [8]. This activity was repeated five times.

3.1.2 90 Degree Turns

Ninety-degree turns were performed to both the left and right. Additionally, the start foot of the subject was dictated such that a spin or step turn could be forced [27]. A spin turn results when the foot on the inside of the turn is used to make the change in direction (Figure 20). The spin turn causes the subject to pivot around the turning foot creating a larger transverse plane moment about the lower limb. A step turn results when the outside foot is used to change direction (Figure 21). The outside foot of the step turn brakes and redirects the motion resulting in less rotation in the lower limb. Subjects were first instructed to turn however felt most comfortable and natural to them. Starting position was adjusted as needed to facilitate clean strikes on the individual force plates. After successful trial set the subject was then instructed to change their start foot, and thus change the turn type. Five trials were taken for turns on the prosthetic limb, three trials for turns on the sound limb. This procedure was performed first for left turns, and then repeated for right turns.

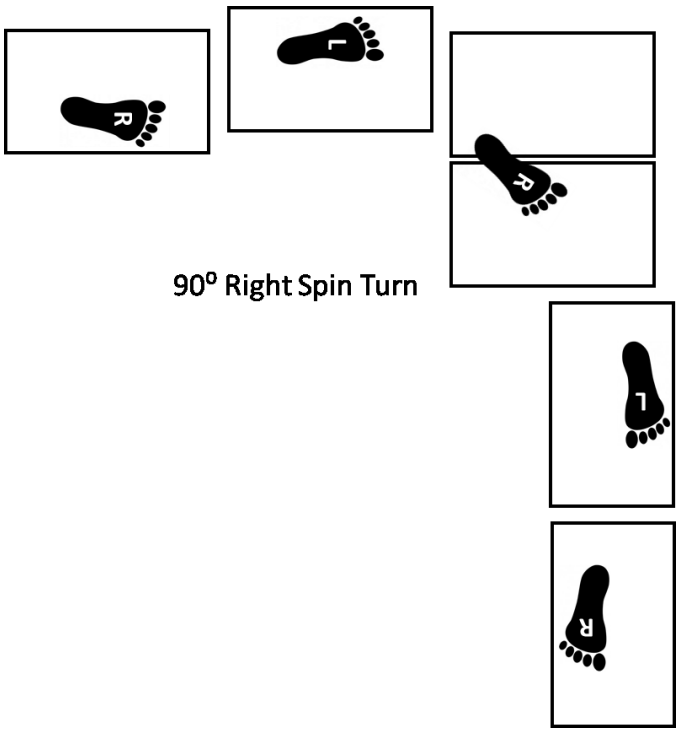

Figure 20: Right 90° spin turn example with spatial characteristics labeled. Numbered rectangles indicate in-ground force plates.

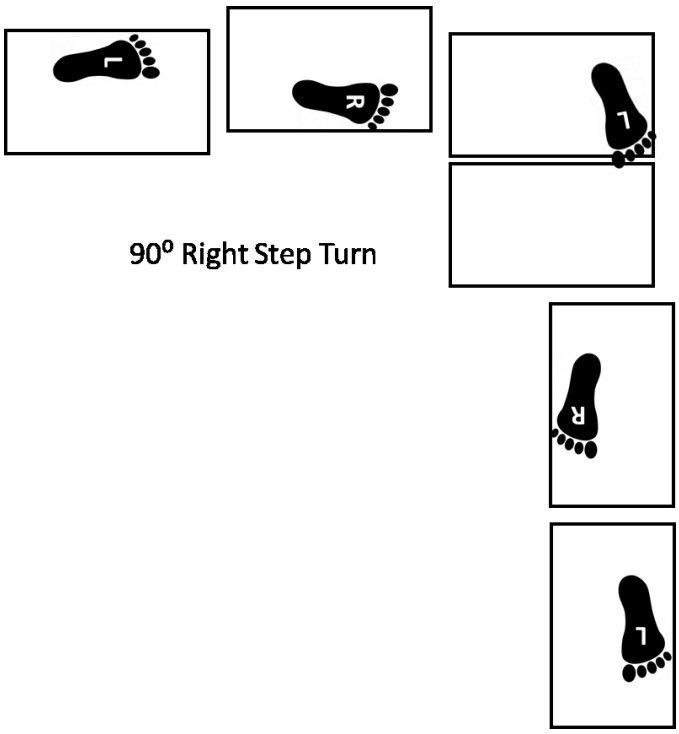

Figure 21: Right 90° step turn example with spatial characteristics labeled. Numbered rectangles indicate in-ground force plates.

3.1.3 180 Degree Turns

One-hundred and eighty degree turns were then performed to investigate large changes in direction. Subjects were lined up similarly to the straight walking trials. They were instructed to turn around when they reached the last force plate. Initially, subjects were instructed to make the turn in a comfortable manner, but were then given further instruction if needed to facilitate a pivot turn that allowed for single steps on each force plate (Figure 22). Subjects could turn to whichever direction was most comfortable for their first trials. The start foot was then changed to force a turn to the opposite direction on the opposite foot. Five trials were taken for each turn direction at each stiffness setting.

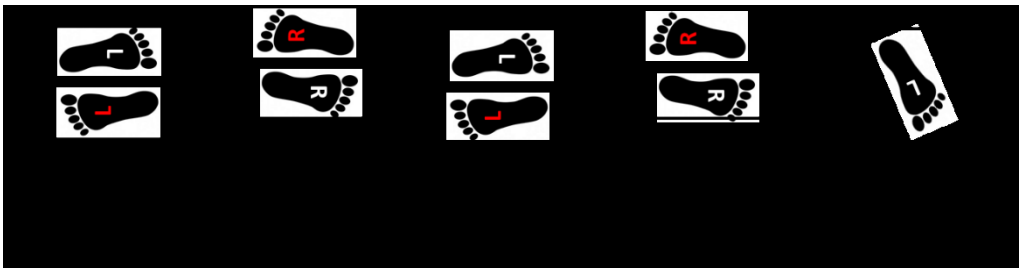

Figure 22: Right 180º pivot turn example. Steps labeled in red are return steps. Numbered rectangles indicate in-ground force plates.

3.1.4 Standing Reach

A standing reach test was done to simulate more static maneuvers that might involve large twisting motions. Subjects were instructed to stand with their feet on two separate, adjacent force plates. They were then to reach across their body to reach for an imaginary object at about shoulder level, like reaching for an item on a shelf. If possible they were instructed to keep their feet planted. This motion was performed both the right and left, five trials each.

3.1.5 L-Test of Functional Mobility

The L-Test of Functional Mobility is a modified Timed Up and Go test (TUG) [18]. This test was used as a clinical measure of mobility as it has shown a less significant ceiling effect as compared to the TUG. Additionally, the L-Test contains 90° turns to both the left and right as well as a single 180° turn, representing a walking activity that includes two of the turning maneuvers of interest. The L-Test of functional mobility is a timed test with the subject starting in a seated position, they then stand, walk 3 meters, turn 90°, walk another 7 meters, turn 180°, and return along the same path back to the seated position. For this test the subjects are instructed to perform the turns in whatever manner is most comfortable for them. Subjects are not required to travel over the force plates for these trials, however, iPecs data was recorded if comparisons to previous turn trials is desired later. Three trials were performed for each stiffness setting.

3.2 VSTA I Human Subjects Testing: Results

Five male, unilateral, transtibial amputees (mean ± standard deviation; age: 53 ± 14 years, mass: 87 ± 12 kgs, height: 1.82 ± 0.05 m) participated in the study (Table 9). The randomized order of stiffness settings for each subject can also be found in Table 9.

To validate the results from the iPecs a comparison to kinetic values calculated from the inverse dynamics of the in-ground force plates was evaluated (Figure 23). Use of in-ground force plates for inverse dynamics is the gold standard for determining joint loading and provided a good basis on which to compare the iPecs output [28]. It was found that the iPecs corresponded well to the inverse dynamics calculation with the iPecs having an overall smoother signal. While a low-pass, Butterworth filter, with a cutoff frequency of 25 Hz, applied to the kinematic signal from the force plates reduced some signal noise, the rough signal remained. The inverse dynamic signal uses double differentiation of the position markers to obtain acceleration to calculate forces and moments. This can lead to high levels of noise in these indirect force signals. Additionally, there was an offset between the two signals corresponding to a large dip in moment seen at the beginning of force plate signals that was not seen in the iPecs data. Future data collection done without the benefit of the iPecs will investigate these phenomena more closely. It was found that load cell data from the iPecs corresponds well to similar testing performed by Neumann et al. [29]. Due to the relatively good correlation with the inverse dynamics and previous research, smoother results, and the fact that the iPecs is a measurement directly in the pylon as opposed to an indirect calculation, the iPecs signal is used for all comparisons of transverse plane moment. By convention internal rotation is positive, and external rotation is negative.

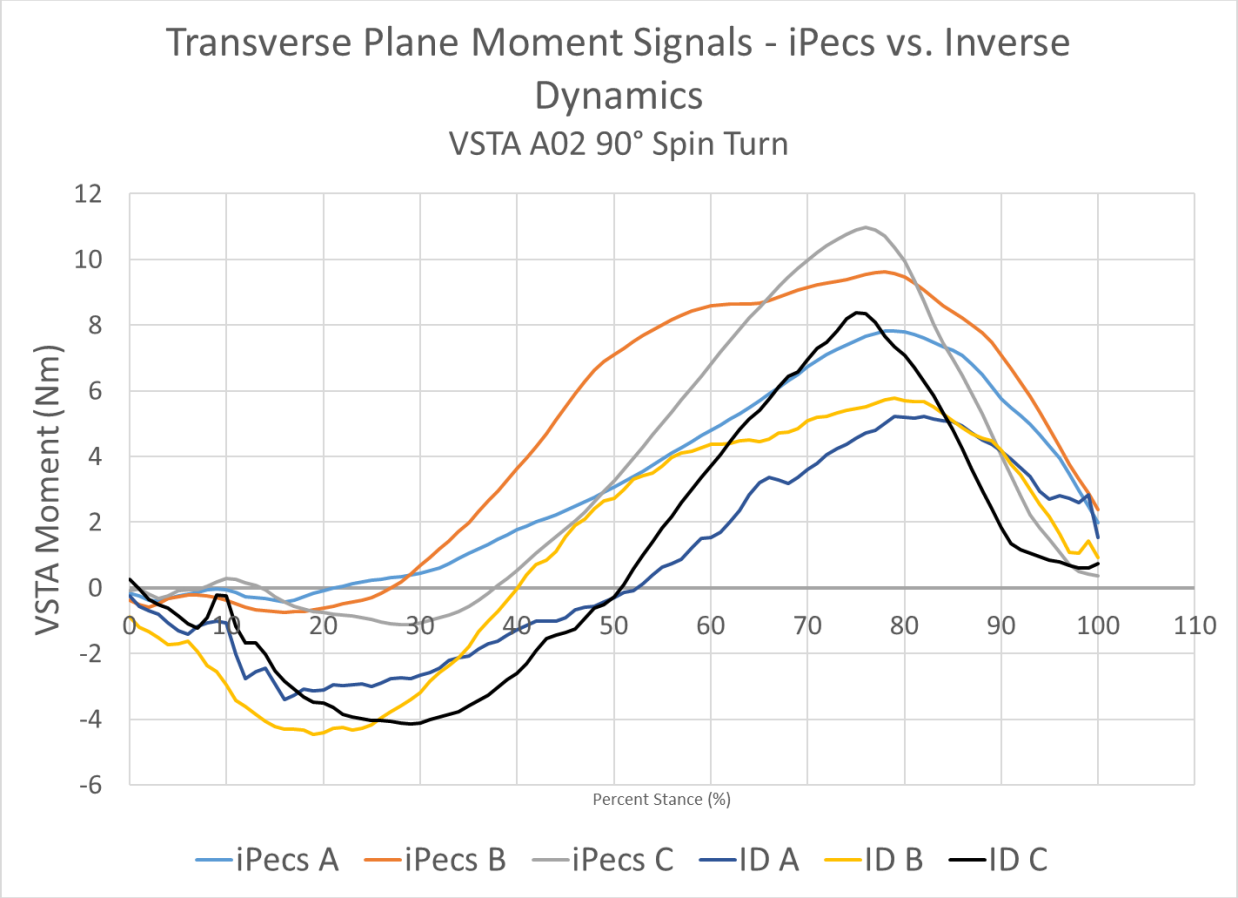

Figure 23: Comparison of iPecs calculation of transverse plane moment (iPecs A, B C) compared with inverse dynamics (ID A, B, C) from the in-ground force plates. (A: 0.30 Nm/°, B: 0.57 Nm/°, C: 0.91 Nm/°).

Transverse plane moment at the distal end of the socket is not a direct measurement of the shear stresses between the socket and residual limb that lead to soft tissue breakdown and discomfort. Shear stresses in the soft tissues of the residual limb result from motion between the socket and limb [7]. A transverse plane adapter serves to absorb this motion, where peak load is directly related to displacement and is an indicator of shear stress. This study uses peak transverse plane moment measured by the iPecs load cell fixed to the distal end of the VSTA (Figure 19) as the primary indicator of residual limb loading [8], [29]. Results are shown in Table 10.

Table 10: Peak transverse plane moment values taken from the iPecs sensor, normalized by body mass. Internal rotation is positive, external rotation is negative. Self-Selected Walking Speed (SSWS) during straight walking trials and time to complete the L-Test of functional mobility, (n= 5). Values are mean plus or minus the standard error. $p<0.05$ considered significant. Significant values are highlighted in bold. Static Reach (SR)

Activity		VSTA Setting			p(A vs B)	p(A vs C)	p(B vs C)
		Compliant (A)	Intermediate (B)	Stiff (C)			
Straight Walk	(Nmm/kg)	82 ± 24	70 ± 18	88 ± 20	0.161	0.394	**< 0.001**
90° Spin Turn	(Nmm/kg)	132± 18	151 ± 22	172 ± 25	**0.040**	**< 0.001**	0.134
90° Step Turn	(Nmm/kg)	-51 ± 13	-51 ± 12	-65 ± 13	0.937	**0.028**	**0.025**
180° Turn	(Nmm/kg)	-65 ± 6	-85 ± 9	-109 ± 18	**0.002**	**0.003**	**0.036**
SR Over Prosthesis	(Nmm/kg)	56 ± 9	94 ± 12	73 ± 15	**< 0.001**	**0.015**	**0.044**
SR Over Intact	(Nmm/kg)	-52 ± 9	-68 ± 14	-48 ± 9	**0.002**	0.269	**0.003**
SSWS	(m/s)	1.30 ± 0.02	1.35 ± 0.04	1.32 ± 0.03	0.093	0.186	0.147
L-Test Time	(s)	22.1 ± 0.5	22.4 ± 0.8	22.3 ± 0.7	0.378	0.644	0.719

3.3 VSTA I Human Subjects Testing Discussion

The data presented above summarizes human subject trials performed using a variable stiffness torsion adapter (VSTA) in a lower limb prosthesis. It is known that the addition of a transverse rotation adapter may help reduce transverse shear loading of the residual limb leading to soft tissue breakdown [5], [7], [8], but little has been quantified regarding the relationship between transverse plane stiffness, limb loading, and mobility. Specific hypotheses included: 1) use of the VSTA at lower stiffness settings will reduce the peak value of transverse plane moment in the lower limb when performing turning and twisting maneuvers similar to everyday activities; 2) the mobility of the user will not vary between stiffness settings.

Significant reductions in peak transverse plane moments between the stiff and compliant settings confirm the first hypothesis. The greatest reductions occurred for both the 90° spin turn and the 180° turn, the maneuvers with the greatest transverse plane motion. Both had an average reduction of 40 Nmm/kg between the stiff and compliant settings, a 40% reduction in peak moment for 180° turn and a 23% reduction for the 90° spin turn. One subject did not keep his foot planted during the 180° stiff trials. This resulted in a reduction of the peak transverse plane moment and did not compare appropriately to the other participants. Thus, the analysis excludes data from those trials.

The 90° step turn which featured a lower amount of transverse plane motion had a statistically significant difference between compliant and stiff ($p = 0.028$), and between intermediate and stiff ($p = 0.025$), but relatively no difference between the compliant and intermediate settings. Between the compliant and stiff settings, the 90° step turn showed a reduction in peak transverse plane moment of 14 ± 6 Nmm/kg. While the magnitude of the reduction is relatively smaller than the other turns, it still represents a 22% reduction in peak transverse plane moment, like the 90° spin turn. Data from 90° spin and step turns is consistent with previous transtibial amputee data performing a constant radius turn around a one-meter circle [8]. Results also align well with data from intact individuals performing 90° spin and step turns [30] and amputee data utilizing a similar load cell measurement setup [29].

Straight walking showed no significant difference in peak transverse plane moment between the compliant and intermediate settings or between the compliant and stiff settings as expected and consistent with the data from Segal et al. [8]. Significance is seen between intermediate and stiff ($p < 0.001$); however, this is only due to the negative trend between compliant and intermediate causing a greater gap between intermediate and stiff.

The static standing reach results were less easily interpreted. Reaches over the prosthetic side showed significant differences between all stiffness settings. Additionally, reaching over the intact limb resulted in significant differences between compliant and intermediate and between intermediate and stiff. While significant differences occurred, no clear trend could be interpreted for either condition. For both reaching tasks limb loading increased for increasing stiffness between the compliant and intermediate settings, and then limb loading decreased during the stiff setting. It was found that when reaching over their intact limb, three subjects lifted their heel to make the reach possible, which may account for the reduction in moment, and indicate a need to compensate for the higher stiffness. No explanation for the reduction in limb loading could be found for reaching over the prosthetic limb. The static reach test is not a standard test performed with amputees and no data could be found for comparison. More subject testing would be needed before any substantial inferences could be made from the current data.

The mobility metrics detected no significant difference between any of the settings for either self-selected straight walking speed or for the L-test of functional mobility ($p>0.093$). Amputees wearing the VSTA averaged 1.32 m/s for all trials, slightly slower than the 1.46 m/s found by Lemann et al. and 1.47 m/s reported by Hillery et al. indicating that the VSTA may have slowed their walking [31], [32]. However, self-selected walking speeds varied on average no more than 0.05 m/s. While changes in walking speed can have a significant effect on the biomechanics of a subject [33], previous studies have generally considered a value of ±10% to be acceptable [8]. A variation of 0.05 m/s is less than a 4% variance and so is considered both statistically and clinically insignificant. The L-Test showed a maximum average difference of 0.3 seconds between the compliant and intermediate settings, however, a difference of ±6.2 seconds is generally necessary to be 95% certain there is a change between conditions [18]. Mobility results are consistent with

those found by Segal et al. using a six minute walk test comparing a standard TRA with a rigid pylon [13]. This indicates that the subjects were equally as mobile at any setting of the VSTA at their self-selected walking speed.

This testing represents a pilot study on a prototype device and some limitations should be noted. This data is from a small sample size, solely male, and while statistical significance was found for many of the outcomes, more subjects should be tested to better apply these results to the general population. Additionally, all subjects were capable walkers, able to compensate well to changes in stiffness of the VSTA. Testing with less able walkers may show that not all individuals are able to tolerate excessively low transverse plane stiffness while maintaining mobility. All subjects in this study, regardless of body mass, were tested on the same three stiffness settings. Further testing is needed to determine how stiffness settings should be modified to accommodate users of varying mass and ability. Additionally, the VSTA and iPecs combination was heavy at 2.1 kg. While studies have shown that additions up to 3.50 kg have no significant effect on self-selected walking speed [31], all the subjects commented on the mass of the VSTA and noted that it would be too heavy for daily use. Testing of the VSTA did not include a locked condition. While the stiffest setting of 0.91 Nm/° is stiff when compared to the maximum settings on current TRA devices [14], it does not compare to the stiffness of a fully rigid aluminum pylon. Future testing should include a locked setting for more complete comparison of the effects of lowered stiffness.

Testing also help served to evaluate the VSTA prototype design and function. The function of the VSTA performed as expected, however its size and mass were limiting factors. Appropriate subjects able to accommodate the height of the VSTA and iPecs assembly proved difficult to find. Future iterations of the VSTA concept should strive to reduce mass and height.

4 VSTA II Design

Three main concerns were identified with the design of the VSTA I. First, it was heavy, and every subject commented about the added weight. Second, the height of the VSTA I was found to prohibit the number of subjects that could fit the device in their pylon space. Eliminating the 46-mm height of the iPecs for future testing would help significantly, but the 89-mm height (without adapters) of the VSTA I could be reduced to help include amputees with longer residual limbs, or to eliminate the need for low profile feet. Lastly, the VSTA I was deemed unfit for use outside of the lab due to internal deflections at higher loads, and the lack of a stand-alone power source and control system, as discussed in Chapter Two. These three criteria became the driving design specifications for a new VSTA II. Specifically, improvement criteria became mass less than one kilogram, height less than 50 mm, and a standalone controller.

4.1 VSTA II Design Criteria

The design criteria for the VSTA II remained the same as the VSTA I, and were further enhanced by the improvement criteria. The initial requirements for the VSTA I were split into two categories; functional, and structural.

Functional Requirements

- Rotate ±30° [19]
- Vary stiffness around a median of 0.6 Nm/° [19]
    - Meeting or exceeding the 0.12-0.91 Nm/° of the VSTA I
- Vary the stiffness within a single swing phase of gate (less than 0.25 seconds [25])

Structural Requirements

- Compression loading for 130 kg individual [20]
- Axial Torsion up to 65 Nm [20]
- Bending Load up to 163 Nm [19]

An additional design criteria was added over the original VSTA I. The VSTA II will only be required to make variations in stiffness during the swing phase of gait, when the device is unloaded. While the VSTA I's electric motor is capable of adjusting stiffness under load, testing was never attempted due to internal deflection issues under high load. Additionally, the use of active stiffness profiles during the stance phase of gait is not within the scope of the VSTA I human subjects testing, and it has solely been used as a state machine with static, linear settings during deflection. Little information is known about what stiffness settings might be optimal for different tasks, and to save weight for the VSTA II a smaller activation motor can be used if variations in stiffness are only required during the no-load conditions of swing phase.

4.2 VSTA II Design Iterations

Many design possibilities were identified during the initial concept generation for the VSTA I. These included series elastic actuators, variable length elastomer springs, and planetary gear trains, and all were re-evaluated to improve the VSTA I given the design criteria and improvement criteria. The main idea that presented itself from multiple sources was to eliminate the coil spring and use the lever arm itself as a cantilever beam spring. Three design iterations were devised, each developed to the point of infeasibility, at which point a new concept was derived and developed.

4.2.1 VSTA II V1: Steel or Carbon Fiber Beam Springs, Infinitely Variability

This first concept consisted of multiple beam springs arranged around a central carrier. The central carrier could be adjusted up and down via an electric motor and ACME lead screw. By adjusting the height of the carrier, the effective length of the beams could be adjusted, and the stiffness modulated (Figure 24).

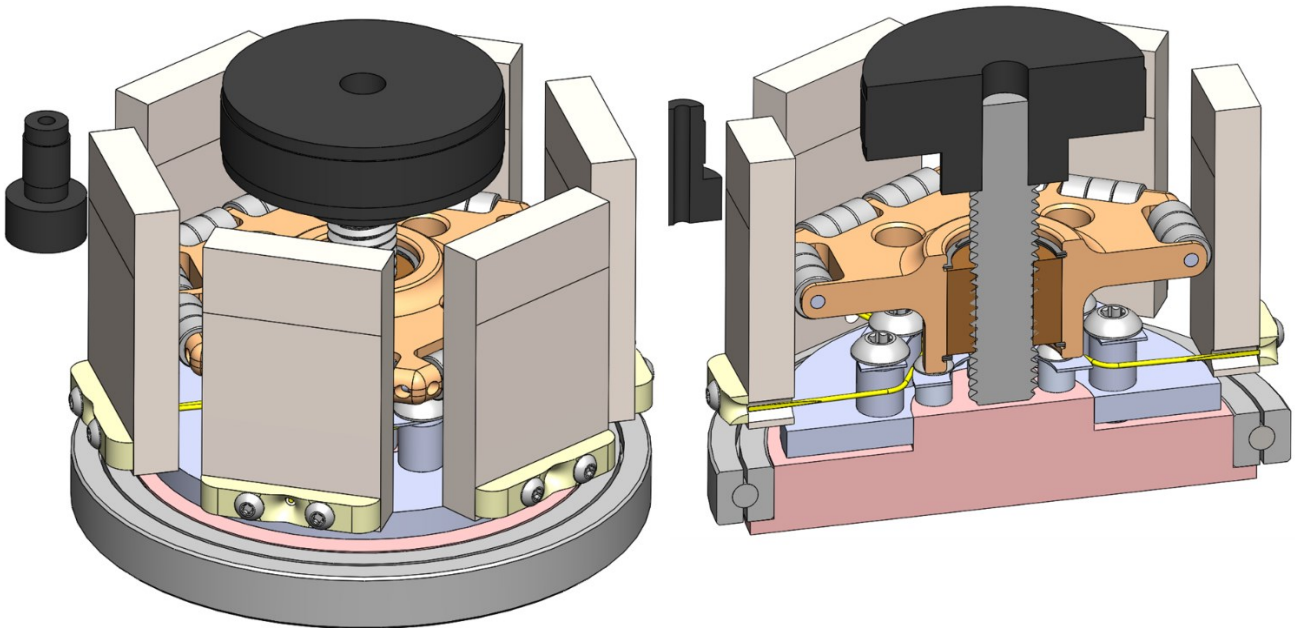

Figure 24: VSTA II V1, Variable Beam Spring Concept

Initially, steel beams were considered due to their ease of calculation and availability for purchase. It was quickly found that a single steel beam would not be appropriate due to over stress in the material during the high deflections needed to achieve the ±30° functional requirement. A leaf spring consisting of multiple, thinner, springs was then considered. This resulted in a leaf spring that was capable of the loads and deflections necessary, but it also required greater overall thickness which greatly increased the mass. Calculations determined that each spring would weigh approximately 50 grams, with six springs necessary for the assembly. This led to the investigation of carbon fiber as a spring material, however, the material specifications of commercially available

carbon fiber are not well defined, making it difficult to calculate the stiffness and stress limitations of the proposed springs. Another design challenge was determining the most efficient way to convert the linear force from the beam spring into the torsional loads needed for the VSTA II. In the V1 concept, this was achieved by pulling the springs with Kevlar thread and routing the thread around a post to align the tension force tangentially to the rotation of the VSTA II. The proposed thread attachment method also led to questions regarding the thread strain under load, ease of assembly and adjustability, as well as maximum load capability.

To investigate these unknown quantities, a test fixture was devised to physically test the materials and setup on the MTS (Figure 25). This allowed for direct testing of intended materials and geometries before moving forward with complete design.

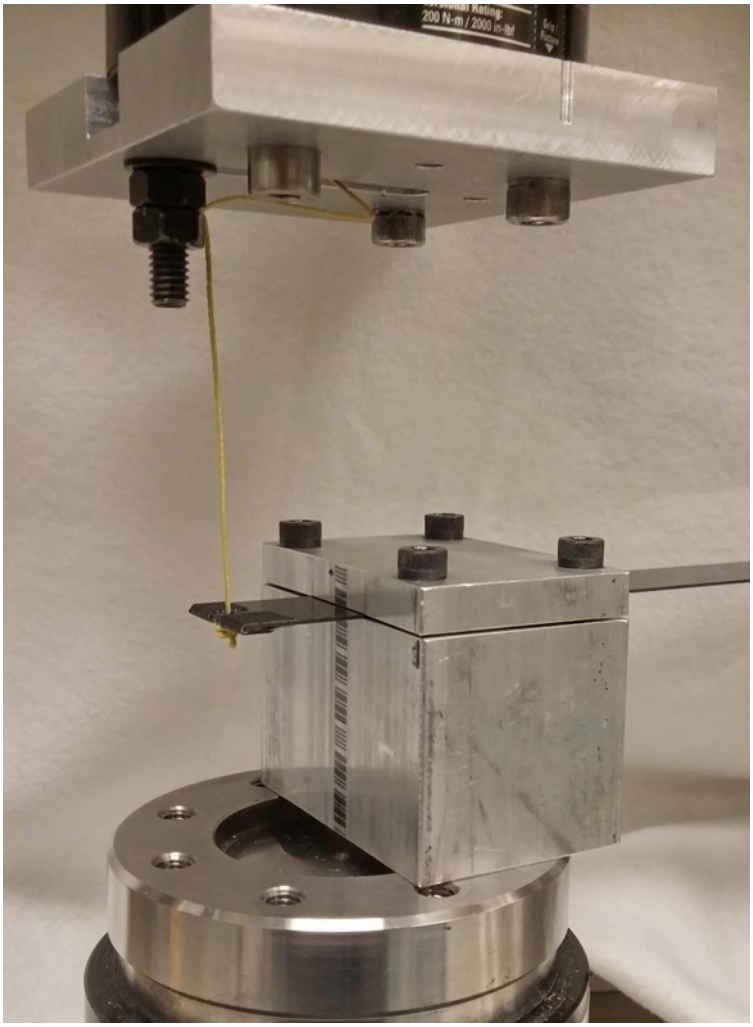

Figure 25: Material Test System Setup - Carbon Fiber Spring and Thread Attachment

Utilizing the MTS setup allowed for characterization of the modulus of elasticity and bending yield stress for the carbon fiber material. Additionally, attachment and activation using the Kevlar thread was evaluated. At this point the V1 design encountered its limit of feasibility. It was found on the MTS that the Kevlar thread was unable to hold the loads necessary, and exceeded the appropriate amount of strain for the application. Furthermore, the design at this point was estimated at 430 grams without housings, motor, or controller, and would be a minimum of 70 mm tall and Ø90 mm. While the issues with the Kevlar thread and relatively high mass might have

been accommodated, the large height was undesirable. At this point development on the VSTA II V1 was abandoned.

4.2.2 VSTA II V2: Horizontal Carbon Fiber Beam Springs- Electroadhesion or Finite Variability

Due to the VSTA II V1's height, it was decided to try aligning the springs in a horizontal orientation. Orienting the springs in a radial pattern around the axis of the device greatly decreased the height of the assembly, but also made modulation of the effective beam length difficult. A method for varying the radial length of all the beams at once was not successfully devised, additionally, it was concluded that the inclusion of an electric motor to facilitate modulation added excess mass, both from the motor and from the battery necessary to operate it. Instead of varying the beam's length, a method to modulate its thickness was investigated. Using a leaf spring configuration, multiple thin beams can be assembled together to make one larger beam that has greater flexibility, with lower force, than a solid beam of similar thickness. Using a high voltage, low amperage electric current an electroadhesive shear force can be generated between the leaves to effectively bond them together. By bonding different amounts of the leaves together, the thickness of the beam could effectively be varied with only an electric signal and the stiffness of the beam varied finitely by adding or subtracting leaves to the beam thickness. To determine the feasibility of this technique, a calculation was performed to determine the shear force that would need to be maintained between two leaves to securely bond them when flexed. A diagram for two leaves is shown (Figure 26).

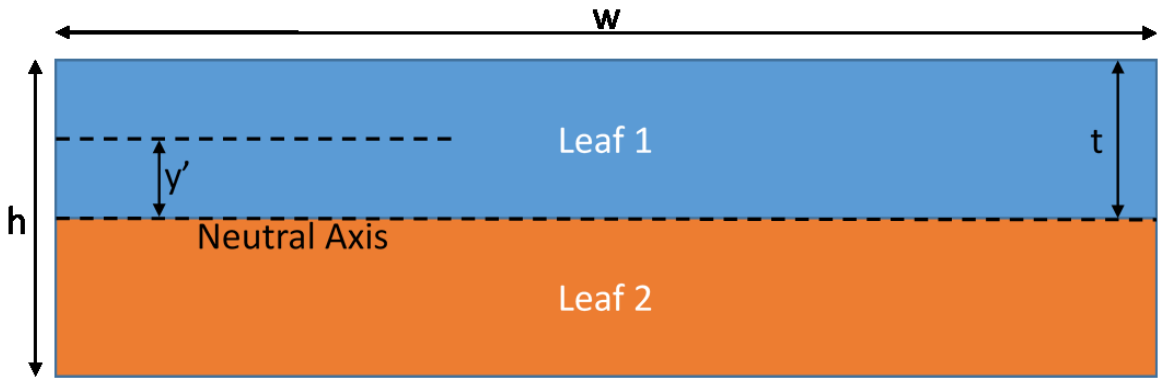

Figure 26: Diagram for two adjacent leaves for the calculation of necessary electroadhesive shear force

Calculation of the shear force between the two leaves was estimated using the spring dimensions from the V1 design [34].

- Individual Leaf Thickness, t = 0.79 mm (1/32")
    - This is the thickness of the commercially available carbon sheet previously tested and found to be appropriate as a leaf spring.
- Spring Width, w = 25.4 mm (1")
- Total spring thickness (2 leaves stacked), h = 2*t = 1.59mm (1/16")
- Distance from the neutral axis to the central axis of a single leaf, y' = 0.5*t = 0.397 mm (1/64")
- Max Shear Load, V = 100 N
    - This value was calculated for a beam with two leaves, 30 mm long, deflected 10 mm using equation [16].

Starting with the calculation of Q, the first moment of the area between the location of the shear stress (bonding between two leaves), and the neutral axis of a single leaf (location of zero shear).

$$Q = A * y' = (0.79\ \text{mm} * 25.4\ \text{mm}) * 0.397\ \text{mm} = 7.97\ \text{mm}^3 \quad [13]$$

Use the moment of inertia for the entire cross section:

$$I = \frac{1}{12} * w * h^3 = \frac{1}{12} * 25.4\ mm * (1.59\ mm)^3 = 8.51\ mm^4 \quad [14]$$

Then calculate the shear flow, or force per unit length at the interface between the two leaves:

$$q = \frac{VQ}{I} = \frac{100\ N * 7.97\ mm^3}{8.51\ mm^4} = 94\ \frac{N}{mm} \quad [15]$$

For a beam 30 mm long, it gives a total load of 2810 N. From the work of Sintake et al., it was found that a setup using a 5 kV source provides 3.5 N/cm^2 [35]. For a beam 2.54 cm wide and 3.0 cm long, this would equate to 26.7 N, many times less than the 2810 N required. At this point the idea of electroadhesion was abandoned.

The idea for discrete thickness increases instead of infinite variation of length gave the idea that the device didn't necessarily need to have infinite variability, which might eliminate some of the complexity of the design. From this, a new concept was derived using the horizontal beam layout. Each beam spring in the device could be activated, or deactivates such that the springs added in parallel, giving discrete increases in stiffness (Figure 27).

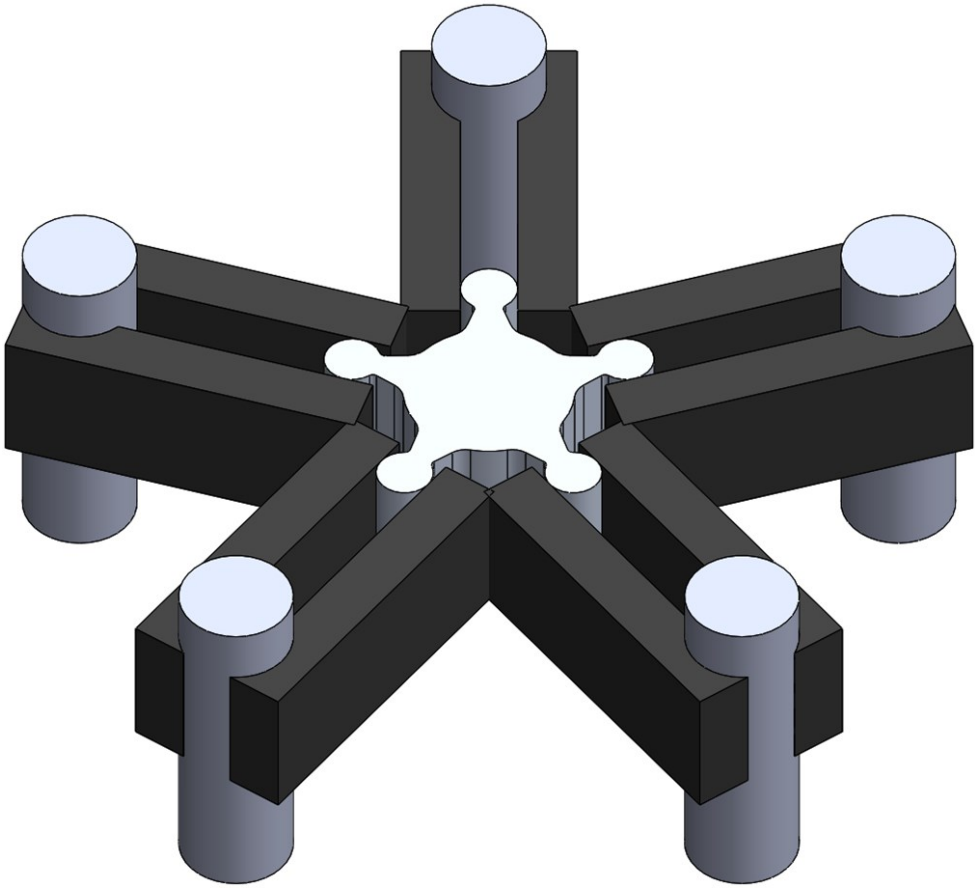

Figure 27: VSTA II V2, Discrete Horizontal Carbon Springs

In the VSTA II V2 design, each of the spring sets was a fixed length and attached at the outside of the device by a rotating hub. A solenoid below the spring layer would activate a lock pin that would allow the hub to lock to the housing or rotate freely. This would allow each spring set to provide force, or move freely without adding to the device stiffness. Again, these carbon beam springs would be made of multiple leaves allowing more flexibility for deflection. Using the data collected during the MTS testing of the carbon material, a mathematical model was created to find the optimal combination of leaf spring thickness, width, and length [36].

$$F = \frac{1000 * E * n * W * d * t^3}{4 * \psi * L^3} \quad [16]$$

$$\psi \cong \frac{3}{2 + \frac{n' + 1}{n}} \quad [17]$$

$$\sigma = \frac{6 * F * L}{n * W * t^2} \quad [18]$$

Where:

F = Spring Force at deflection point (N)

L = Spring Length (Distance from anchor point to deflection application in mm)

E = Modulus of Elasticity (GPa)

n = Number of spring leaves

n' = Number of extra full length leaves (Taken as n-1 for all full length), $\psi = 1$

W = Spring Width (mm)

d = deflection of the beam end in the y-direction (mm)

t = Thickness of individual Leaf (mm)

σ = Stress (MPa)

Given these equations, multiple iterations for width, length, thickness, number of leaves, and number of spring sets were considered to find a spring configuration that would fit within the design specifications. It was found that to sustain the deflection necessary without exceeding the bending yield stress of the carbon fiber material that the spring would have to be excessively long, putting the diameter of the device around 100 mm. This might have been acceptable, however, the number of leaves required to achieve the necessary torsional loads caused interference between the components, noticeable in Figure 27 at the corner of the springs near the center. Additionally,

it was found that because the springs did not rotate with the center portion of the design the length of the beam lengthened as rotational deflection increased. This caused a falling rate in the springs that further decreased the force abilities and made the design unsuitable. At this point, the design was abandoned.

4.2.3 VSTA II V3: Torsion Springs, Finite Variability

After great amounts of work with cantilever beam leaf springs, the idea of torsion springs was revisited with the new concept of finite stiffness variability. In the original VSTA I, the single torsion spring had to be very large as it was the only stiffness element in the device. The original stiffness target for that spring was 0.6 Nm/°; however, the maximum stiffness spring that could be made for that configuration was 0.33 Nm/°. The new discrete stiffness concept meant multiple, smaller, torsion springs were possible, increasing feasibility. Additionally, the discrete concept meant that the spring did not have to change location as it did in the VSTA I design, making it easier to mount the springs without the internal deflection issues found in the VSTA I. After initial investigation, it was found that this design would be able to meet all the design requirements and was pursued fully. Specific details of the design are outlined in the next section.

4.3 VSTA II Design Specifications

Design of the multiple torsion spring VSTA II with finite variability began with the torsion spring. Two primary design considerations drove the specifications for the spring. The minimum stiffness of the VSTA II is determined by the stiffness of a single spring, when only one spring in the parallel set is providing resistance for the device. Based on the design and testing of the VSTA I, a maximum single spring stiffness was set at 0.30 Nm/°. The second design consideration for the spring was the placement of the mechanism used to engage and disengage the spring force from the system. Initially, a single electric motor was sought for this task. In this configuration,

the motor would rotate to sequentially lock or unlock the spring from the set. However, placement of a single electric motor would require a central location between all the springs, area that was determined necessary for other components of the VSTA II described later. The ideal location to house an actuator is nested inside the coils of the torsion springs. A low power solenoid was identified as a candidate. Sourcing from Digi-Key (Thief River Falls, MN) identified the DSTL-0216-05 (Delta Electronics, Fremont, CA) (Figure 28) as the smallest solenoid that would be able to nest within the torsion springs. The DSTL-0216-05 solenoid weighs only 9 grams allowing for minimization of mass, even with multiple units. Additionally, the solenoid consumes only 1.1 W at 5.4 volts and can be switched on or off allowing for fast activation of individual springs in the set.

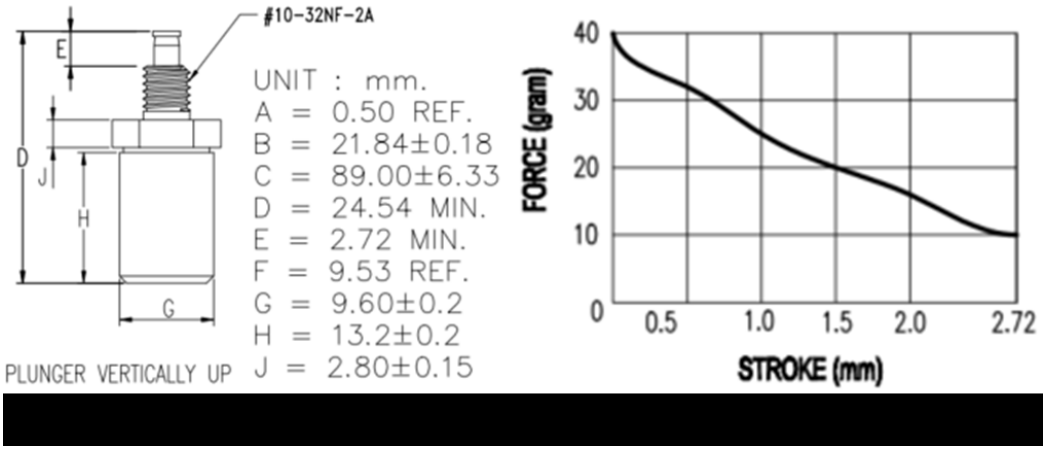

Figure 28: DSTL-0216-05 Solenoid, (a) Physical Dimension (b) Force-Deflection Capabilities

Using the constraints of maximum spring torque, and a minimum inside diameter able to accommodate the solenoid a specific spring was then designed. Gears will be used to activate the set of springs spread radially around a central shaft. This brought up the constraint regarding the functional range of the spring. The VSTA II is specified for a deflection of ±30°, but use of gears allows the motion ratio between the input and the springs to be varied. Previous work with the VSTA I allowed for a starting point in spring design. The main variables of wire diameter (d_w in

mm), mean coil diameter (D_m in mm), number of coils (N), working deflection (θ in degrees), and material (modulus of elasticity, E in MPa) were the inputs for the spring force and stress equations [23]:

$$\text{Spring Rate } (\frac{\text{Nm}}{^\circ}) = \frac{d_w^4 * E}{4000 * N * D_m} \quad [19]$$

$$\text{Spring Stress } \sigma \text{ (MPa)} = \frac{d_w * E * \theta}{392 * N * D_m} \quad [20]$$

Spring stress in a torsion spring must then be corrected to account for shearing stresses due to curvature. The correction factor interpolated from figure 20 in [23] gives the appropriate multiplier (K) needed to determine allowable working stress.

$$\text{Spring Stress Correction Factor } \sigma_c(\text{MPa}) = \sigma * K \quad [21]$$

After making initial calculations, the spring manufacturer used for the VSTA I springs (Diamond Wire Spring (DW), Tyler, TX) was contacted to verify feasibility and availability. When comparing numbers with their calculations it was found that there was a slight difference. The manufacturer was kind enough to share their spring design spreadsheet and it was found that there were slight differences in the constants used in their formulas.

$$\text{DW Spring Rate } (\frac{\text{Nm}}{^\circ}) = \frac{d_w^4 * E}{3888 * N * D_m} \quad [22]$$

$$\text{DW Spring Stress } \sigma \text{ (MPa)} = \frac{19 * d_w * E * \theta}{1994 * \pi * N * D_m} \quad [23]$$

Specifically, the differences in Diamond Wire's formula lead to a slightly higher estimation in spring force output, and a significant increase in the predicted internal stresses. Additionally, Diamond Wire uses the Wahl stress correction factor to adjust for the shear stress when estimating the working stress of the spring.

$$\text{Wahl Corrected Spring Stress } \sigma_c(\text{MPa}) = \sigma\left(\frac{4\left(\frac{D_m}{d_w}\right)-1}{4\left(\frac{D_m}{d_w}\right)-4}+\frac{0.615}{\left(\frac{D_m}{d_w}\right)}\right) \quad [24]$$

Additionally, Diamond Wire suggested designing the spring stress to no more than 75% of the tensile yield strength for the material to guarantee spring durability and longevity. Due to their superior experience in spring design, the altered versions of the spring equations were used for further design refinement. One design flaw of the original VSTA I was its inability to utilize stiffness settings between the stated 0.91 Nm/° max and the infinitely stiff setting. This was due to overestimation of the spring's abilities during the design phase, which these adjustments should correct.

Multiple iterations were made modulating the wire size, mean coil diameter, number of coils, and the motion ratio between limb rotation and the spring rotation via the gears selected to rotate the springs. This was done to produce a minimum range of 0.3-1.0 Nm/° (similar to the VSTA I), and to minimize the VSTA II package size. The final design consisted of the following specifications:

- Wire Size = Ø 4.318 mm (0.170")
- Mean Coil Diameter = 24.638 mm
- Active Coils=3.0
- Motion Ratio = 1:1
- Spring Working Deflection = ±30° * Motion Ratio
- Material = ASTM A228 (Music Wire, E = 207 GPa, Max Design Stress= 1288 MPa)
- Spring Stiffness = 0.25 Nm/°

Using these specifications, the general layout for the interior of the VSTA II began. The next design consideration was to determine the gear specifications. The motion ratio of 1:1 dictated that the central drive gear would be the same size as the driven gear for each spring. The estimated spring stiffness dictated that at least four springs were required to achieve the desired functional range. However, it was previously found that the actual spring output in the VSTA I was lower than the estimated value. To provide a factor of safety on the functional range of the VSTA II five springs will be used. To ensure that the springs would not contact each other, the pitch diameter of the gear needed to be larger than 24.63 mm (Figure 29). Additionally, as detailed later, the alignment of the gears will be critical to the design, and to enable manufacturing of gears that are identical the number of gear teeth must be divisible by the number of springs in the VSTA II.

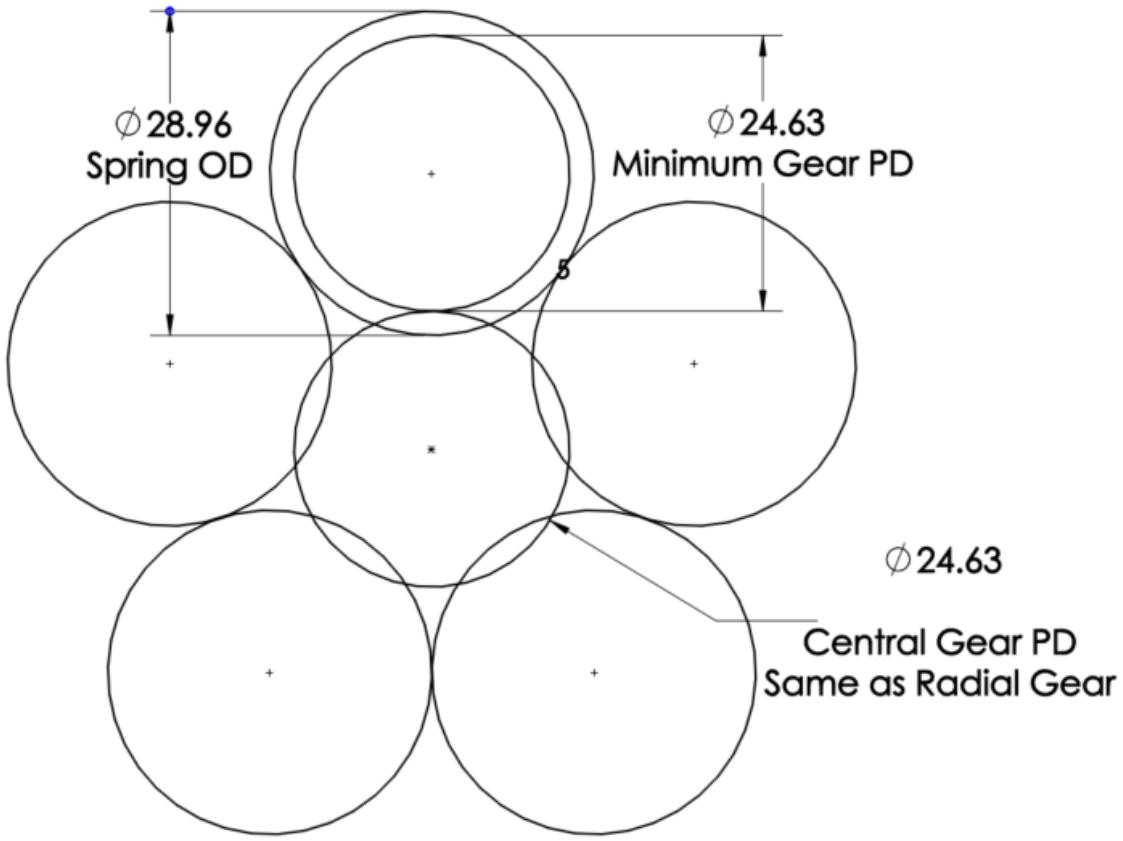

Figure 29: Sketch of spring and gear layout to determine minimum gear pitch diameter (PD)

With the general size and tooth count of the gears established, the diametrical pitch and pressure angle could be designated. The selection of gear parameters was limited by availability. Custom cut titanium gears were initially considered to help reduce mass, however, the high cost of custom gears was deemed unnecessary for the limited weight savings titanium would provide (33-gram reduction for all gears). W.M. Berg (Cudahy, WI) was identified as an appropriate supplier as they had a wide range of gear sizes in various materials available for purchase at a reasonable price. Given the size constraints, a gear with a pitch of 48 and 50 teeth fit best into the design. The gear's load bearing capacity then dictated the face width, pressure angle, and material. For each spring with a rate of 0.25 Nm/°, a maximum deflection of 30°, and a gear pitch diameter of 26.47 mm the gear would have to be capable of 7.5 Nm of torque, or a tangential load of 284 N at the pitch diameter. The Lewis bending strength equation was then used to estimate the gear's capacity [24], [37]:

$$W_t = \frac{S * F * Y}{DP} \quad [25]$$

Where:

W_t = Maximum transmitted tangential load at the pitch diameter (N)

S = Maximum bending tooth stress = 1/3 of the material tensile strength (table C, page 5 of [37])

Y = Lewis Factor (page 3 of [37])

DP = Diametrical Pitch = 48

Using the strongest material offered, 17-4 PH Stainless Steel (tensile strength = 1040 MPa), reduced the availability to a single configuration with a pressure angle of 20° and a face with of

4.7625 mm (3/16”). This worked out to a maximum tangential load capacity of 355 N, giving a safety factor of 1.25 over the expected maximum load of 284 N. This capability was deemed acceptable and the W.M. Berg gear (P48PH28-50) was selected for use in the VSTA II as both the drive and driven gear.

At this point the main components dictating the VSTA II layout were selected and design of the locking mechanism was undertaken. Using these dimensions, a method to hold and activate the spring was then designed. Torsion springs work best when deflected in the direction of winding such that the body contracts. Another shortcoming of the original VSTA I was use of the torsion spring in both directions. Although testing showed that there was no significant difference in the loading profiles between the two directions, the increased stress forced operation of the VSTA I at a lower than desired maximum stiffness. To correct this, a design was needed that could operate in both the clockwise and counterclockwise directions, but that would only deflect the spring in one direction. To achieve this, a double arm mechanism was used that would change the end of spring being deflected based on the direction of operation.

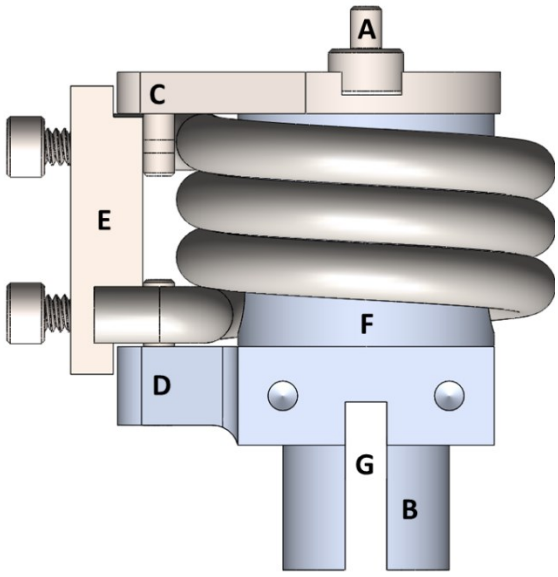

Figure 30: Spring Post Assembly, A) Upper Pilot (Dowel), B) Lower Pilot (Bushing), C) Upper Arm, D) Lower Arm, E) Ground Bar, F) Spring Post Body, G) Lock Bar Slot

The Spring Post assembly (Figure 30) allows for operation of the VSTA II in both directions while only deflecting the spring in the direction of the wind. The upper and lower pilots (Figure 30A and Figure 30B respectively) support the assembly and allow it to rotate freely around the axis of the spring. The two arms (Figure 30C and Figure 30D) are fitted with dowel pins that allow interaction with the spring arms. The Ground Bar (Figure 30E) is anchored to the outer housing via the pictured bolts and provides the spring a reaction point during deflection. The Spring Post Body (Figure 30F)) provides the center support for the spring and is sized to allow enough contraction of the spring without interference. When the assembly is rotated clockwise (as viewed from above) the Upper Arm will tend to rotate into the adjacent arm of the spring, the lower arm of the spring is held firm against the Ground Bar, the Lower Arm moves into open space and the spring is deflected. Similarly, for counterclockwise operation, the Lower Arm will push the lower spring arm and Ground Bar holds the upper spring arm. In this manner, the spring is operated in both directions while only winding it into contraction. With operation addressed, the locking mechanism was tackled.

The premise of the VSTA II is to have five parallel torsion springs that can be engaged or disengaged to increase or decrease the torsional stiffness. Operation of the engage/disengage function is performed by a solenoid and Lock Bar (Figure 31).

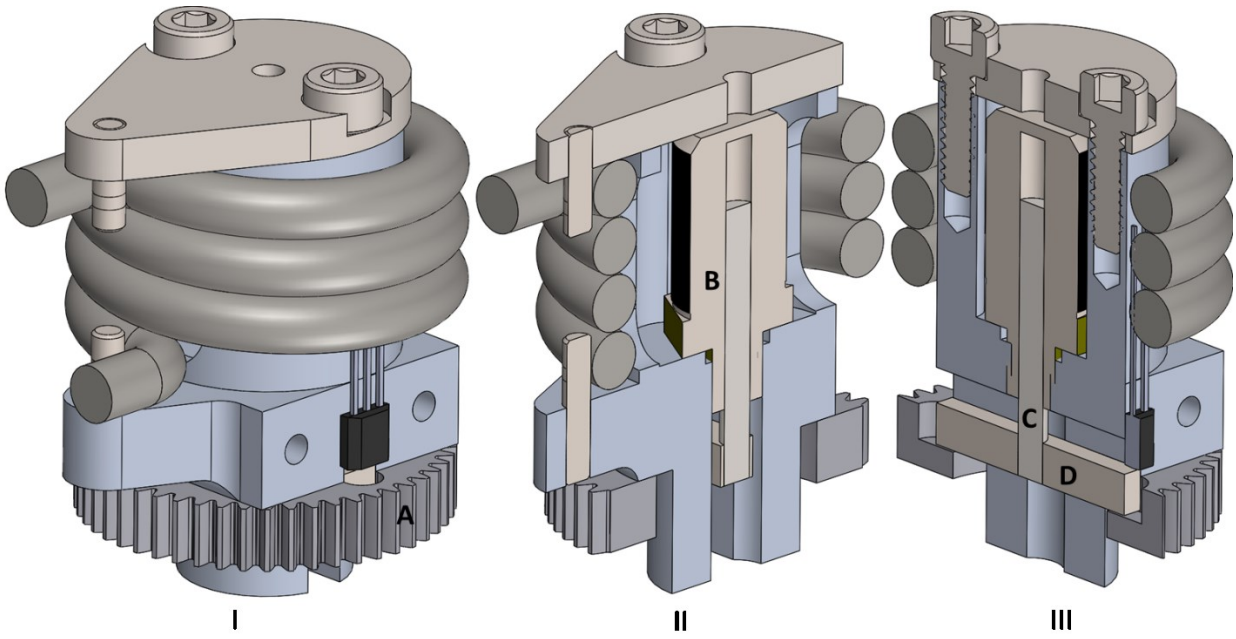

Figure 31: Spring Post Lock Detail I) Full View, II) Lateral Section, III) Frontal Section; A) Driven Gear, B) Solenoid, C) Solenoid Plunger, D) Lock Key

The Driven Gear (Figure 31 I-A) can spin freely around the Lower Pilot and is driven by a Central Gear (shown later) to activate each of the five Spring Posts individually. The Solenoid (Figure 31 II-B) is threaded directly in the aluminum housing of the Spring Post and uses an electric current to generate a magnetic field which is used to draw the Solenoid Plunger (Figure 31 III-C) toward the top of its body. When power is turned off the spring inside the Solenoid (not pictured) along with gravity push the Plunger back downward. Attached to the Plunger is the Lock Key (Figure 31 III-D) that allows the Gear to be locked or unlocked from the Center Post. The Lock Key rides in the Lock Bar Slot on the lower side of the Spring Post and is grounded to the

Lock Bar Slot. The Driven Gear (Figure 32) is a modified version of the stock component procured from W.M. Berg. Its bore has been increased to fit around the Spring Post and a slot has been cut (Figure 32A) to allow engagement to the Spring Post Body (Figure 30F) via the Lock Key.

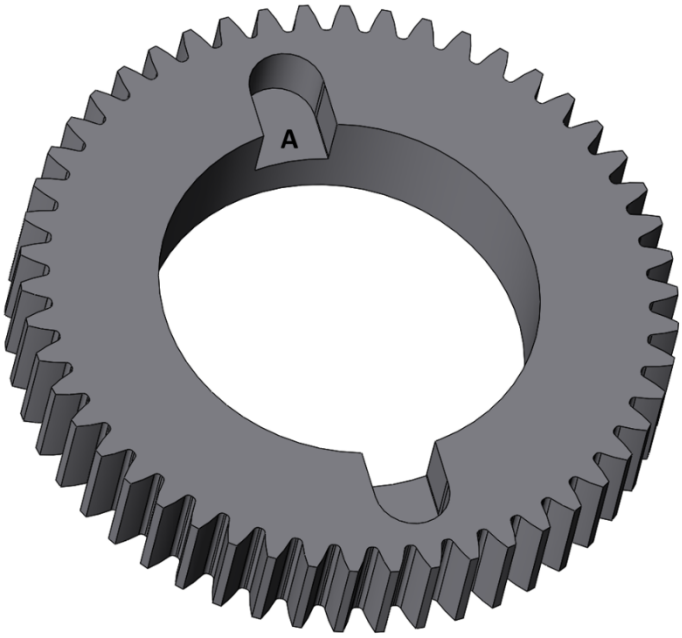

Figure 32: Driven Gear Detail, A) Lock Key Slot

The Solenoid minimum stroke is 2.72 mm with a maximum pulling force of 40 grams. These numbers seem small, however, since locking or unlocking of the spring sets occurs under no load during swing phase there should be little to no resistance during activation. When the VSTA II is under load and a spring set is deactivated the Solenoid will be powered on and attempt to draw the Lock Key out of engagement. When the subject goes into swing phase, the load will be removed and the Lock Key will be able to move. Conversely, if a spring set is activated during the stance phase the Solenoid will be deactivated and the spring force will push the Lock Key against the face of the Driven Gear. When the subject goes into swing phase, the VSTA II will tend back toward its neutral position, aligning the slot in the gear with Lock Key allowing the key to push back into the slot, locking the assembly together again. The unpowered condition of the

VSTA II is with all the spring sets locked. This was done as a safety precaution in the event of a power loss, allowing for the stiffest VSTA II setting.

With the primary functional designs completed, the final components could be finished. The surrounding elements consisted of the housings, central shaft, and surrounding support systems (Figure 33).

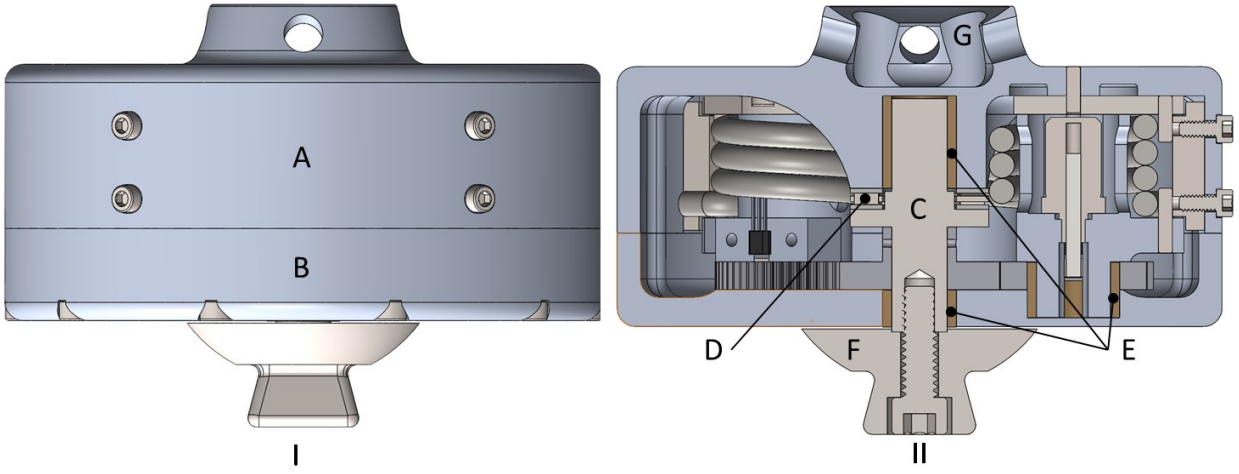

Figure 33: VSTA II I) Exterior, II) Cross-Section; A) Upper Housing, B) Lower Housing, C) Center Shaft, D) Main Thrust Bearing, E) Support Bushings, E) Male Pyramid Adapter, F) Female Pyramid Adapter

The Upper Housing (Figure 33 I-A) and Lower Housing (Figure 33 I-B) are bolted together and provide the support for the internal components. The Center Shaft (Figure 33 II-C) runs axially between the housings and is able to support the loads of walking via the Main Thrust Bearing (Figure 33 II-D). The thrust bearing is designed for walking loads of a 130 kg person as previously described in the design specifications. When walking, compression loads (ground reaction force during single support) are generally around 1.2 times body weight, 1.6 times body weight when walking downhill, and 3 times body weight when running [38], [39]. To accommodate for this, the main thrust bearing must be able to accommodate 390 kg (3 x 130 kg). Because this will be the main mode of loading for the VSTA II it was decided to give the greatest capacity possible. The

maximum bearing capacity that was capable of fitting in the design space is capable of 871 kg, 6.7 times body weight. This should be sufficient to support the loads during testing, plus any unforseen compressive loading. To support the rotation of the Center Shaft, Spring Post, and Gears, bronze Support Bushings are included (Figure 33E). These Support Bushings serve to enable rotation by reducing friction between components while supporting radial loads. The loading case for the Support Bushings is when the VSTA II is in bending or side load, which will be discussed more in the next section. Finally, standard style pyramid adapters were integrated to allow attachment into the pylon of a lower limb prosthesis. A standard pyramid adapter uses a four bolt pattern with spacing of 36 mm. Unfortunately, the configuration of the five Spring Post assemblies and their connection into the housings prevented to inclusion of bolt holes that could accommodate the standard bolt pattern without adding additional material height. Addtionally, the standard pyramid adapters' attachment flanges can add as much as 10 mm of height, contrary to the design goal of minimizing the integrated height of the VSTA II. Due to these two conflicts it was decided to customize the adapters to better integrate with the VSTA II. The Male Pyramid Adapter (Figure 33 II-F) is bolted directly to the Center Shaft, and has a small clearance below the Lower Housing to allow for free rotation. The Center Shaft and the Male Pyramid adapter are keyed together to allow for a secure connection without relative rotation (Figure 34). The Female Pyramid Adapter (Figure 33 II-G) is integrated directly into the Upper Housing. This eliminated a significant amount of build height and the construction of the adapter from aluminum, as opposed to the steel or titanium standard adapters, further reduces the overall mass of the VSTA II.

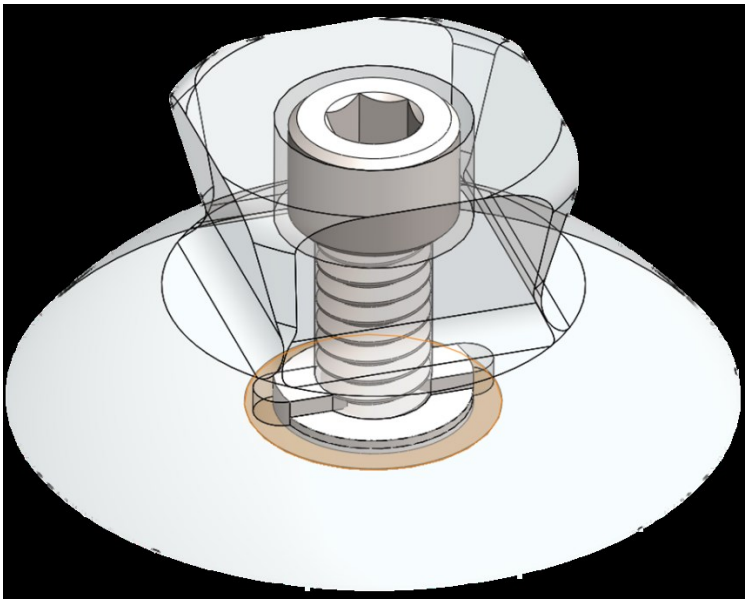

Figure 34: Detail of key feature locking the Male Pyramid Adapter to the Center Shaft

Final design elements for the VSTA II were to include the ability to sense the position of individual locks as well as the displacement of springs. During normal operation there will be no way to visualize if an individual lock key is engaged or disengaged. Simply powering a solenoid on or off does not guarantee the state of an individual lock. To help determine the actual condition of the VSTA II during operation, each Spring Post is equipped with a Hall effect sensor to determine the location of the key (Figure 35).

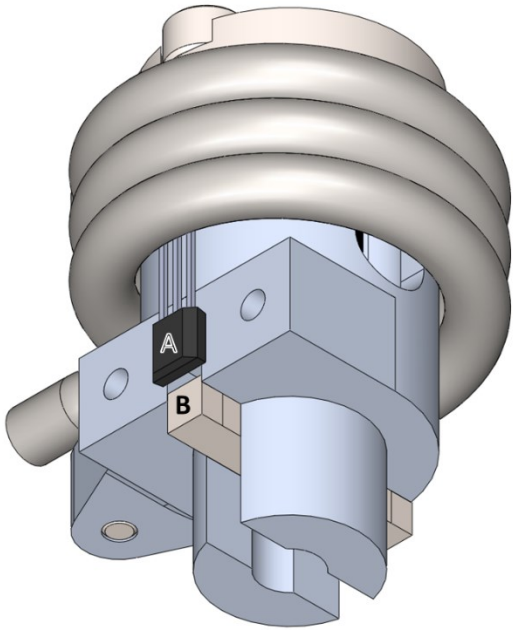

Figure 35: Lock Key position Hall effect sensor detail, A) Sensor, B) Lock Key

The Hall effect sensor (Figure 35 A) chosen is a HAL 835 (Micronas, Zurick, Switzerland) is able to detect the presence of a manetic field. The Lock Key (Figure 35 B) is ferrous and a small magnetic field will be imparted to the end via electrostatic induction. As the Lock Key moves into the disengaged postion (up) it moves closer to Hall effect sensor which will be registered resulting in a change to the sensor output voltage. The output will then be linked to a controller (discussed later) and the position of an individual key can be known. A position sensor is also included to determine the position of the springs at any given time (Figure 36).

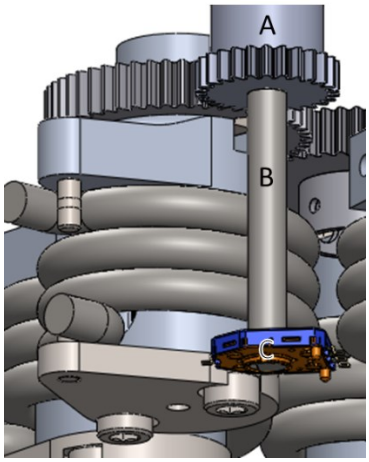

Figure 36: Position sensor detail, A) Sensor Gear, B) Layshaft, C) Position Sensor

Displacement sensing is performed with three components. A small gear (Figure 36A) is meshed with one of the Spring Post gears. Because all the gears move together whether they are engaged or not, the state of locking will not affect the sensing ability. The gear transmits rotation via a Layshaft (Figure 36B) down to the SV01A103AEA01B00 rotary variable resistance-based position sensor (Figure 36C) (muRata, Kyoto, Japan). The ratio of VSTA II movement to sensor displacement will be determined by the gear ratio between the Spring Post gear and the Sensor Gear, which can then be read and interpretted by the controller. At this point in the design, the components were at a stage of rough completion. Finite element analysis was used to refine the geomtry of each part based on their expected loading condition.

4.4 Finite Element Simulations

A finite element model (SolidWorks) was utilized to investigate the loading conditions expected on the VSTA II. Given the reliability of the materials used for construction and the predetermined conditions for maximum loading, a factor of safety of at least two is ideal; however, in order to meet weight and functionality goals a factor of 1.25-1.5 is acceptable [24]. Simulations were first run on the Spring Post assembly to test the ability of the parts when reacting to the spring loads at full deflection. For all tests regarding the spring load an input moment of 8 Nm was used.

This was determined from the expected spring rate of 0.25 Nm/° at 30° of deflection (7.5 Nm) and gave an extra cushion to account for variations that might manifest in the physical setup. Simulation of the main Spring Post body were performed by applying load to the Lower Arm at the dowel pin while holding the Lock Key reaction faces fixed. Sliding constraints were applied to the lower cylindrical surface as the support bushing, as well as the face where Upper Arm attaches (Figure 37). Initially, the factor of safety was calculated around 0.9, which led to thickening of the arm, bringing the final simulation to a factor of 1.7. Aluminum 6061 is used for the Spring Post Body, and while adjusting the material to steel (+29 grams each) or titanium (+10 grams each) would greatly increase the load capability, the weight increase was deemed significant. Changes to help remove material, to better utilize a material like titanium, were not significant enough to offset the weight gains. This was due to geometry being constrained by the interaction between the mating components, and as such further modifications to the shape would require changes to the primary design components. Considering these aspects, the 1.7 factor of safety was acceptable. Simulation of the Spring Post body also included holding the top face of the Spring Post Body fixed and applying the 8 Nm load to the Lock Key faces (Figure 38). This investigated the scenario of the load applied to the opposite side of the spring at the Upper Force Arm. This similarly resulted in a factor of safety of 1.8, also deemed acceptable.

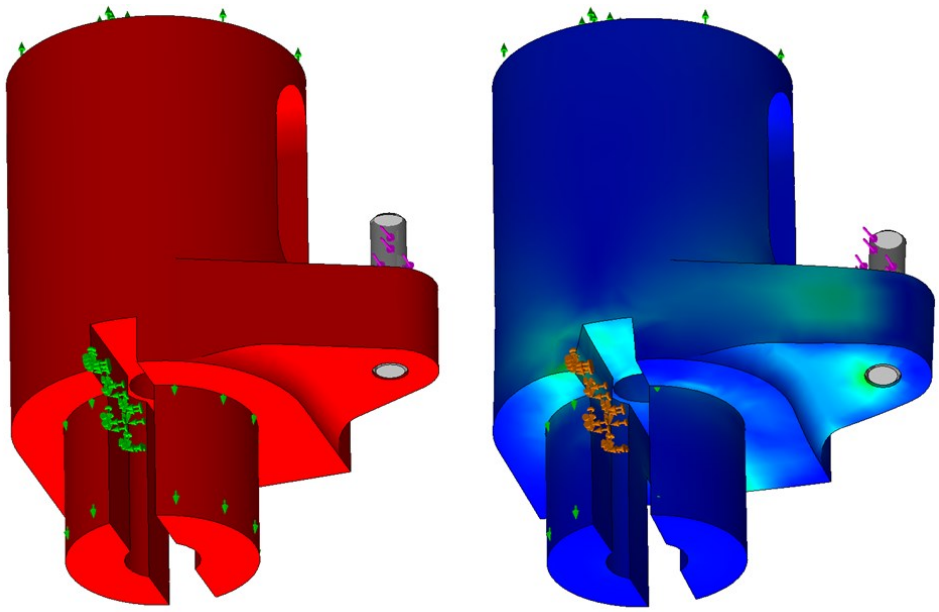

Figure 37: Simulation of Spring Post body loaded at Lower Arm resulting in a factor of safety = 1.7. Factor of Safety Distribution (Left), von Mises Stress Distribution with deformation (Right)

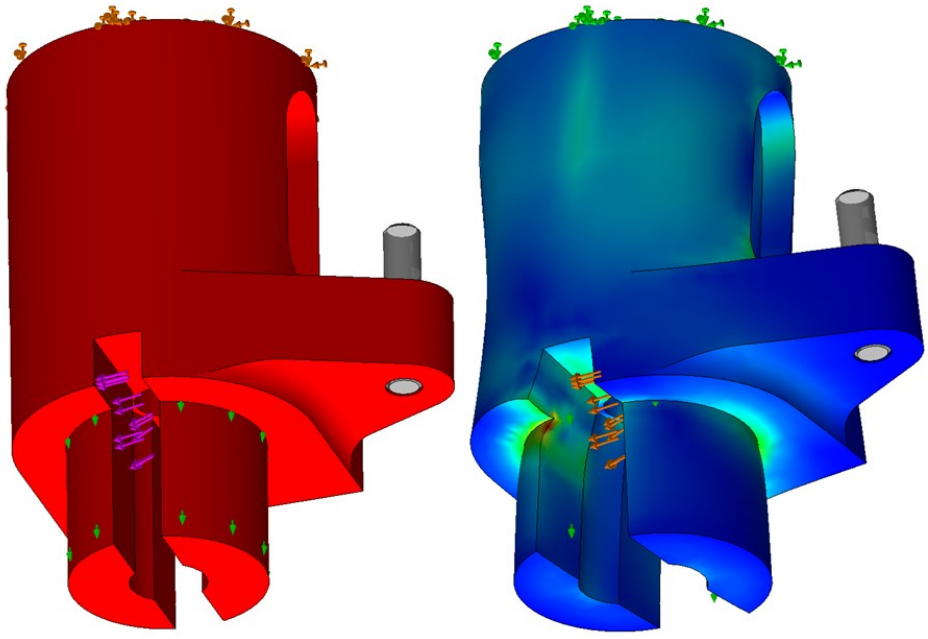

Figure 38: Simulation of Spring Post Body loaded at Upper Arm resulting in a factor of safety = 1.8. Factor of Safety Distribution (Left), von Mises Stress Distribution with deformation (Right)

The Upper Arm is a separate component that bolts to the Spring Post Body to allow for ease of machining and assembly of the components. The Upper Arm needed to be as thin as possible as the height of the Spring Post assembly dictates the overall height for the VSTA II. To

attain the thin form with sufficient strength, and low mass the material was chosen as Grade 5 titanium. Simulation was completed similarly to the Spring Post Body with an 8 Nm load applied to the dowel pin and the bolt attachment faces fixed (Figure 39). Simulation resulted in a factor of safety of 2.7, beyond ideal and accepted.

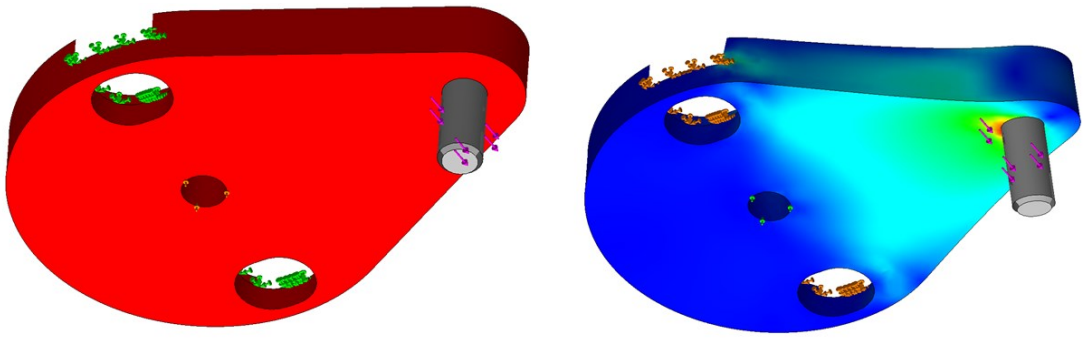

Figure 39: Simulation of Lower Arm loaded at the dowel pin resulting in a factor of safety = 2.7. Factor of Safety Distribution (Left), von Mises Stress Distribution with deformation (Right)

The VSTA II locking mechanism was next for simulation, starting with the Lock Bar (Figure 40). The Lock Bar was similarly loaded with an 8 Nm moment at the faces that contacted the gear, while being held fixed at the faces that contact the Spring Post Body, resulting in a factor of safety of 5.3.

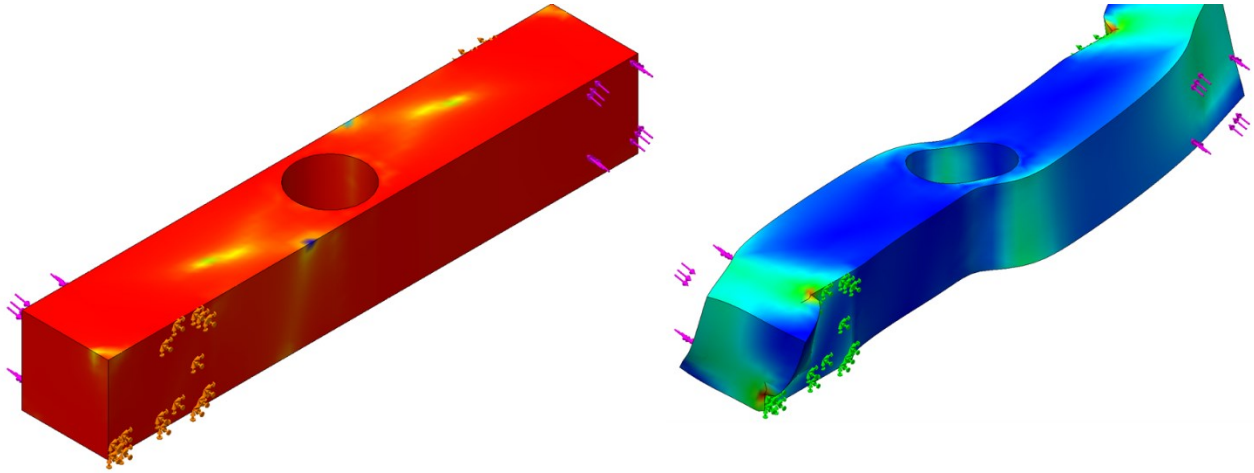

Figure 40: Simulation of the Lock Bar resulting in a factor of safety = 5.3. Factor of Safety Distribution (Left), von Mises Stress Distribution with deformation (Right)

Reacting against the lock bar is the Driven Gear (Figure 41). Simulations were performed by applying the 8 Nm moment to the faces in contact with the Lock Bar and fixing the outside diameter. Because the strength of the gear teeth was already evaluated by equation [25] the gear teeth were removed for this simulation to isolate the body of the gear. Simulation resulted in a factor of safety of 1.7, like previous components. To increase the strength of the gear body and lock face, the engagement of the Lock Key would have to be increased which would require more stroke from the solenoid. Increasing the capability of the solenoid increased its size significantly such that it would not be able to fit within the Spring Post Body. Due to these factors, the Driven Gear design was accepted with the 1.7 factor. Investigation of the Lock Bar with the Spring Post Body was performed earlier when simulating the Lower Arm and so simulations regarding the Spring Post Assembly were concluded.

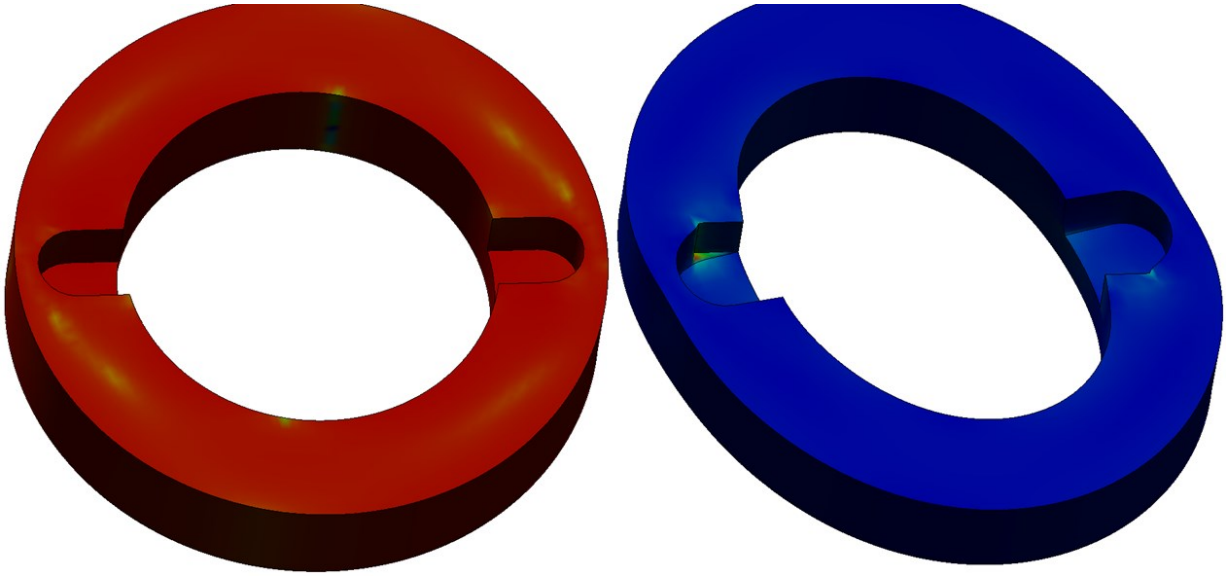

Figure 41: Simulation of the Driven Gear lock face resulting in a factor of safety = 1.7. Factor of Safety Distribution (Left), von Mises Stress Distribution with deformation (Right)

The main load bearing member of the VSTA II, the Center Shaft, was simulated next. Forces on the Center Shaft are derived from the design specifications. Specifically, compressive strength for a 130-kg individual, torsional loading up to 65 Nm, and bending up to 163 Nm. To save weight while maintain high strength, the Center Shaft was specified as Grade 5 titanium. Compressive simulations were performed first by fixing the face interacting with the thrust bearing and applying load to the top of the shaft where the Male Pyramid Adapter attaches (Figure 42). This resulted in a factor of safety of 33 which makes it suitable for loading far exceeding three times body weight as previously discussed.

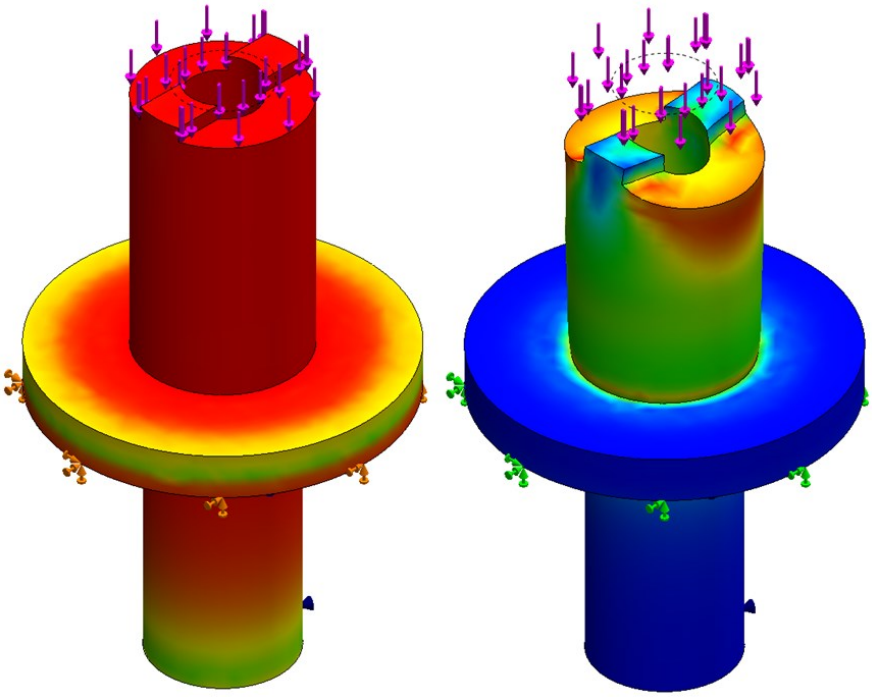

Figure 42: Simulation of the Center Shaft in compression resulting in a factor of safety = 33. Factor of Safety Distribution (Left), von Mises Stress Distribution with deformation (Right)

Torsion of the shaft is specified up to 65 Nm. This was simulated by fixing the shaft where pyramid adapter attaches and applying the moment to the face where the Center Gear will be pressed onto the shaft (Figure 43). The factor of safety is estimated at 2.6, passing the design guidelines.

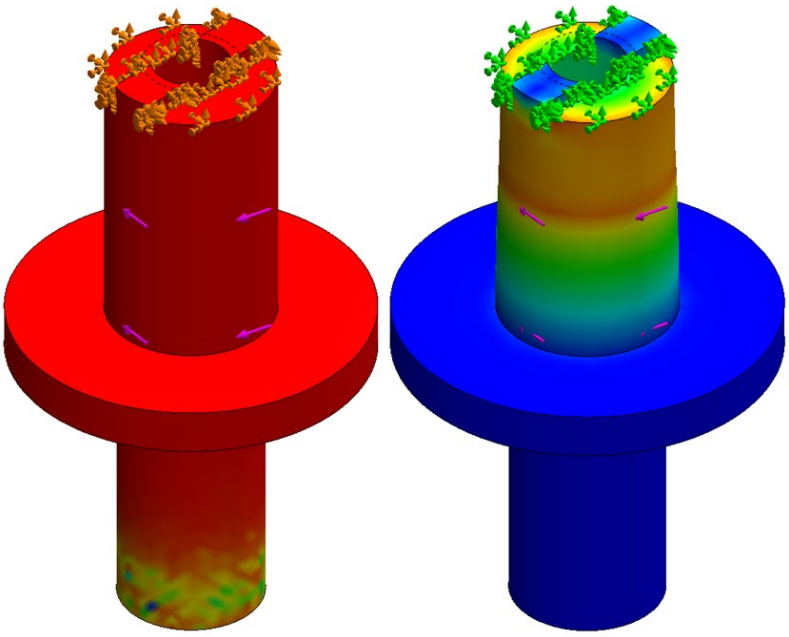

Figure 43: Simulation of the Center Shaft in torsion resulting in a factor of safety = 2.6. Factor of Safety Distribution (Left), von Mises Stress Distribution with deformation (Right)

The design specification for the 163 Nm bending load comes from an indirect source. As discussed previously in chapter 2 it is estimated that the greatest bending load will occur when a person wearing the VSTA II kneels as demonstrated (Figure 44, same as Figure 5).

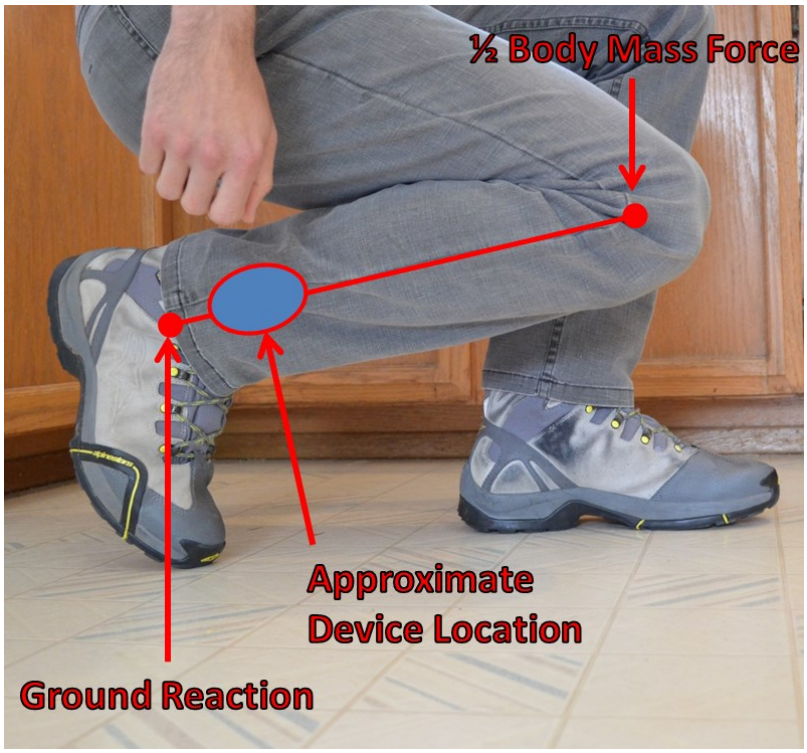

Figure 44: Demonstration of lower limb creating a large bending load on the VSTA II while kneeling.

Using the 130 kg mass to determine the applied body load (65 kg) and a lever arm of 253 mm from a 50th percentile male [20] the 163 Nm bending load is generated. A simulation of the VSTA II in bending was constructed using the Upper and Lower Housings along with the Center Shaft as these are the three components that make up the main structure of the device (Figure 45). Additionally, the center Drive Gear was added because it effectively adds stiffness to the lower section of the Center shaft once the two are press fit together. The simulation was constructed by mating the housings and shaft together with bearing mates, and the gear to the shaft with a bonded mate. The end of the shaft where the pyramid adapter attaches was held fixed and a remote load of 65 kg at 253 mm applied. This resulted in a factor of safety of 0.30, far less than ideal. The diameter of the lower section of the Center Shaft was increased and the safety factor was increased to 0.68, still short of acceptable. The failure point being predicted at the shaft and gear near the interface with the Lower Housing. Further increasing the shaft diameter might help marginally,

however further modifications to the Drive gear would completely remove its collar and reduce its ability to press fit securely on the center shaft. The design specification was revisited to determine if it was appropriate and necessary to meet this requirement. It was determined that this scenario could not be properly simulated without further testing to properly define the loading conditions. It is theorized that during this maneuver, the half body load condition is not accurate. Much of the body load may be borne by the planted foot, instead of an even split between the limbs. Additionally, at the completion of the kneeling maneuver it is believed that the seat of the individual will contact the heel of the foot directly transferring load, and bypassing the bending scenario. Because this scenario will not be part of the testing planned for the VSTA II, it was deemed excessive and no further design changes were implemented to increase the bending strength.

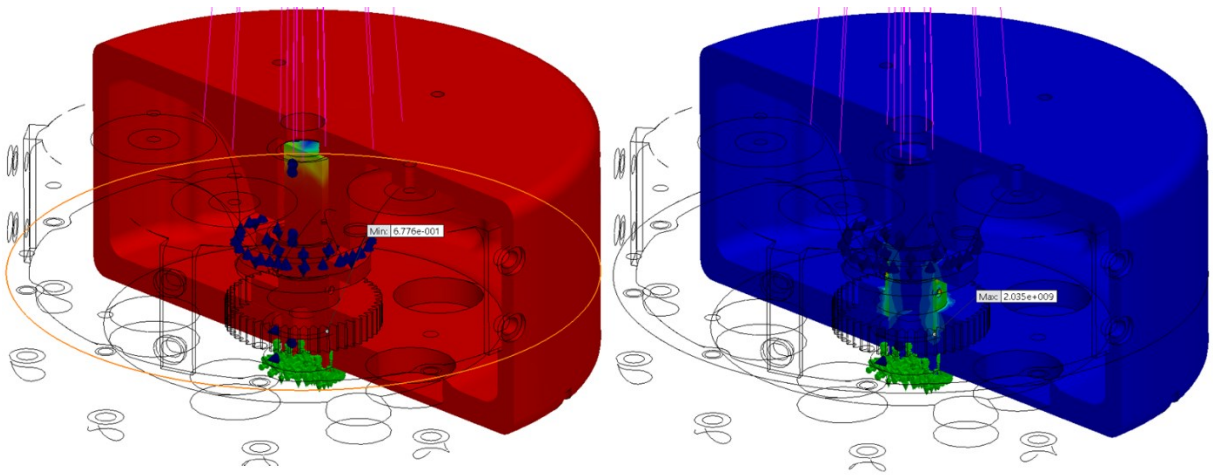

Figure 45: Simulation of VSTA II in bending resulting in a factor of safety = 0.68. Factor of Safety Distribution (Left), von Mises Stress Distribution with deformation (Right)

The resolution of the bending simulation marked the end of the simulation phase of the design. While the design is considered complete at this point, there are still some issues that may present themselves when the physical parts are assembled, they are discussed in the next section. At this point the design was complete enough to begin the process of quoting and manufacturing.

4.5 Design Summary and Possible Issues

This section will provide a summary of the design of the VSTA II and outline initial concerns that were identified as possible failure modes. The VSTA II is a variable stiffness torsion adapter that allows for variable passive spring resistance. It is an improvement over the previous design, and the physical and functional attributes can be compared in Figure 46 and

Table *11*. The VSTA II has a considerable weight and height reduction as compared to the VSTA I, while increasing the functional range.

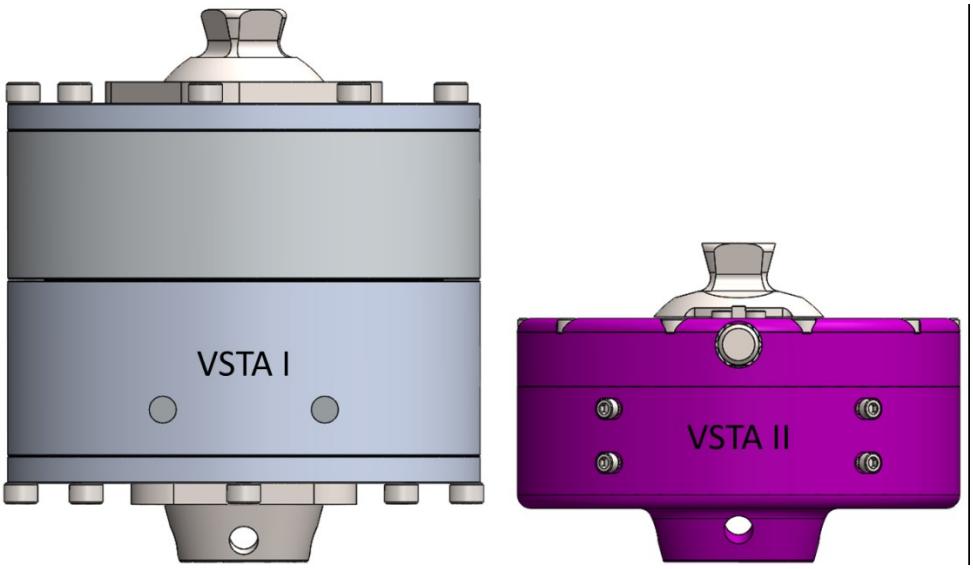

Figure 46: Pictorial comparison of the VSTA I and the VSTA II

Table 11: Comparison of VSTA I vs. VSTA II physical and functional attributes. VSTA II features a 0.92 kg reduction in mass (51%), and a 55-mm reduction in height (42%).

Device	Motion Range	Stiffness Range	Mass (with adapters, no controller)	Size (with adapters)
VSTA I	±30°	0.12-0.91 Nm/° Locked Condition Available	1.8 kg (Actual)	Ø 111 mm x 130 mm
VSTA II (As Designed)	±30°	0.25-1.25 Nm/° Locked Condition Available	0.876 kg	Ø 104 mm x 75 mm

The main concern for the VSTA II is the ability for the solenoids to quickly and accurately lock and unlock the gears. The main obstacles being alignment of the Lock Key with the Driven Gear, and the fit between Lock Key, Spring Post Body, and Driven Gear providing smooth movement without binding and with minimal backlash. To account for any alignment issues, three precautions were taken. First, as previously discussed the gears were chosen with a tooth count divisible by five. This means that each gear can be the same for manufacturing and will not require individualized alignment between the slot and the teeth. The slot must only be oriented the same for each gear during manufacturing which can be done with a properly constructed jig. Second,

alignment of the Lock Key with the Driven Gear slot must correspond to the neutral no load condition from the spring. Variability in the manufacturing of the spring, the slots in the Spring Post, or Driven Gear could cause misalignment in the VSTA II. To accommodate for this, the attachment of the Ground Bar to the Upper Housing uses slotted holes that allow for adjustments of the angle of the Lock Key slots between the Spring Post and Driven Gear up to ±1.7°. Lastly, to reduce backlash, it is ideal to align the two arms in contact with the spring arms so that load is applied immediately when the Spring Post is deflected. Adjustments are allowed via the slotted holes in the Lower Arm that allow up to 5° of rotation between the opposing arm alignments allowing up to 1.4 mm of tolerance in the spacing of the two spring arms.

The fit of the Lock Key is also vital. If the Spring Post or Driven Gear slots are too tight, the key will drag and the solenoid will not be able to move the key or it will bind or chatter. If the slots are too loose, then extra backlash will be introduced to the system and there will be a dead zone of no resistance around neutral displacement. This is a concern that will be investigated using initial test parts that will be discussed later. Initial parts will be constructed on the tighter side of the tolerance zones and then the fits evaluated, and adjusted manually. When initial testing is complete, the full run of manufacturing will be adjusted accordingly.

5 VSTA II Mechanical Testing

Prior to testing the VSTA II on human subjects it will be run through mechanical bench testing. Mechanical bench testing will provide the actual functioning capabilities of the VSTA II while verifying the design and qualifying it for use with human subjects. Mechanical testing will determine the actual stiffness settings available with the VSTA II, the linearity of the stiffness response, and the ability of the VSTA II to vary its stiffness.

5.1 VSTA II Test Unit

To avoid design errors like the internal deflections found in the VSTA I, a VSTA II Test Unit (Figure 47) was devised to allow bench testing of a single functional unit before the full prototype was manufactured.

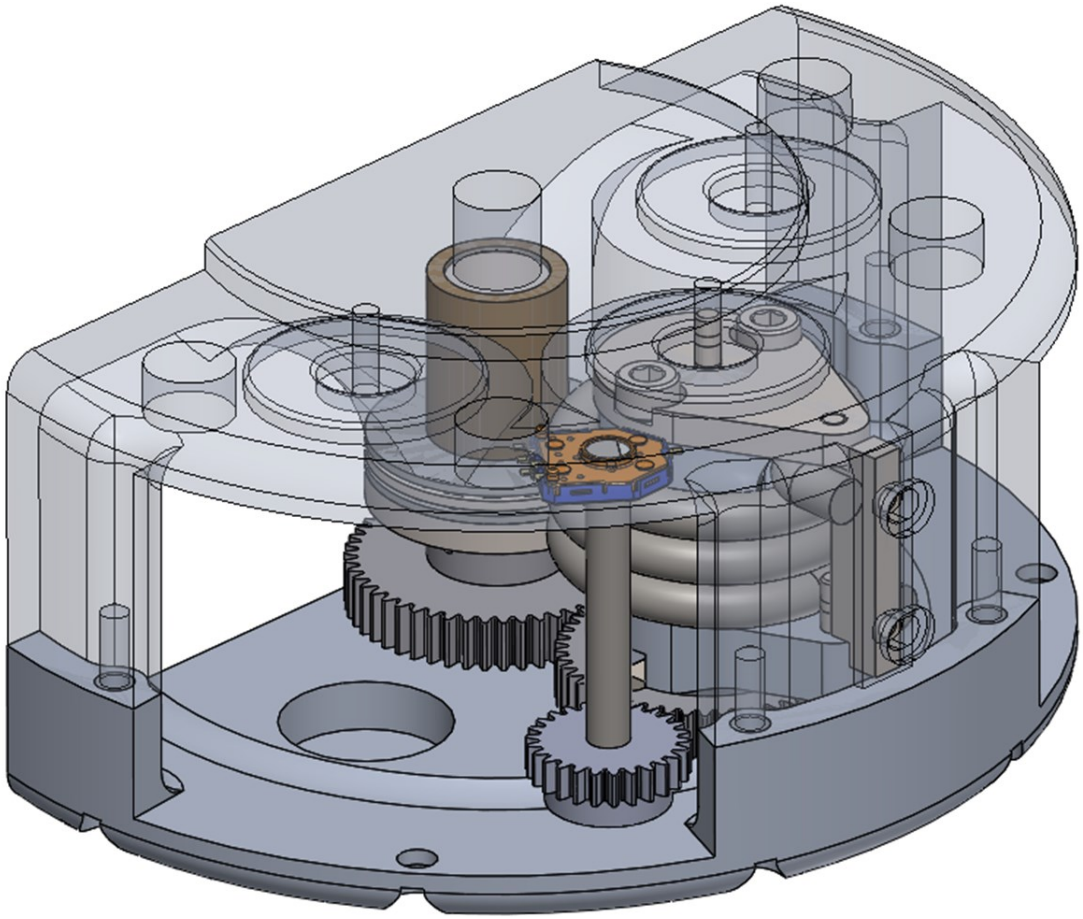

Figure 47: VSTA II Test Unit Assembly

The VSTA II Test Unit features modified housings for easy integration onto a servo-hydraulic test machine. It can test all components featured in the full VSTA II, but with only a single functional unit. The use of a single functional unit allowed for the testing of the actual spring rate achievable for the unit, testing of the solenoid locking mechanism, and evaluation of the component strengths in relation to their simulated performance. In addition to mechanical

testing the VSTA II Test Unit allowed for desktop development of an onboard controller. The VSTA II also included all types of the sensors previously detailed along with a single solenoid.

5.2 VSTA II Test Unit Mechanical Testing

Mechanical testing on the VSTA II Test Unit followed a similar path to the original VSTA I. Bench testing of the VSTA II Test Unit consisted of evaluation on the MTS (Figure 48). The torque-deflection response of the device was measured through its operating range of ±30° for the single unit stiffness. Testing was performed at both 0.5 °/s and 60 °/s to evaluate any effects of speed similar to previous testing, all repeated for three trials each [14], [17].

Figure 48: VSTA II Test Unit on MTS

Ideally, the design should produce a linear torque-displacement curve relating to a constant spring rate, with no dependency on loading rate or direction. However, initial tests indicated that the actual spring rate was almost double the intended design with some dependence on rate, but relatively unaffected by deflection direction. The original design estimated a single spring unit

would produce a 250 Nmm/deg VSTA II rate. Test results showing (Figure 49) indicate that the measured rate was approximately 580 Nmm/deg for 60 deg/s deflection and 470 Nmm/deg for 0.5 deg/s deflection.

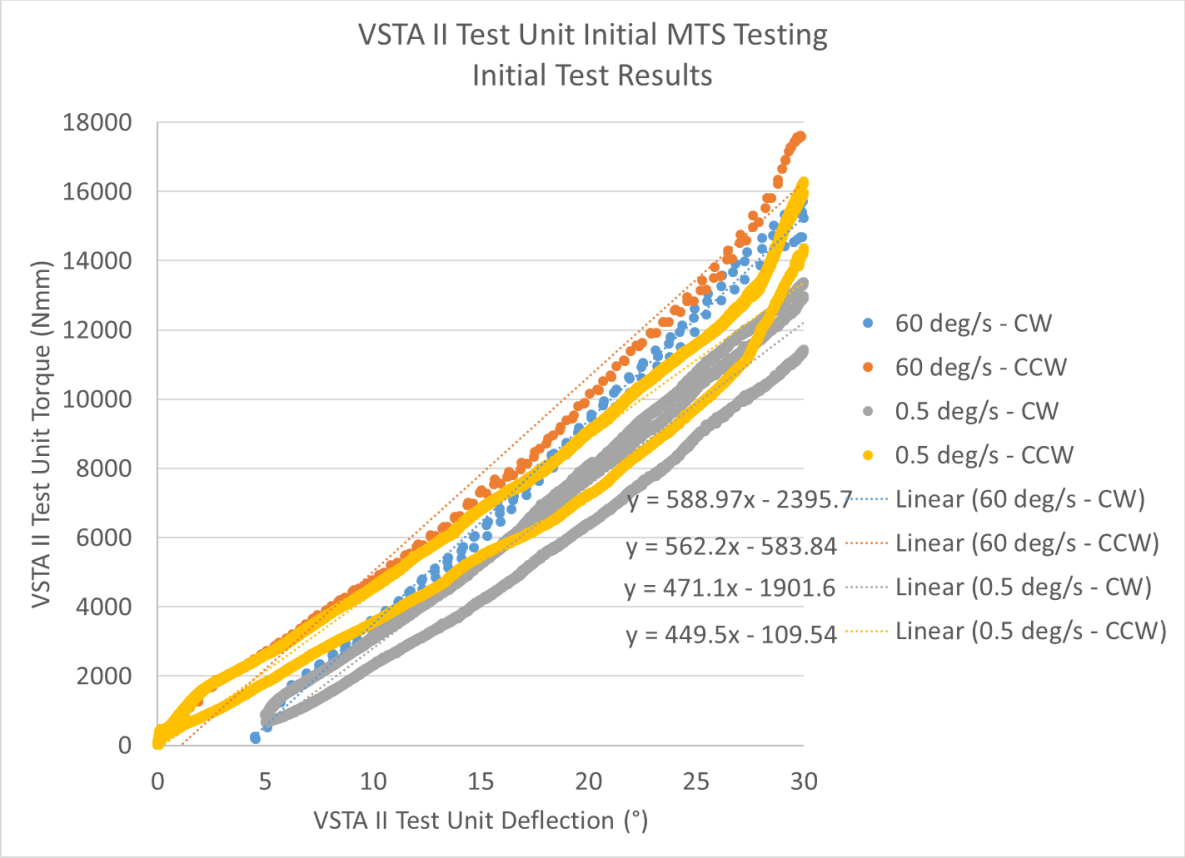

Figure 49: VSTA II Test Unit initial torque-deflection results. Data is the combination of three trials for an individual spring in the VSTA II Test Unit deflected at 60 deg/s and 0.5 deg/s in the clockwise and counterclockwise directions.

Initially, the root of the discrepancy in the design and the actual performance was difficult to determine. After consultation with the spring manufacturer it was determined that the diameter of the Spring Post mandrel that supports the torsion spring was too large. The manufacturer recommended that the mandrel size not exceed 90% of the ID of the spring at maximum deflection. At full 30° of deflection the spring is expected to reduce from its resting ID of 22.5 mm down to 19.77 mm. This new specification would result in a maximum mandrel diameter of 17.79 mm. The

design of the VSTA II Test Unit featured a Spring Post mandrel diameter of 19.56 mm. To verify the new design one of the VSTA II Test Unit Spring Posts was reduced in diameter by 0.75 mm, down to 18.81 mm. Due to limitations of the design at that stage more material removal would have resulted in loss of function. The unit was then retested with the modified Spring Post (Figure 50).

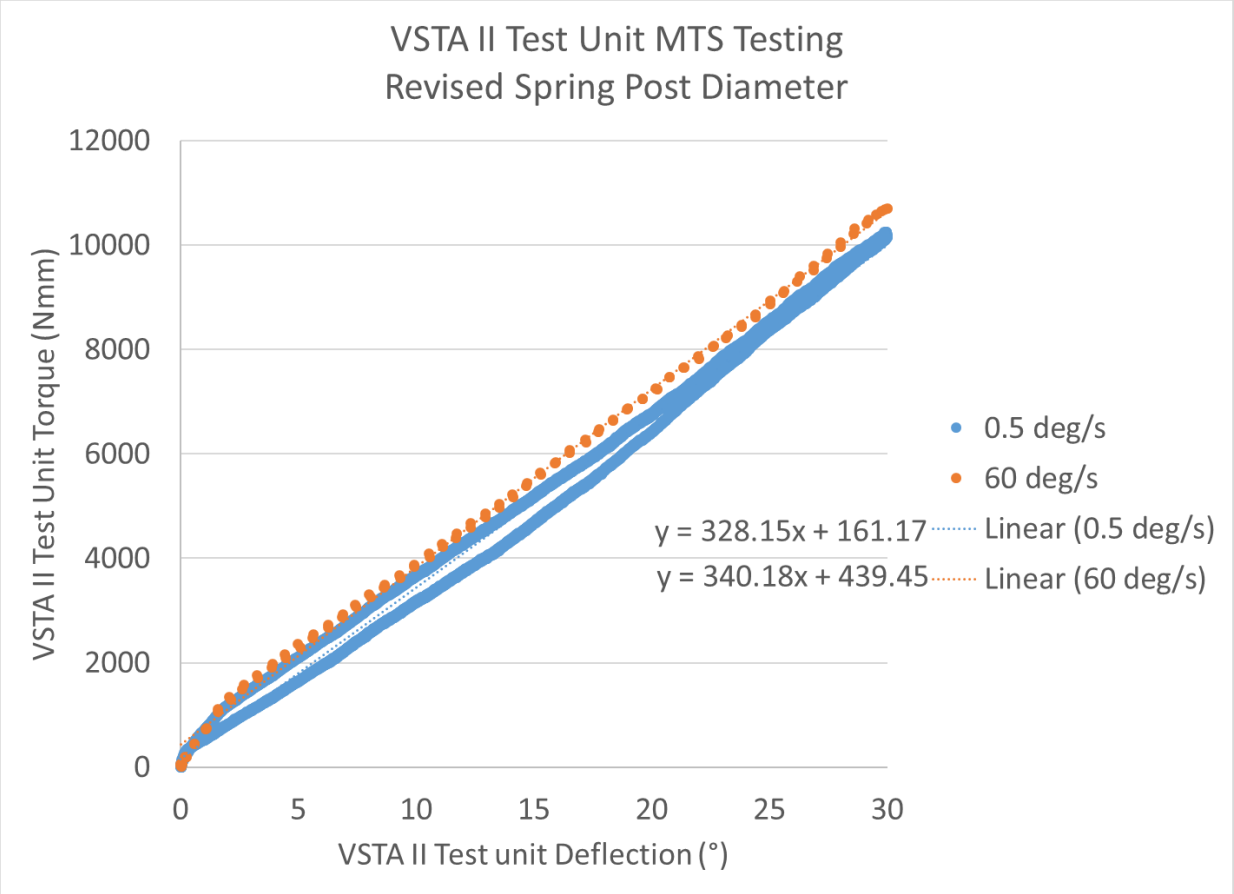

Figure 50: VSTA II Test Unit torque-deflection testing with reduced Spring Post mandrel diameter.

The results showed that just the small amount of diameter reduction had a significant effect on the torque-deflection response of the system. The new system had a spring rate of approximately 335 Nmm/deg. While this was still well above the 250 Nmm/deg estimated value, it was expected that further reduction of the Spring Post's diameter could resolve the difference.

Testing of the VSTA II Test Unit next focused on the function of the locking mechanisms. During the design phase of the VSTA II there was concern that the locking mechanism would not allow for fast and reliable activation of the solenoids. This was a result of the tight tolerances required for the locking system to function properly. Testing of the locking mechanism's performance to both lock and unlock was performed using motion that would simulate the VSTA II being activated during the swing phase of gait, while the VSTA II is unloaded and passing through the neutral point. This was accomplished by moving the VSTA II Test Unit from +30° to -30° deflection at both 0.5 deg/s and 60 deg/s to determine if the gear can be engaged and disengaged dynamically. It was found that the VSTA II Test Unit had no issues engaging the lock mechanism in either scenario.

5.3 VSTA II Test Unit Design Updates

Using the lessons learned from the assembly and testing of the Test Unit critical revisions were made to the final VSTA II prototype design. Most notably for the function of the VSTA II the diameter of the Spring Post mandrel was reduced within the new design constraint. Additional revisions included changes to the tolerances and fits between the internal moving components. It was found that not enough space was reserved in the vertical stack of the Spring Post assembly between the two housings causing the gear to bind. It was also found that no pilot features had been provided between the Force Arm to the Spring Post making axial alignment difficult during assembly. Lastly, the design of the lock mechanism sensor was revised. It is desirable to verify the location of the lock mechanism to indicate the stiffness of the VSTA II during normal operation. Originally, this design called for a small magnet on the end of the lock mechanism that could be read by a Hall Effect sensor. Testing of this system on the VSTA II Test Unit revealed that the addition of the magnet created an attractive force between the lock mechanism and the gear that

the solenoid could not overcome, resulting in the locking system being incapable of disengaging. To remedy the issue, the system was revised to include a circuit that relies on the contact between lock mechanism and a small wire to complete a circuit and indicate location. The new system was prototyped on the VSTA II Test Unit and deemed to work appropriately. Lastly, a locking mechanism was added to the VSTA II to allow a fully locked setting, also controlled by a solenoid. This was accomplished by adding a lock key similar those for the individual gears between the male pyramid adapter and the lower housing that allows the adapter to be locked to the housing. The final, as manufactured, VSTA II is shown in Figure 51.

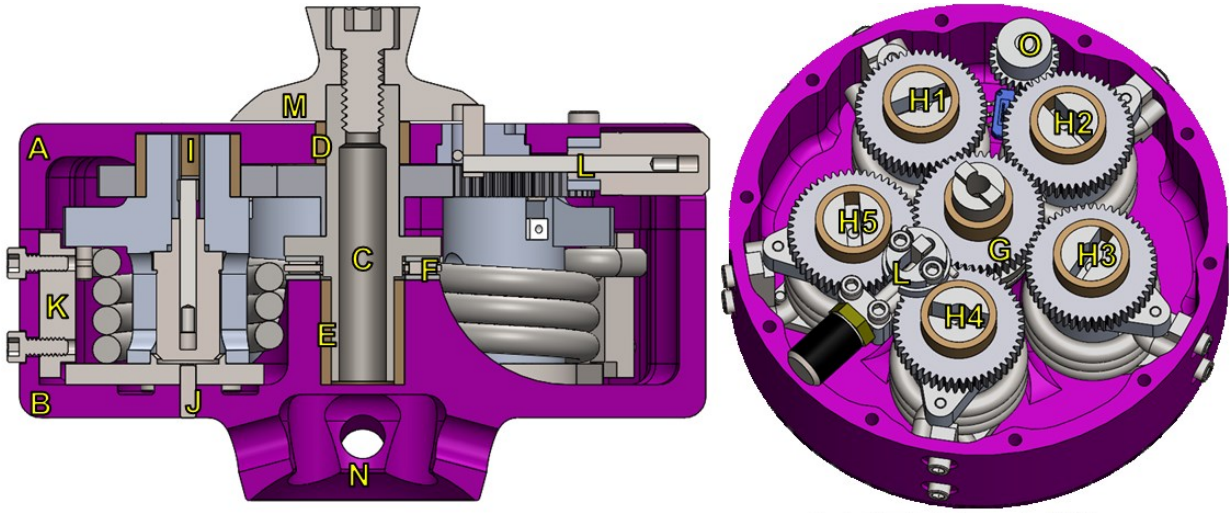

Figure 51: VSTA II Overview: A – upper housing, B – lower housing, C – center shaft, D – upper shaft support bushing, E – lower shaft support bushing, F – shaft needle roller thrust bearing, G – center gear, H 1-5 – five subunits, I – subunit upper support bushing, J – subunit lower support pin, K – ground bar, L – locking mechanism, M – male pyramid adapter, N – female pyramid adapter, O – rotational position sensor.

While producing and testing the Test Unit resulted in an extra project step, it was found valuable. Without the initial testing on the VSTA II Test Unit, critical design errors would have been part of the final VSTA II assembly, compromising its function and success.

5.4 VSTA II Full Prototype Bench Testing

Mechanical bench testing was performed on the VSTA II to determine its functional characteristics as built. Testing was performed using a servo-hydraulic material testing system (Model 858 Bionix^{TM}; MTS System Corporation, Eden Prairie, MN). Testing included three repeated trials at both 0.5 deg/s and 60 deg/s through 30° of motion in both the CW and CCW directions for all five stiffness settings. This procedure mirrors previous testing with the VSTA I and is comparable to testing on existing TRA devices [14], [17]. Testing also included quantification of drag loads by testing the system with no springs installed.

To determine how quickly the stiffness of the VSTA II could be varied, the solenoid actuation time was measured. The time from command (key up - locked) to key contact (key down- unlocked) was tested on four different subunits for five trials each. Lastly, battery testing determined the minimum life of the system on a single charge. While powered to its highest energy consumption state, all five solenoids on, battery voltage was monitored with the lower voltage limit set at 3.5 volts per cell (7.0 volts total). Initial testing was performed with a 2200 mAh battery (later upgraded to 2700 mAh).

5.4.1 VSTA II Full Bench: Results

Mechanical test results for the five individual stiffness settings were fit using least squares optimization to determine the effective linear stiffness at each setting (Figure 52). Testing showed increasing variance between different direction trials (CW vs. CCW) with as little as 2% at the lowest stiffness (1 Spring) and up to 10% variance at the maximum stiffness (5 Springs). Variability between trials of the same direction with varying rates of rotation (0.5 deg/s and 60 deg/s) were within 1%, indicating good repeatability and no rate dependence. Despite the variance, trials were well grouped for each stiffness setting and data for all trials at each stiffness were pooled. The stiffness curves were linear with actual stiffness values over the full range of data exceeding the expected stiffness at all settings (Table 12).

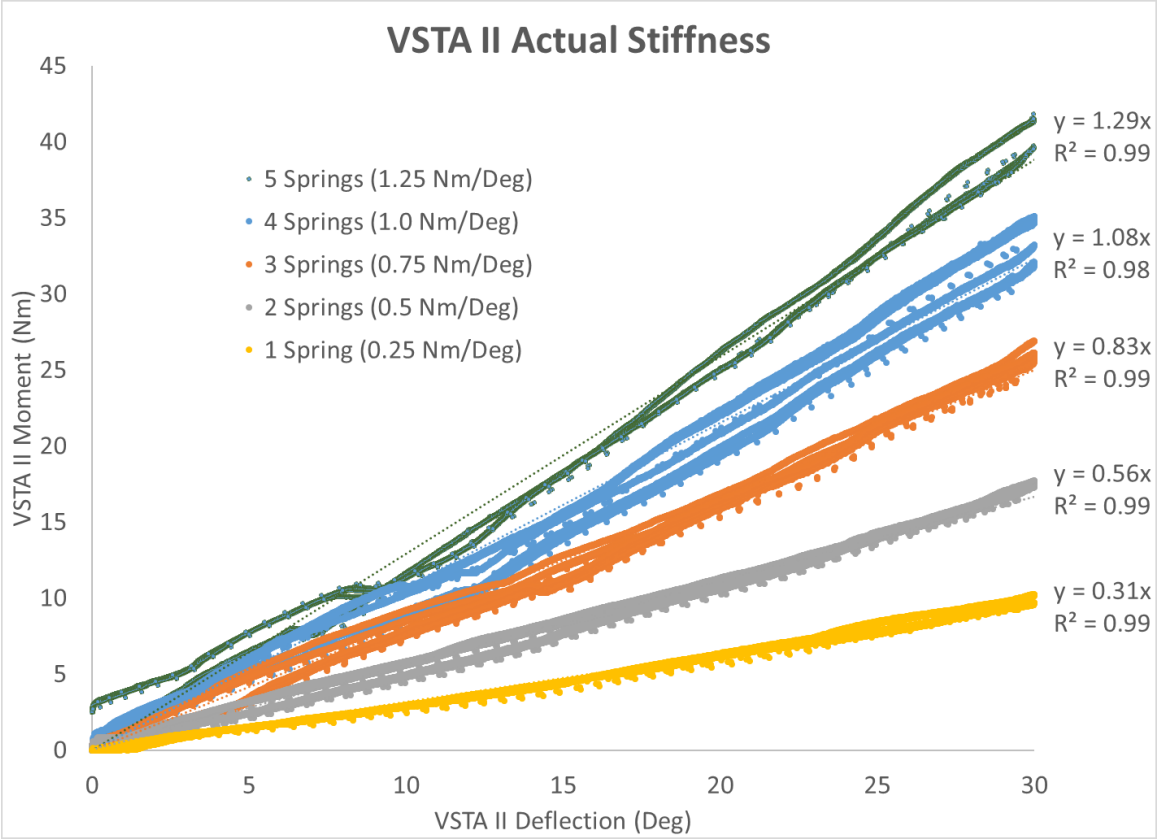

Figure 52: VSTA II MTS results. Each line represents the pooled results from all data at a single stiffness. Actual VSTA II stiffness higher than expected.

Table 12: VSTA testing summary. Deviations of the actual results from the expected are calculated as a percent of the full stiffness range of the device. R^2 value indicate the goodness of linear fit on the pooled data.

Expected Stiffness (Nm/°)	Actual Stiffness (Nm/°)	Deviation from expected as percentage of full scale range (%)	Device fit R^2 (linearity of results)
1.25	1.29	3.2%	0.99
1	1.08	6.4%	0.98
0.75	0.83	6.4%	0.99
0.5	0.56	4.8%	0.99
0.25	0.31	4.8%	0.99

Investigation determined that the spring on each subunit contacts the center post during deflection, inducing friction forces and increasing tested stiffness. The rubbing is also considered the cause of variation between deflection directions. While the friction forces added unexpected stiffness to the system the offset from the expected was relatively consistent and the responses highly linear, and so VSTA II performance was considered acceptable for continued testing. Lastly, on the MTS, the VSTA II was run through the same testing procedure with no springs installed to quantify any drag loads inside the device. It was found that friction loads were less than one Newton-meter and would be inconsequential to the system operation. The final physical attributes of the VSTA II are a stiffness range of 0.31-1.29 Nm/°, displacement range of ±30°, mass of 0.88 kg, and a physical size of Ø104 mm x 75 mm.

The solenoid activation speed was found to be 0.029 ± 0.008 seconds from command to full key movement. When the key is under no load, a stiffness change could occur quickly, well within the swing phase of gait. Finally, the full system powered with a 2200 mAh battery lasted 105 minutes with the system at maximum power consumption. During normal operation, the system is not run continuously at maximum power and actual battery life likely be longer.

5.4.2 VSTA II Full Bench: Discussion

The aim of this project was to create a second-generation prototype of the VSTA that featured a significantly reduced height and mass. The VSTA II design mirrors the function of the original VSTA I, but utilizes a new mechanism. The VSTA II is more capable than its predecessor and can accommodate a wider range of individuals.

Bench testing of the VSTA II showed it is a viable device to replace the VSTA I. MTS testing of the VSTA II followed the same protocol as the VSTA I. The results showed the function of the VSTA II was not rotation rate or direction dependent, functioning similarly at both 0.5 deg/s and 60 deg/s, in both the CW and CCW directions. The VSTA II features discrete stiffness modes from 0.31-1.29 Nm/° in approximately 0.25 Nm/° steps with displacement up to ±30° in addition to fully locked operation. This capability exceeds the tested range of the VSTA I (0.3-0.91 Nm/°) and that of available single stiffness devices tested by Flick et al [14].

The VSTA II is intended for advanced human subject testing to better understand optimal implementation of variable transverse plane stiffness to benefit individuals with lower limb amputation. While it has been shown that reductions in transverse plane stiffness can significantly reduce peak loading on the residual limb during turning activities, the original study only focused on self-selected walking speed [17]. Walking speed can greatly influence stability and limb loading and

therefore could be a significant factor when choosing the optimal VSTA II stiffness [40], [41]. Additionally, the VSTA I study only included five participants as the height of the device limited recruitment. Future studies will seek higher enrollment numbers, facilitated by the VSTA II's reduced height.

The VSTA II's reduced mass and stand-alone controller make it more ideal for testing in and out of the lab. While no well-established amount exists for how much mass can be added to a prosthesis, increased lower limb prosthesis mass has shown no significant effect to gait kinematics up to 3.97 kg and energy consumption up to 2.3 kg [22], [31], [42]. The overall mass of the VSTA II (0.88 kg) is significantly lower than the VSTA I (1.8 kg). Lastly, the VSTA I featured a 0.24 second transit time between the minimum and maximum stiffness settings, a value that pushed the limits of the 0.19-0.25 seconds available during the swing phase of gait. The VSTA II can select between any of its discrete stiffness setting in 0.029 seconds, making it more capable of variations during swing.

While the VSTA II features improvements over its predecessor, it is still considered an early prototype and has some limitations. VSTA II modulation is limited to no load conditions during the swing phase of gait. Additionally, the VSTA II must be in the neutral position to allow alignment of the key mechanisms to lock and unlock subunits. This results in a narrow window to vary stiffness during active use. Another limitation of the VSTA II is the increased variability in stiffness

between deflection directions at stiffer settings. This effect can be contributed to the springs rubbing the center post as it is deflected. As the spring is deflected more, the friction increases causing an increase in apparent stiffness, and less predictable operation. Variability increases with increasing stiffness because each increase in stiffness is the addition of a new subunit. Each subunit is characterized by its own variability, which then adds to the total variability at increased stiffness. At the lowest stiffness, the variability is 2% and it is 10% at the highest. This indicates that each subunit contributes linearly to overall variability. Lastly, the tested battery lasted only 105 minutes during full power operation. Ideally, the battery would last the length of the in-lab tests, approximately four hours. Because actual power consumption will vary depending on the stiffness setting, it is difficult to determine battery life in practice. To remedy any power supply shortfalls, a larger battery (2700 mAh) has been included for future testing.

5.4.3 VSTA II Full Bench: Conclusions

This chapter outlined an upgraded transverse plane rotation adapter for a lower limb prosthesis that features variable stiffness abilities. The VSTA II is capable of discrete stiffness variation from 0.31-1.29 Nm/° in 0.25 Nm/° increments with ±30° of motion in addition to fully locked operation. Stiffness variation is enabled by five independent spring subunits that can be combined in parallel to create different, linear, stiffness settings. Stiffness selection is performed via small

locking mechanisms operated by electro-mechanical solenoids that can vary the stiffness of the VSTA II in 0.029 ± 0.008 seconds while the device is unloaded during the swing phase of gait. The VSTA II features reduced mass and height compared to its predecessor along with a stand-alone control and power system. This will help in future recruitment for human subject studies, and allow for advanced testing both in and out of the lab. Future work with the VSTA II will seek to better understand how variable transverse plane stiffness can benefit lower limb amputees and what stiffness levels might be optimal for varying activities and walking speeds.

5.5 VSTA II Design Updates

While the VSTA II was found to perform well on the bench it was the device needed further updates to perform during human subject testing. Testing on initial human subjects (discussed in chapter 8) revealed that the interface between the pyramid adapter and the center shaft (Figure 51, M and C respectively) was not sufficient to handle the off-axis bending loads experienced during a gait cycle. In initial testing the bolt holding the two components together was found to loosen causing the keyed coupling between them to break in shear and eventually cause the bolt to break and allow the assembly to separate during operation. Design updates were performed to strengthen the connection between the adapter and the center shaft (Figure 53). Primarily, a needle thrust bearing was added between the adapter and housing to support eh bending loads (Figure 53, A). Next, additional key features were added along the length of the shaft to increase coupling strength between the shaft and adapter (Figure 53, B). Last, the shaft length was extended an

additional 5 mm into the body of the adapter to better transfer the loads between the components (Figure 53, C).

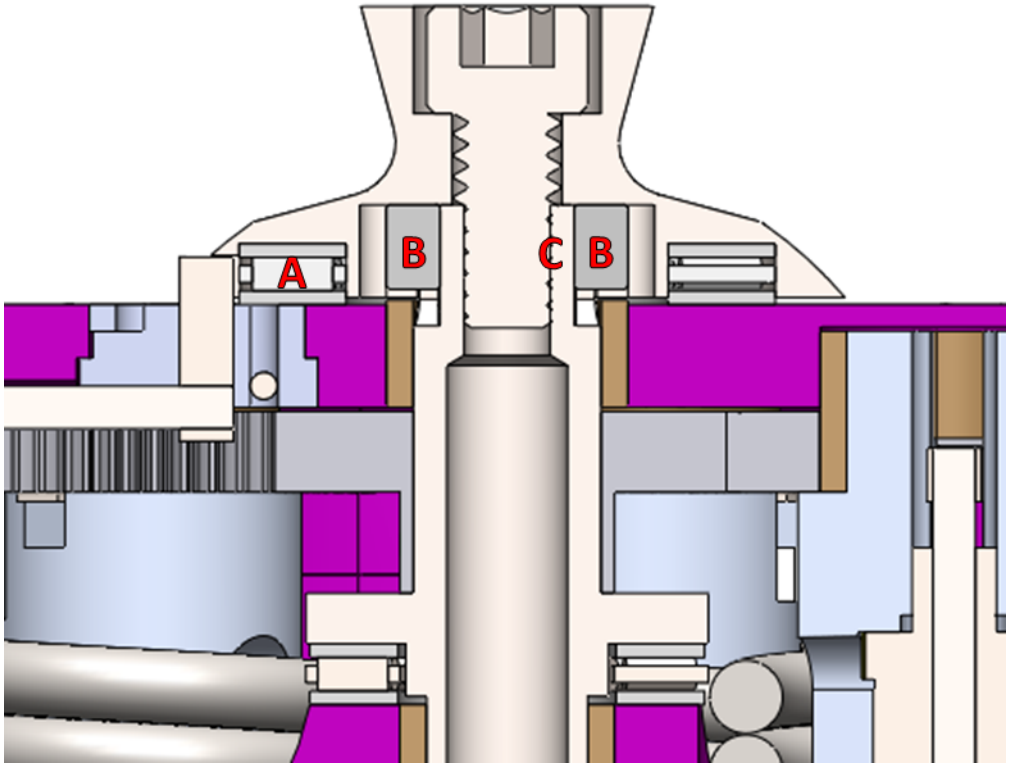

Figure 53: VSTA II design updates. Initial testing found the key features on the shaft and the bolted interface insufficient to withstand off-axis and bending loads while walking. Needle roller thrust bearing added between adapter and housing to support loads (A). Two additional keys added vertically along shaft to augment horizontal keys on top of shaft (B). Shaft extended farther up into the body of the adapter (C).

6 VSTA II Controller

A stand-alone controller was developed for the VSTA II using a BeagleBone Black (BBB) (BeagleBoard Foundation, Oakland Township, MI), coupled with a custom breadboard (Figure 54).

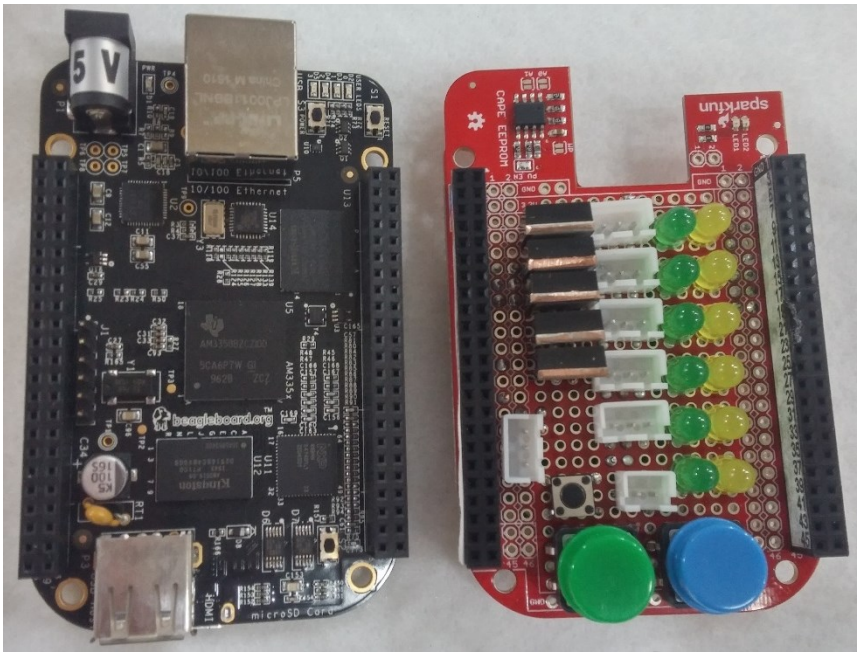

Figure 54: BeagleBone Black (Left) and the custom 'Cape' prototype board for the VSTA II (Right)

The BeagleBone Black's large computing power and ability to directly integrate analog sensor signals made it the ideal choice when compared to other modular control systems. The BeagleBone Black is a complete computer which allows it to run script to control the VSTA II as well as import and process data from sensors in real time. The VSTA II controller was designed to accomplish the following tasks:

- Manipulate the On/Off states for the 5 VSTA II solenoids (manual buttons)
- Indicate control command and actual VSTA II stiffness state (LEDs)

- Read and Interpret Sensors
    - VSTA II Angular Position
    - Lock Key Position – Determine if spring is engaged or disengaged
- Log data from sensors

To complete the desired tasks, the BBB is coupled with a custom board that allows for input and output from the VSTA II components. Initial prototyping of the board was accomplished with a solderless breadboard and all the individual components necessary to implement the controller (Figure 55). This allowed for the design to be revised easily without soldering.

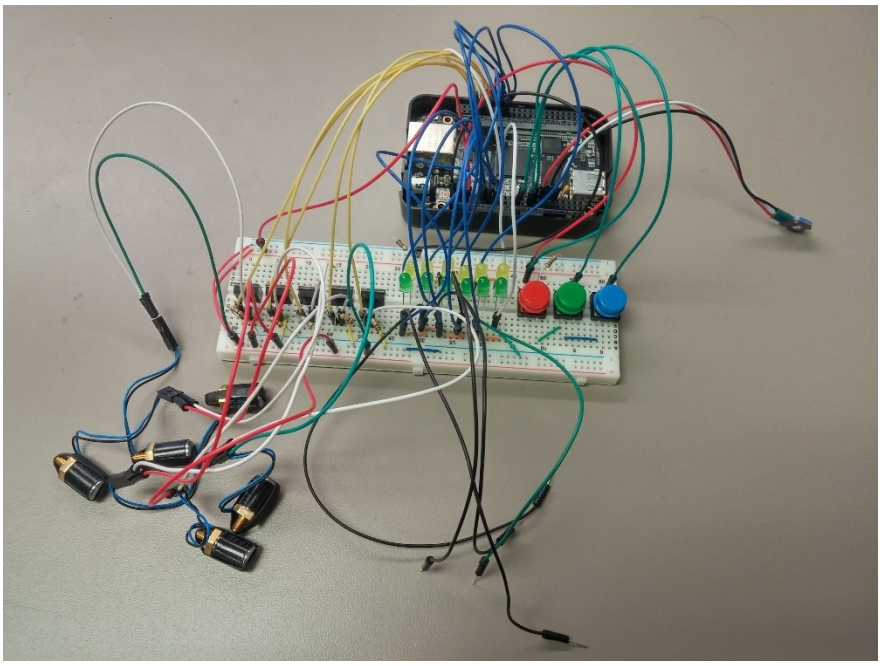

Figure 55: BeagleBone Black computer controller with breadboard components in prototype setup.

After the rough layout, had been determined a detailed layout was prepared using EAGLE PCB Design (CadSoft, San Rafael, CA) software. The detailed layout allowed for specific routing of individual components and declaration of intended resistor values (Figure 56). The schematic has been outlined with boxes to help identify the individual components sets.

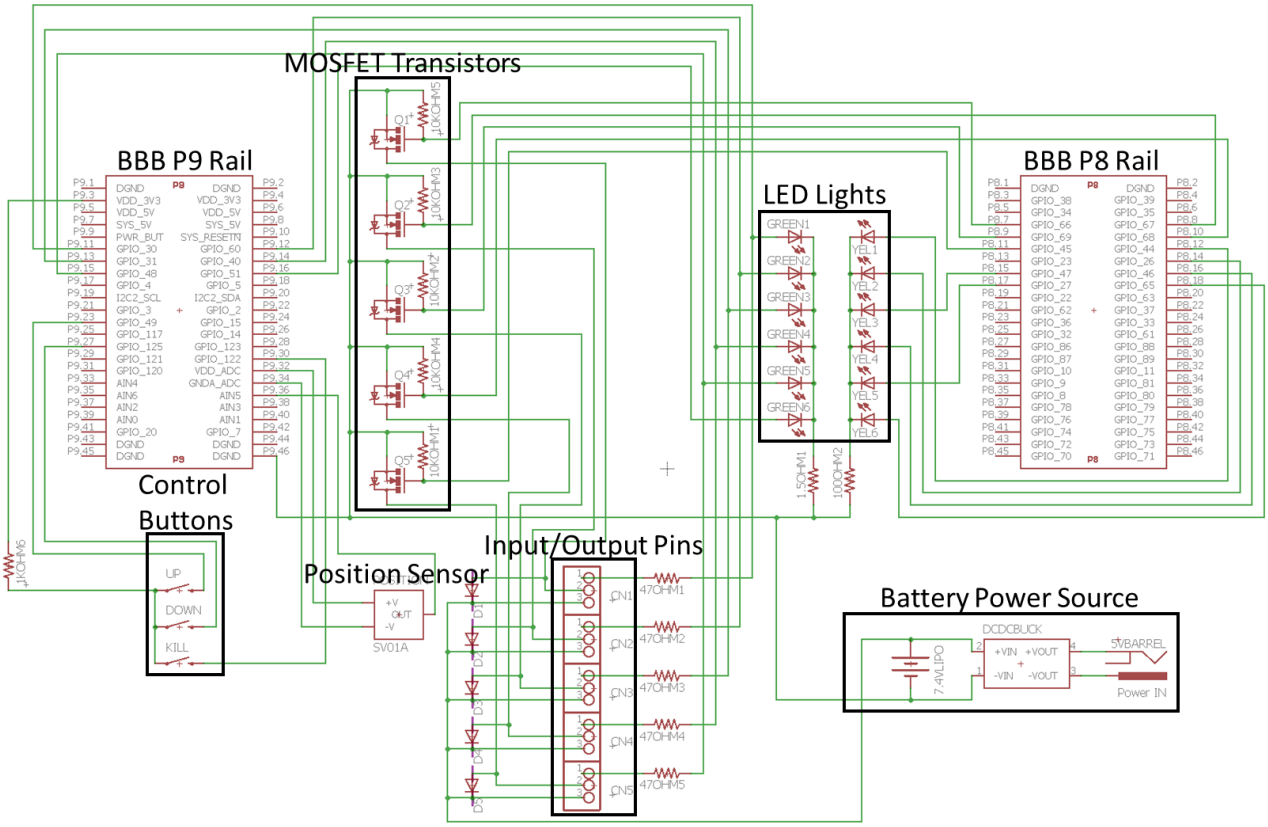

Figure 56: Detailed schematic of controller components.

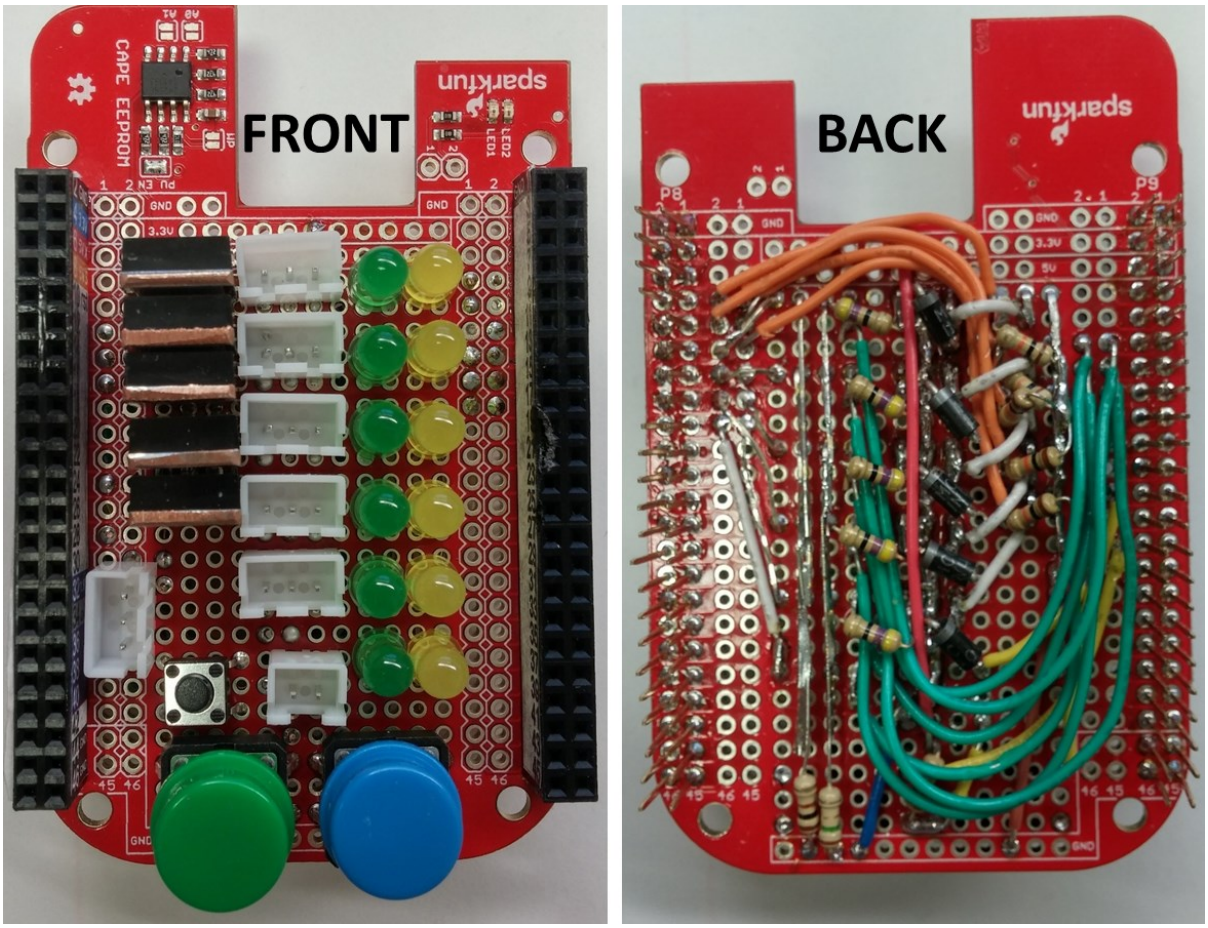

Figure 57: Final component breadboard for use with BeagleBone Black

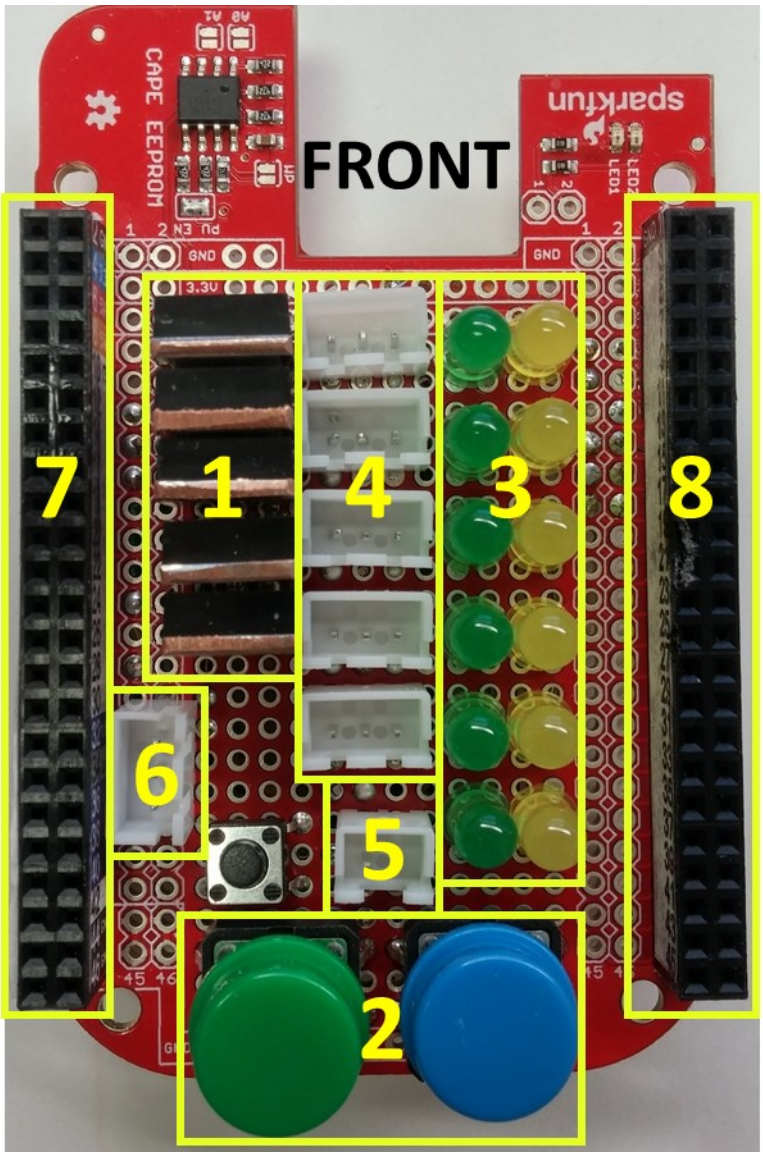

Figure 58: Detailed sections of the BBB prototype board. 1) MOSFET Transistors, 2) Control Buttons, 3) Function Indicator LEDs, 4) Solenoid Connectors, 5) Solenoid Power, 6) Rotary Position Sensor Port, 7 & 8) Header Connections

The final design was then prototyped onto a BBB Proto Cape (SparkFun, Niwot, CO) (Figure 57). The following details of how the board satisfies the design goals, its setup, and components are as follows, and refer to the outlined sections of the prototype board (Figure 58). The main objective of the controller was to manipulate the On/Off state of the individual solenoids to vary the stiffness of the VSTA II by unlocking or locking the individual springs. Each individual solenoid (DSTL-0216-05, Figure 28) requires a 5.4-volt (1.1 W) signal to activate, however, the

BBB is only capable of providing a low power 5-volt source. Five FQP30N06L-ND N-Channel MOSFETs (Fairchild Semiconductor, Sunnyvale, CA) achieve the goal of switching the solenoids (Figure 58, box 1). The MOSFET transistors provide ground switching of each solenoid, with power being supplied to the solenoids directly from the battery power source. This allows the solenoids to run at high power using the low power switching signal from the BBB. Manual control of the solenoid states is set by pressing the green and blue buttons at the bottom of the board (Figure 58, box 2). Each press of the green button increases the stiffness (locks one spring to the set), and pressing the blue button releases a spring from the parallel set. To indicated at what stiffness setting the VSTA II is currently operating LED lights were added (Figure 58,box 3). Twelve LED lights total (six green, six yellow) comprise the set. Yellow LEDs indicated the commanded number of spring sets to engage, Green LEDs indicate the number of spring sets that are physically engaged. There are six individual levels of stiffness (five spring sets plus fully locked). When all lights are illuminated the VSTA II is at its highest stiffness setting (fully locked). When only one level of LED lights is illuminated the VSTA II is at the lowest stiffness (one spring engaged). Yellow LEDs are activated directly by the controller corresponding to the stiffness setting commanded. The green LEDs activate based on a switch build into the Spring Post of the VSTA II. When the solenoids are powered they draw the locking mechanism into the unlocked position (Figure 35). At that time, the key contacts a small grounding wire, completing a circuit that illuminates the corresponding green LED, indicating that the VSTA II has reached the commanded stiffness. Five individual, 3-wire, JST connectors provide connection between the control board and the VSTA I (Figure 58, box 4). The three wires correspond to solenoid power, switched ground from the MOSFET, and the lock position signal. As previously discussed the solenoids require power directly from the battery source to achieve the appropriate power levels.

The battery connects power and ground via a 2-wire JST connecter that then distributes common power to each of the solenoid connectors (Figure 58, box 5). The controller also required sensing of the angular position of the VSTA II. This is accomplished with the previously discussed rotational potentiometer (Figure 36) which is powered and read by the analog channels of the BBB (Figure 58, box 6). Lastly, two header bars provide connection into the headers of the BBB board (Figure 58, boxes 7 and 8).

The final design requirement also included the ability to log data during operation. The BBB includes an onboard micro SD card slot which can be used for this purpose. The output from the positions senor, as well as the state of the command and lock key positions can all be recorded during each cycle of the code. The cycle is slowed to 4 Hz to allow appropriate interaction with the manual control buttons. If the cycle is increased too far the buttons become overly sensitive making it hard to select a specific stiffness level. This cycle rate could be varied if a higher resolution data stream was required.

Powering the BBB and solenoids is performed by a 2 cell (Tenergy, Fremont, CA) 2200 mAh battery that nominally outputs 7.4 volts. The BBB requires maximum 5 volts input, and so the battery voltage is converted using a DC-DC voltage converter (R-78E-0.5, Recom Power, Gmunden, Austria). The solenoids are then powered separately using a lead from the same battery source, allowing them to be powered by the higher 7.4-volt signal. The solenoids are designed for a 5.4-volt signal, but it was determined that powering them at the higher voltage signal would allow for faster, and more forceful activation, improving the performance of the VSTA II. Testing of the solenoids was performed at the higher power level and was determined to be acceptable. Specifically, the solenoids were tested for thermal stability at the higher power. Energizing the solenoids at the peak battery voltage (full charge) of 8.36 volts continuously resulted in a stable

surface temperature of 88 ºC, well within the specified maximum operating temperature of 130 ºC. After sustained operation for three hours the solenoid was then retested for function and found to have no deficit. This provided the basis for full time operation at the higher power level.

With all final components in place the controller was tested for power consumption and battery life. First the system was tested for power consumption; this was accomplished by hooking the system to a AC/DC variable power supply. The system was tested with all five solenoids engaged to determine maximum power draw, at both 7.4 V (nominal battery charge) and 8.4 volts (maximum battery charge). It was found that the system drew 1.40 amps at 7.4 volts and 1.42 amps at 8.4 volts. Additionally, the system's lower power state was tested (all solenoids off) and was found to draw 0.5 amps at 7.4 volts. Given the measured power draw the battery longevity could be estimated given the battery capacity. Using the Digi-Key battery life calculator formula:

$$\frac{\text{Battery Capacity (mAh)}}{\text{Device Consumption (mA)}} * 0.7 = \text{Battery Life (hours)} \quad [26]$$

This estimated a battery life of 1.1 hours for the 2200 mAh battery. To confirm this the battery life was directly tested. The fully charged battery was set with the system running and all five solenoids under power. Lithium polymer batteries are sensitive to excessive discharge and discharging the individual cells below 3.5 volts (7 volts battery total) can damage the battery. The battery was monitored and found to last a total of 105 minutes (1.75 hours), with the final voltage of each cell at 3.467 volts (Figure 59).

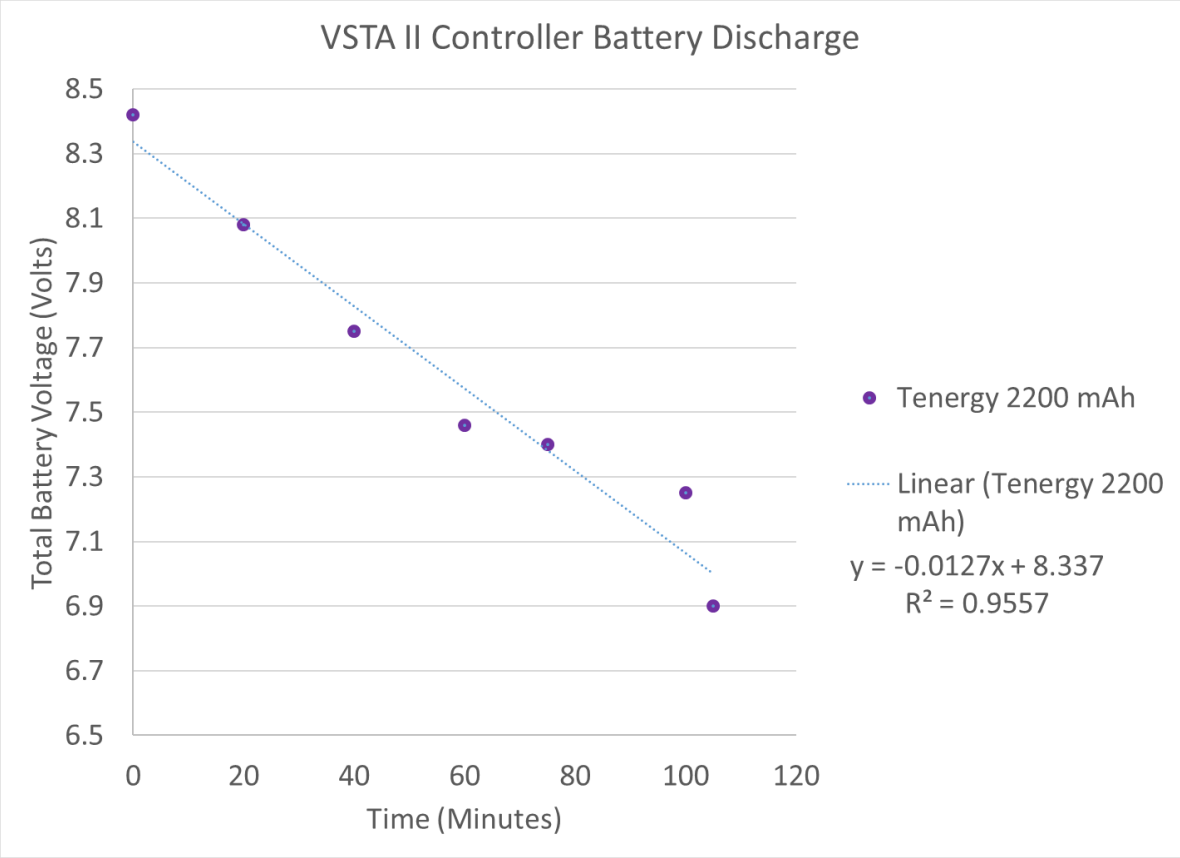

Figure 59: VSTA II controller battery discharge test

It was found that the battery lasted longer than expected, with a relatively linear discharge rate of -0.0127 mAh/min. Near the end of the test there were some anomalous readings however the trend returned during the last reading. Ideally, a single battery would last for at least one day of laboratory testing (3-4 hours), however, increasing the battery capacity would increase the mass of the overall system. This could potentially have effects on the user's gait kinematics [22] and so it was decided to use the smaller battery and change battery units mid test. It should also be noted that the power consumption and battery tests were performed with all solenoids active, corresponding to the lowest stiffness setting. Operation of the VSTA II will not always be at the lowest stiffness setting, and so actual battery consumption will vary depending on how it is utilized.

To house the complete controller a custom, 3D printed, case was constructed (Figure 60). The case features a loop on each side that allow it to attach to the user via a 2-inch elastic Velcro strap. The strap is ideally placed around the socket of the user for maximum comfort and to keep it close to the VSTA II for ease of routing signal wires.

Figure 60: Complete VSTA II controller inside the custom housing with battery attached.

7 Turn Intent Prediction

Pilot testing of the VSTA I indicated that reductions in transverse plane stiffness during turning maneuvers can significantly reduce peak loading of the residual limb that could lead to soft tissue breakdown and discomfort, without adverse effects on subject mobility [43]. Information regarding how to appropriately modulate the transverse plane stiffness is limited, and initial testing utilized manual control of the VSTA I stiffness settings when walking. Ideally, the VSTA could interpret real-time information to determine the optimal stiffness setting required for a given walking condition and modulate the transverse plane stiffness accordingly.

Control of advanced prostheses are often task specific, implementing different schemes depending on the phase of gait and locomotion mode [44]. Classification algorithms have been developed to determine if a subject is walking on level ground, on a slope or stairs, and sitting or standing [45]–[48], but limited research has been performed on identifying turns in real time [49], [50]. Classifier algorithms can take many forms such as decision trees, discriminant analysis, support vector machine, nearest neighbor, neural networks and spectrograms [51]–[59]. Inputs to these classifiers have included mechanical (force and torque), kinematic (acceleration, velocity, and position), and electromyography (EMG) signals [45], [50], [54], [60]. Utilizing all these signals has demonstrated the highest classifier accuracy [45], [54], [60], but may not always be feasible. Measurement of EMG signals requires direct contact with the skin, increased processing power, and is subject to motion artifact making the use of EMG outside of a lab setting uncomfortable or difficult [61]. Embedded IMUs are a practical alternative, but may provide less accurate classifications [45], [60]. Practically, an IMU integrated with the VSTA in the shank of a lower limb prosthesis would provide the most ideal packaging,

Control of the VSTA is constrained to the swing phase of gait. To make the VSTA as light as possible, low power elements are used to modulate the stiffness and are not intended operate under body weight loads. The VSTA controller must predict an upcoming turn during the swing phase preceding the heel strike of the turning step with enough time to process and activate the mechanical components. The goal of this study is to identify a classification algorithm that can accurately predict a turn using IMU signals from the shank with adequate time to enact a change in stiffness, before the foot is loaded during a turn.

7.1 Turn Intent Prediction Methods

Using previously collected data from VSTA I human subject trials simulated IMU data was calculated in Visual 3D (C-Motion Inc., Germantown, MD) using a composite model with 63 retroreflective markers. IMU signals included three-axis translational velocity and three-axis angular velocity from the upper segment of the VSTA joint. Derivation of translational velocity data to obtain segment acceleration was performed in MATLAB (Mathworks, Natick, MA) and utilized a moving average filter, with a window size of seven consecutive data points, to smooth the signal. All signals taken with respect to the upper segment coordinate system to simulate the movement of an IMU in the shank of the prosthesis.

Data for each subject consisted of 90° spin, 90° step, and 180° turns, and straight walking at the subject's self-selected pace. Each activity included testing at three different stiffness settings of the VSTA, with three to five trials per setting for each activity and subject. Previous results indicated that the stiffness setting to minimize peak transverse plane moment was independent of turn type [43]. Furthermore, different stiffness levels had no significant effect on self-selected walking speed or the L-Test of functional mobility, indicating that the approach and negotiation of turns is unaffected by stiffness setting [18], [43]. Therefore, data from all turning types and

stiffness settings were combined to create a larger pool of data for training and testing. An individual data set used for analysis consisted of data from all trials, activities, and stiffness settings concatenated into a single array, with only the steps on the prosthetic limb considered for data analysis. Data labels indicating the activity being performed included: 1) the swing phase immediately preceding the turn, the time from toe-off to heel strike of the prosthetic limb leading into the turn, 2) the stance phase during the single step turn, the time from heel strike to toe-off during the actual turn, and 3) all remaining data labeled as self-selected straight walking with no differentiation for gait phase.

A review of the literature [53], [54], [57], [58] and preliminary analysis using five-fold cross validation on the data set suggested analysis of three classifiers was warranted: support vector machine (SVM) with a fine Gaussian kernel, K nearest neighbor (KNN) with a weighted kernel, and a bagged decision tree ensemble (Ensemble). SVM classifiers attempt to separate data in the training set using oriented hyperplanes [62], [63] and have previously been used for similar activity classification algorithms [51], [54], [60]. KNN classifiers make predictions based on the data point to be classified's distance from other known points in the training data set when plotted in an n-dimensional space, where 'n' is the number of different signals being used to make the classification (e.g., six dimensions for a 6-axis IMU). Classification is then determined by the known class of the 'K' closest points from the training set. A weighted KNN normalizes the magnitudes of the different input signals, which if significantly different, can bias the results [46], [56], [63], [64]. Ensemble classifiers use multiple models in combination and is analogous to a Venn diagram, where each model is a circle that encompasses a certain range of data. When data falls into the range of a singular model, it is used to predict the outcome. When multiple models cover the same range, each makes a prediction and the prediction with the greatest number of

'votes' is used. A bagged (bootstrapped aggregated) decision tree ensemble uses an aggregated set of decision trees that are generated by randomly sampling the training data (bootstrapping) to create multiple subsets of training data. The generated training data subsets become a set of decision tree models (ensemble). This method has been shown to help reduce overfitting, with better performance than a single decision tree but requires longer computation time [63], [65].

Training and testing of classifier models was performed both for each individual and for all the individuals pooled together utilizing MATLAB software. Training data for individuals consisted of all the data for a single subject minus randomly selected trials which became the test data. The test data set for each individual consisted of one trial from each activity at each stiffness setting, for a total of nine turning events (three each from the three turn types), and three trials of straight walking, totaling 12 trials of data to be used to validate the individually trained model. This accounted for an approximate 80/20 split of the total data.

Pooling data from all individuals for training would be ideal as this provides a greater number of data points to train the classifier and requires less training for new individuals to use the device. This approach has not shown strong results for level walking, ramp, and stair classification, but has not yet been investigated for turning [66]. Pooled training consisted of the total data for four of the five subjects, then model testing on the total data for the fifth subject. The holdout subject was then rotated to determine the effect for each individual. All classifier testing employed the default MATLAB parameters.

Because a classifier's predication ability can be dependent on the number and type of input features used for classification [63] the input features were varied to determine if a reduction of input signals influenced overall classifier accuracy. After running the classifier training with all

six IMU signals the process was repeated with only the three accelerometer signals and again with only the three gyroscope signals for each model and the overall classifier accuracies compared.

Overall classifier accuracy is based on all the points in the data set but may not necessarily correspond to the accuracy of a controller using the classifier output. Creation of a simple control scheme allowed for determination of how the classifier output might be used by a controller in real-time. Implemented on the models' predictions on the test data the control law designated a trigger to identify an upcoming turn, and was defined as four adjacent time steps containing the label indicating the swing before a turn. This trigger would then be used to activate the VSTA into a stiffness setting different from the one used for straight walking. The amount of time a prediction trigger preceded the heel strike of the turn gave the length of time the controller would have to enact changes to the device. Because the exact window needed to modulate a device can vary, prediction times less than 100 ms were arbitrarily counted as a missed prediction [35]. Model predictions were also evaluated to determine how often straight walking steps were mistaken for turns, indicating changes to the device parameters when no change is warranted. Straight walking steps were separated into two categories, transitional steps (i.e., the straight steps that immediately precede and follow a turn) or constant straight walking, as transitional steps can be harder to classify than steady state activity [48], [54], [60]. Furthermore, there may be less consequence to the user for misclassifying a transitional step as the user is expecting a change, compared to an unexpected change during steady state operation.

Statistical analysis of overall model prediction results consisted of a McNemar test to determine if the predictions made by each model on the test data yielded significant differences ($p<0.05$). Analysis of control scheme results utilized linear mixed effect models with fixed effects for classifier model, VSTA stiffness setting, turn type, and random slope and intercept effects for

subject for the continuous prediction time results. Individual and pooled prediction time means were compared using a two-sample t-test with two-tailed probability. Differences in percent accuracies achieved by the control scheme were evaluated overall using a one-way ANOVA with individual significance values between models using one-sample paired t-tests with two-tailed probability and Bonferroni correction for the multiple tests between models.

Lastly, it is intended that the classifier models would be part of a larger control scheme that could run in real-time on wearable, tether-free hardware. An initial prototype controller would be based on an existing device that can be purchased off the shelf, and so simulation of controller processing was performed on a BeagleBone Black, Rev C (BeagleBoard Foundation, Oakland Township, MI). Processor in the loop testing was only performed with the SVM model as it is the only model of the three supported directly by the MATLAB software; however, the SVM model is rated as the slowest of the three, and will give the worst-case processing scenario. Additionally, models were tested in the primary workstation hardware (Dell M4800, Windows 10 64-bit operating system, Intel® Core™ i7-4710MQ CPU @ 2.50 GHz, 8.00 GB of RAM) to give a relative comparison of the time needed to process classification at a single time point. Processor in the loop testing was completed for each subject individually by running the entire data set through the BeagleBone and taking the mean and standard deviation of the time to process a single data point across all subjects.

7.2 Turn Intent Prediction Results

The classifiers' overall ability to predict an upcoming turn during the swing phase preceding a turn were analyzed with confusion matrices (Table 13). The results show the ability to recognize straight walking (SSW) was high for all models and subjects (96% or greater), while the ability to identify the swing phase of gait before a turn (Swing) varied from 55-92 The

identification of Swing is most often mistaken for SSW, indicating that a controller using these classifiers might inadvertently mistake turning for straight walking. Classifier models evaluated on the test data yielded 90.6%, 90.0%, and 90.2% overall percent accuracies for the SVM, KNN, and Ensemble models across all individual subjects. McNemar tests on each model's prediction abilities indicated that the KNN and Ensemble models had essentially the same performance, while the SVM had significantly different accuracy than both the KNN and Ensemble ($p<0.001$ and $p=0.001$ respectively). Additionally, the confusion matrices imply that the pooled data may have decreased performance in comparison to individual training. Looking at the classifier's dependence on the input features revealed that utilization of all six inputs yielded the best result. Overall classifier accuracies for all three models ranged from 66-77% between individuals when using only the accelerometer signals and from 83-90% using only the gyroscope signals.

Table 13: Confusion matrices for each subject and classifier method. The vertical labels of each matrix represent the true activity label, whereas the horizontal labels represent the activity predicted by the classifier. The diagonal of each matrix represents the classifier's accuracy predicting the true label correctly (SSW – Straight walking, Stance – Stance phase during the turn, Swing – Swing phase just prior to turn). Off diagonal values show the percentage of labels that were predicted incorrectly. The overall value is the total accuracy percentage tested on the complete data set.

Subject	Label	Classifier								
		Support Vector Machine			K Nearest Neighbor			Ensemble		
		SSW	Stance	Swing	SSW	Stance	Swing	SSW	Stance	Swing
A01	Overall	96.2%			96.5%			96.2%		
	SSW	98%	1%	1%	98%	1%	1%	98%	1%	1%
	Stance	11%	89%	1%	8%	91%	1%	10%	90%	1%
	Swing	7%	1%	92%	8%	1%	92%	9%	1%	90%
A02	Overall	95.2%			94.9%			94.8%		
	SSW	98%	1%	1%	97%	1%	1%	98%	1%	1%
	Stance	10%	90%	1%	9%	91%	1%	10%	90%	1%
	Swing	17%	1%	82%	15%	1%	84%	19%	1%	80%
A03	Overall	90.7%			90.4%			90.3%		
	SSW	98%	1%	1%	96%	2%	2%	97%	1%	1%
	Stance	21%	79%	1%	20%	80%	1%	23%	77%	1%
	Swing	44%	1%	55%	32%	2%	66%	36%	2%	62%
A04	Overall	92.7%			92.6%			92.1%		
	SSW	98%	1%	1%	97%	1%	2%	97%	2%	1%
	Stance	19%	80%	1%	18%	81%	1%	18%	81%	1%
	Swing	18%	1%	81%	17%	1%	82%	21%	1%	78%
A05	Overall	93.0%			94.4%			93.8%		
	SSW	98%	1%	1%	97%	1%	2%	97%	1%	2%
	Stance	19%	81%	1%	10%	89%	1%	10%	89%	1%
	Swing	14%	1%	86%	14%	1%	86%	14%	1%	86%
Pooled	Overall	90.5%			91.2%			90.5%		
	SSW	97%	2%	1%	96%	2%	2%	97%	2%	1%
	Stance	26%	74%	1%	20%	79%	1%	23%	77%	1%
	Swing	29%	2%	69%	24%	2%	74%	30%	3%	67%

The accuracy and prediction time of a controller utilizing the classifier output was evaluated with a simple control scheme (Table 14). The time between the control trigger and the heel strike of the turn (Pred Time) is relatively consistent between individuals, but is significantly reduced for the pooled data ($p<0.001$). Individual training was found to be the best method with

all three classifier models (SVM, KNN, Ensemble), able to predict a turn (Turn Acc, Table 14) with high accuracy (96%, 93%, and 91% respectively), approximately 400 ± 70 ms before the heel strike of the turn. The accuracy predicting a turn (Turn Acc) and the accuracy for steady straight walking (SSW Acc) were high overall for the individual results, but varied widely between subjects. Often four of the five subjects would achieve 100% accuracy, while the fifth subject had a less desirable result that significantly affected the overall average. Additionally, the control scheme could properly identify the transition straight walking step immediately before and after a turn (Trans Acc, Table 14) with 85%, 82%, 97% for the SVM, KNN, and Ensemble models respectively with all three having the same prediction accuracy for sustained straight walking, 92% (SSW Acc, Table 14).

Statistical analysis of the control scheme results indicated no significant difference in the prediction time between the three algorithms. Moreover, the prediction time between the varying stiffness settings and turn types had no significant difference, further reinforcing the assumption that all data could be grouped together for this analysis. Regarding the percent accuracies, all three models had non-significant differences in their turn prediction accuracies (Turn Acc) or their ability to not mislabel straight walking steps during steady state walking (SSW Acc). However, the Ensemble model had a significantly better ability ($p = 0.002$ overall) to recognize the transition straight walking step immediately before and after a turn (Trans Acc).

Table 14: Control algorithm results using the three classifier models. Individual results are for a model trained on data from only that subject, pooled results are from models trained on the other four subjects. Prediction time (Pred Time) indicates the amount of time before the heel strike of the turn the controller identified turn intent, with standard deviation (Std Dev). Turn accuracy (Turn Acc) gives the accuracy of correctly predicting a turn before it happens. Transition accuracy (Trans Acc) denotes the accuracy distinguishing a straight walking step adjacent to a turn step. Steady straight walking accuracy (SSW Acc) is the accuracy during pure straight walking trials, the ability for the classifier to not mistake straight walking for turning. Three classifiers tested: Support Vector Machine (SVM), K Nearest Neighbor (KNN), Bagged Tree Ensemble (Ensemble). An * indicates a significantly significant result at the $p<0.05$ level.

Subject	Classifier	Individual					Pooled				
		Pred Time (ms)	Std Dev (ms)	Turn Acc	Trans Acc	SSW Acc	Pred Time (s)	Std Dev (s)	Turn Acc	Trans Acc	SSW Acc
Overall	SVM	404	61	96%	87%	92%	0.30	0.11	50%	62%	76%
	KNN	407	72	93%	84%	92%	0.29	0.12	76%	39%	27%
	Ensemble	400	73	91%	97%*	92%	0.26	0.11	62%	58%	70%
A01	SVM	424	46	100%	95%	100%	0.31	0.06	55%	78%	97%
	KNN	425	48	100%	86%	100%	0.37	0.09	84%	48%	8%
	Ensemble	423	48	100%	100%	100%	0.26	0.11	92%	67%	82%
A02	SVM	371	88	100%	81%	100%	0.31	0.08	69%	44%	55%
	KNN	393	72	100%	81%	100%	0.28	0.11	95%	46%	55%
	Ensemble	385	84	100%	86%	100%	0.23	0.08	93%	52%	76%
A03	SVM	414	66	78%	95%	100%	0.18	0.10	30%	61%	51%
	KNN	437	55	78%	90%	100%	0.19	0.06	35%	26%	0%
	Ensemble	412	65	78%	100%	100%	0.19	0.08	35%	38%	29%
A04	SVM	389	41	100%	80%	100%	0.33	0.08	9%	87%	94%
	KNN	356	101	89%	80%	100%	0.24	0.09	78%	41%	0%
	Ensemble	400	39	78%	100%	100%	0.22	0.03	18%	75%	92%
A05	SVM	418	56	100%	71%	63%	0.33	0.13	80%	50%	79%
	KNN	425	67	100%	71%	63%	0.32	0.13	87%	38%	71%
	Ensemble	381	111	100%	100%	63%	0.34	0.12	78%	66%	71%

Results for processor in the loop testing are shown in Table 15. As expected the SVM classifier was the slowest of the three, with KNN being the fastest by an order of magnitude. The classifier run time on the BeagleBone processor was considerably slower than on the workstation.

Table 15: Workstation versus embedded controller processing time for an individual time point for each classifier model. processing time is given as the mean and standard deviation (Std Dev) to process a single time point across all subjects. Processor in the loop using BeagleBone Black (BBB) evaluation of Support Vector Machine model.

Hardware	Classifier	Processing Time (ms)	Std Dev (ms)
Workstation	Support Vector Machine	0.0684	0.0127
	K Nearest Neighbor	0.0081	0.0011
	Ensemble	0.0226	0.0122
BBB	Support Vector Machine	1.53	0.19

7.3 Turn Intent Prediction Discussion

This study aimed to identify a classifier that could accurately predict an intended turning maneuver prior to the stance phase of the turn. Classifier models were compared utilizing data from five individuals with lower limb amputations performing 90° spin turns, 90° step turns, 180° turns, and straight walking, all at a self-selected speed. Training and validation performed on both individual and pooled data utilized input from a simulated IMU located in the shank of the lower limb prosthesis. A simple control scheme allowed for analysis of each classifier's ability to predict turn intent before heel strike, and evaluate the amount of time the prediction would give a controller to enact changes in a semi-active prosthetic device.

Whereas, the overall classifier accuracy is generally stated to denote model ability [48], [54], and was high for the three models tested, that metric is not optimal when determining how well the classifier would be able to predict turn intent. Testing of the three models on test data yielded about 90% overall accuracy for all three. While the SVM model showed a significant difference in overall accuracy it does not seem to give substantial overall gains compared to the

other two. Evaluation of confusion matrices gave a more in-depth analysis of the models' ability to predict the swing phase preceding a turn (Swing) (Table 13). The classifiers' accuracy in recognizing the Swing label fell below the overall accuracy. The reason overall accuracy can be high while accuracy to identify the stance during a turn (Stance) and Swing states is low, is that the self-selected straight walking label (SSW) occurs more frequently than the other two, and makes up 73% of the 128,024 total data points between all subjects. This means SSW accuracy will have a greater influence on the overall accuracy than the other two labels. The classifiers' ability to identify Swing is relatively low and widely varied (55-92% depending on subject), however, it should be noted that the confusion matrix accuracy relates the total number of actual Swing labels to the number identified by the classifier, and a controller would only need enough labels to denote that a turn may be imminent and enact changes to the prosthetic device.

Analysis of input features indicated that the best result was obtained using all six IMU signals. It was interesting to note that the gyroscope signals alone yielded a better result (83%-90% accuracy on training data) than accelerometer signals alone (66%-77% accuracy on training data). This suggests that the gyroscope signals are primary for identification of turn intent.

Implementing the control law, individual training was found to be the best method with all three classifier models (SVM, KNN, Ensemble), able to predict a turn with high accuracy (96%, 93%, and 91% respectively), approximately 400 ± 70 ms before the heel strike of the turn (Table 114), with no significant differences found between the models for either turn prediction accuracy or time. While methods that utilize multiple sensors and EMG can reach accuracies of 97-99% [45], [46], [54], [60], this system has a reduced level of complexity, using only an IMU, and would be easier to implement in conjunction with a device like the VSTA [10]. Often, intent recognition systems need to reach 99% or greater classification accuracy, particularly with stair detection,

where a missed recognition could result in the fall and injury of the user. However, VSTA operation at varying stiffness levels does not have an adverse effect on the user's mobility at self-selected speeds [43]. This indicates that a missed prediction would not necessarily result in injury to the user, only a lessened benefit while using the VSTA, and that the classifiers identified in this work would be suitable for use with the VSTA.

Results for pooled training were less encouraging with far lower accuracy to predict a turn (50%, 76%, and 62% respectively) and a significantly reduced prediction time (Table 14), consistent with previous findings [50], [66]. It would be ideal to train classifiers on a group of pilot subjects and apply that to all future users, reducing the effort to apply devices to a new individual. However, the results presented here suggest that each user should have the model trained to their specific gait.

While the main intent of the controller is to identify when a turn is about to occur, misclassifications of straight walking as turns must also be considered. Straight walking steps were separated into two categories: transitional and steady state. Transitional steps can be difficult to identify as turn preparation and recovery may be occurring, which can account for the generally lower accuracy when using the SVM and KNN classifiers (Table 14 'Trans Acc' column). The Ensemble classifier, however, had 100% accuracy during transitions for four of the five subjects, and a significantly greater overall accuracy of 97% for transitional steps, compared to 87% and 84% for SVM and KNN classifiers, respectively. Steady, straight walking steps (Table 14, 'SSW Acc' column) were 100% accurate for four of the five subjects for all three classifier models. This suggests the controller could maintain the ideal stiffness setting during steady state operation and not surprise the user with an unexpected stiffness change.

All three classifier models had approximately the same prediction time (400 ± 70 ms), which is similar to previous research with SVM classifiers [54]. Previous work with the VSTA has shown that modulation of the full stiffness range could be performed in 380 ms, with smaller increments performed more quickly [35]. This indicates that for the intended purpose, control of this nature would be adequate.

Finally, control requires integration into a stand-alone, onboard controller that would be part of the complete device package. To ensure the ability of these algorithms to run on a wearable, untethered computer, classification simulations were run with the BeagleBone Black processor in the loop (Table 15). It was found that for the slowest classifier algorithm (SVM) the onboard processor could perform the classification of a single time step in 1.53 ± 0.19 ms. For a sampling rate of 120 Hz (8.33 ms), any of these classifiers would readily run on the BeagleBone Black or similar onboard processor.

Determining the most ideal classifier model is not straightforward. Initially, the SVM method would seem the best choice with the highest turn prediction accuracy of 96%, however, it had a relatively low accuracy during transition steps, at 87%. On the other hand, the Ensemble classifier with the lowest overall turn prediction accuracy (91%) had the best accuracy during transition steps, at 97%. Statistical testing indicated all three models ability to detect turns were not significantly different even with the 5% difference, suggesting that the Ensemble classifier would be best overall. However, initial pilot testing indicated that negotiating a turn at low stiffness settings, including the transition steps, did not have an adverse effect on subject mobility [43]. If transition step identification is a lower priority than turn prediction, then the SVM might still be a better choice. Additionally, the pilot testing had constant stiffness setting throughout the activity, and did not challenge the subject with stiffness switching during the transition steps, so it is

unknown how the transition between stiffness settings might affect user gait. Future studies should include the effect on an individual when transition steps are randomly misclassified as a turn. Additionally, the speed of the classifier must be considered. While the BeagleBone Black was capable for all three classifiers, it has a relatively powerful processor. If a less powerful computer is being considered, the fastest classifier (i.e., KNN) may be necessary.

This study represents an initial investigation into a controller for the VSTA or similar device for a lower limb prosthesis, and some limitations should be noted. First, the IMU data used as the input is simulated from motion capture kinematics. While simulated signal was compared to actual IMU data and qualitatively found to have a similar domain and range, the data is not the same as real IMU output. Additionally, the simulated IMU data was collected at 120 Hz, whereas actual IMU data is often collected at 100 Hz [50], [60] and the lower sampling rate could worsen the prediction time. However, the lower frequency signal could require less processing power. Next, an arbitrary control method was used to positively identify turn intent during swing (i.e., Swing classification at four consecutive time steps). Future implementations should consider alternative control schemes. Next, the training data was lab-based where turn types were specifically prescribed. Results from data gathered while walking in a natural environment may be different. Moreover, the subject sample is limited to five individuals with lower limb amputations who were relatively capable walkers. Each classifier was trained on an individual and more training data would not necessarily increase classifier performance [52], but more subjects would be required to show that this type of training is applicable to the general population with lower limb amputations. In example, four of the five subjects had excellent results with one or more of the individual classifiers reaching 100% accuracy for turn prediction, and three of five having 100% accuracy for all three models (Table 14). However, subject A03 had relatively poor

performance with all classifiers for turn prediction, resulting in a lower overall average. This variation can also be found in the steady straight walking steps (SSW Acc) where only A05 had lower than 100% accuracy for all three classifiers. Data from a more varied subject pool would be required to determine if these represent true outliers, or if classifier selection should be individually-based. Lastly, the training data was only performed at self-selected speeds. Future testing is planned to ascertain how variations in subject walking speed and activity affect control performance.

7.4 Turn Intent Prediction Conclusion

The goal of this study was to identify a classification algorithm that can accurately predict a turn using IMU signals from the shank with adequate time to enact a change in stiffness before the foot is loaded during a turn. Three classification models were trained and tested: SVM, KNN, and Ensemble. Training for an individual gave superior results over training on a pooled set of five individuals. Coupled with a simple control scheme, the SVM, KNN, and Ensemble classifiers attained 96%, 93%, and 91% accuracy (no significant difference), respectively, predicting an upcoming turn 400 ± 70 ms prior to the heel strike of the turn. However, misclassification of straight walking as turning during transitions occurred. Given available test data the Ensemble classifier would be most ideal as it had a similar ability to predict turns and a greater ability than the other two to predict transition steps. However, optimal controller specifications are limited and priorities must be set when determining the best control model. While the Ensemble had the best overall result, the SVM had a slightly more accurate result on the overall accuracy and might be ideal if identification of turning is the highest priority and misclassification of transition steps is inconsequential. Lastly, the KNN is best if processing time is a concern. While control of the

VSTA was the primary drive for this research, it would be useful to help determine a classifier strategy for any lower limb device seeking to predict turn intent.

8 VSTA II Human Subjects Testing

To properly implement the VSTA II on an amputee, more information is needed to determine the optimal stiffness setting for an individual during different daily activities. Initial tests performed with the VSTA I investigated different activities, but did not consider varying walking speeds and user preference, both of which are hypothesized to have a significant impact on the optimal stiffness setting of the VSTA [40], [41], [67]. Specifically, it is hypothesized that peak transverse plane moments related to skin breakdown and discomfort when ambulating will increase with increased walking speed. That reductions in transverse plane stiffness will produce the greatest reductions in peak transverse plane moment when turning vs. walking straight. Additionally, user preference for stiffness will vary based on walking speed and activity.

8.1 VSTA II Human Subject: Methods

Five male, unilateral, transtibial amputees (mean ± standard deviation; age: 52 ± 16 years, mass: 90 ± 5 kgs, height: 1.82 ± 0.04 m) provided informed consent to participate in an IRB approved protocol. Gait kinematics and kinetics were collected using a 12-camera Vicon system (Vicon, Centennial, CO), 8 in-ground force plates (AMTI, Watertown, MA), and an iPecs (College Park, Warren, MI) 6-axis load cell installed axially to the VSTA II (Figure 61). Kinematic and kinetic analysis was performed using Visual 3D (C-Motion Inc., Germantown, MD) and a 63-marker composite model modified to include the VSTA II and iPecs in the lower shank of the amputated limb.

Figure 61: VSTA II installed in pylon of lower limb amputee with iPecs attached axially.

Subjects performed testing to determine their stiffness preference during different activity and speed combinations: three different activities (straight walking, spin turn, step turn) and three different walking speeds (self-selected, ±20%). Straight walking performed over-ground along a 7-meter walkway and turning simulated by walking around a 1-meter radius circle [8]. Turning was split into walking in both directions around the circle, prosthesis on the inside of the turn (spin turn) and prosthesis on the outside of the turn (step turn). A paired preference, A-B-C testing flow, allowed determination of preferred stiffness from one of three blinded stiffness settings (A: 0.31 Nm/°, B: 0.83 Nm/°, C: 1.29 Nm/°) for each speed-activity combination (Figure 62). For a given activity and speed, the user performed three to four trials at setting A, then three to four trials at

setting C. The subjects were then required to choose their preference between the two (P1). Subjects then compared their preferred setting, P1, from round one to a third setting, B, after three trials each [68]. The overall stiffness preference (P2) resulted from the flow. Nine preference testing flows were completed for each subject (3 speeds for each of the 3 activities) over the course of two days (straight walking on day on, turning on day two). After fitting the device and following changes to the stiffness settings, subjects were instructed to walk and acclimate until they felt comfortable, generally lasting no more than 5 minutes. Administration of the patient specific functional scale at the beginning of each day allowed for assessment of each subject's physical status to determine consistency of physical performance between the separate days [69]. Round one of preference testing was always between settings A and C to give the greatest contrast and round two between P1 and setting B. Self-selected walking speed was calculated as the mean of four trials walking at each activity. Fast and slow speeds were then determined by adding or subtracting 20% from the self-selected mean. All speeds were controlled within 10% of their mean to ensure no overlap in speeds. The order of speed, activity, and stiffness setting within each round was randomized for each subject.

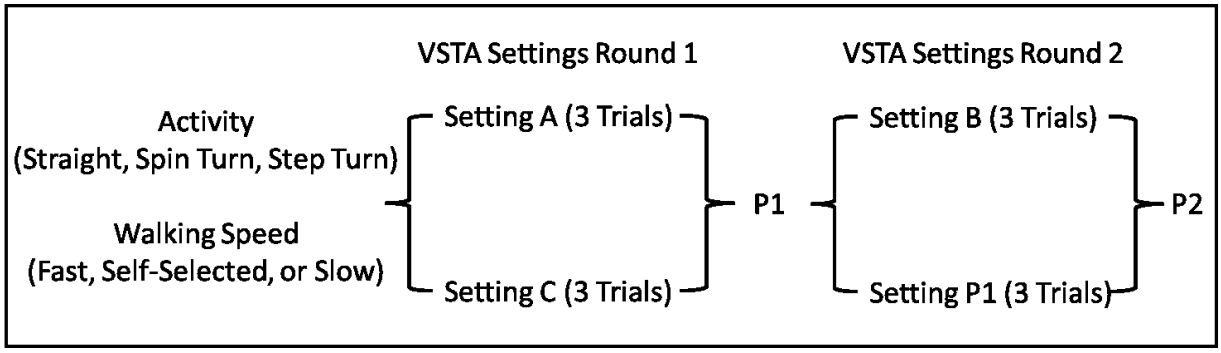

Figure 62: VSTA II A-B-C preference testing flow.

Statistical analysis (Matlab, MathWorks, Natick, MA) of peak transverse plane moments utilized a linear mixed effect model with fixed effects for stiffness and speed and random intercept

for subject. Analysis of preferences utilized an exact multinomial test to determine if the distribution of stiffness preferences represented a random distribution or a significant trend within each activity-speed combination and a chi squared test determined if any difference existed between the activities. A p-value less than 0.05 indicated statistical significance.

8.2 VSTA II Human Subject: Results

The results from this study feature two main measures as outcomes. First, the peak transverse plane moment at the distal end of the socket. The objective of the VSTA II is to reduce shear stresses in the soft tissues of the residual limb, however, that outcome is not easily measured. Because shear stresses are the result of motion between the socket and limb [7], the transverse plane moment can be used to indicate the loading on the socket that induces that motion [7], [8], [29]. To facilitate comparisons between conditions, the peak transverse plane moment at the distal end of the socket is the primary outcome from this testing. The second outcome consists of the responses from each subject during the paired preference testing. Administration of the patient specific functional scale at the beginning of each day showed no difference in subject ability between the two days.

The intercepts of the linear models indicated the magnitudes of the peak transverse plane moments measured for each stiffness setting and speed for each of the individual stiffness and speed effects (Table 16). Significance values indicate if the varying peak transverse plane loads in the limb were significantly different from one another (Table 17). Differences in peak transverse plane moment for varying stiffness conditions do not exist for straight walking, but are present for turning. Specifically, for the prosthesis inside (spin) turns between settings A and C and between A and C as well as A and B for the prosthesis outside (step) turn. Varying speeds show differences for all effects during the three activities, except between slow and fast while straight walking and

between slow and self-selected during prosthesis inside turning. Combining information from Table 16 and Table 17, a summary of changes is given in Table 18. Changes with the greatest magnitude occurred during prosthesis inside turning while the largest percent change was experienced during prosthesis outside turning. During straight walking, self-selected pace presented the lowest peak transverse plane moment with a negative trend between slow and self-selected.

Table 16: Peak transverse plane moment intercept values (Nmm/kg) with standard error for each fixed effect and activity

	Peak Transverse Plane Moment Intercept ± Standard Error (Nmm/kg)		
Fixed Effect	Straight Walking	Prosthesis Inside Turn	Prosthesis Outside Turn
A	87 ± 15	127 ± 23	40 ± 5
B	88 ± 15	130 ± 23	42 ± 5
C	90 ± 15	131 ± 23	44 ± 5
SLW	90 ± 15	127 ± 23	39 ± 5
SSW	84 ± 15	126 ± 23	41 ± 5
FSW	92 ± 15	136 ± 23	46 ± 5

Table 17: P-values for different stiffness and speed comparisons, $p < 0.05$ significant (Bold). A – Compliant (0.31 Nm/deg), B – Moderate (0.83 Nm/deg), C – Stiff (1.29 Nm/deg). Slow (SLW) and Fast (FSW) speeds are 20% slower or faster than the individuals Self-selected pace (SSW) for the given activity.

	P-values for Varying Stiffness and Speed Combinations ($p<0.05$ in bold)		
Effect Comparison	Straight Walking	Prosthesis Inside Turn	Prosthesis Outside Turn
A vs C	0.113	**0.045**	**< 0.001**
A vs B	0.864	0.081	**0.020**
B vs C	0.186	0.957	0.091
SLW vs FSW	0.594	**< 0.001**	**< 0.001**
SSW vs FSW	**< 0.001**	**< 0.001**	**< 0.001**
SLW vs SSW	**<0.001**	0.785	**0.011**

Table 18: Total difference (Tot Diff) and Percent Diff for significantly different effects. Percent difference is expressed as the percent increase (positive) or decrease (negative) of the second effect over the first.

	Total and Percent Difference between Effects					
Effect Comparison	Straight Walking		Prosthesis Inside Turn		Prosthesis Outside Turn	
	Tot Diff (Nm)	Percent Diff	Tot Diff (Nm)	Percent Diff	Tot Diff (Nm)	Percent Diff
A vs C	-	-	4	3%	4	10%
A vs B	-	-	-	-	2	5%
B vs C	-	-	-	-	-	-
SLW vs FSW	-	-	9	7%	7	18%
SSW vs FSW	8	10%	10	8%	5	12%
SLW vs SSW	-6	-7%	-	-	2	5%

Box plots for the individual conditions are given to better illustrate the differences between the varying settings and conditions. Plots for each activity: straight walking (Figure 63), prosthesis inside (Figure 64), prosthesis outside (Figure 65), are shown in pairs. Each pair gives the same information arranged differently to emphasize comparisons between stiffness or speed. The top plot has bars grouped by walking speed to highlight the difference between stiffness settings at individual speeds. The bottom plot has bars grouped by stiffness setting to accentuate differences between walking speeds at a given stiffness. Significant trends are difficult to identify visually as box plots do not account for random effects factors in the linear model. Looking at straight walking no major trends stand out as expected by the previously reported p-values (Table 17). A trend of increasing peak moment with increasing stiffness can be seen during slow walking (Figure 63, top), but it is not consistent for the other speeds. During prosthesis inside and outside turning, the trend of decreasing transverse plane moment with decreasing speed is visible at all stiffness settings (Figure 64 and Figure 65, bottom). The hypothesized trend of increasing transverse plane moment with increasing stiffness is not clearly apparent during prosthesis inside turning, but is

visible during prosthesis outside turning at the self-selected and slow speeds (Figure 63 and Figure 64, top). This may account for the lower p-values found for data during prosthesis outside turns as compared to straight walking and prosthesis inside turns (Table 17). Additionally, interaction effects between stiffness and speed were investigated with no significant correlation found.

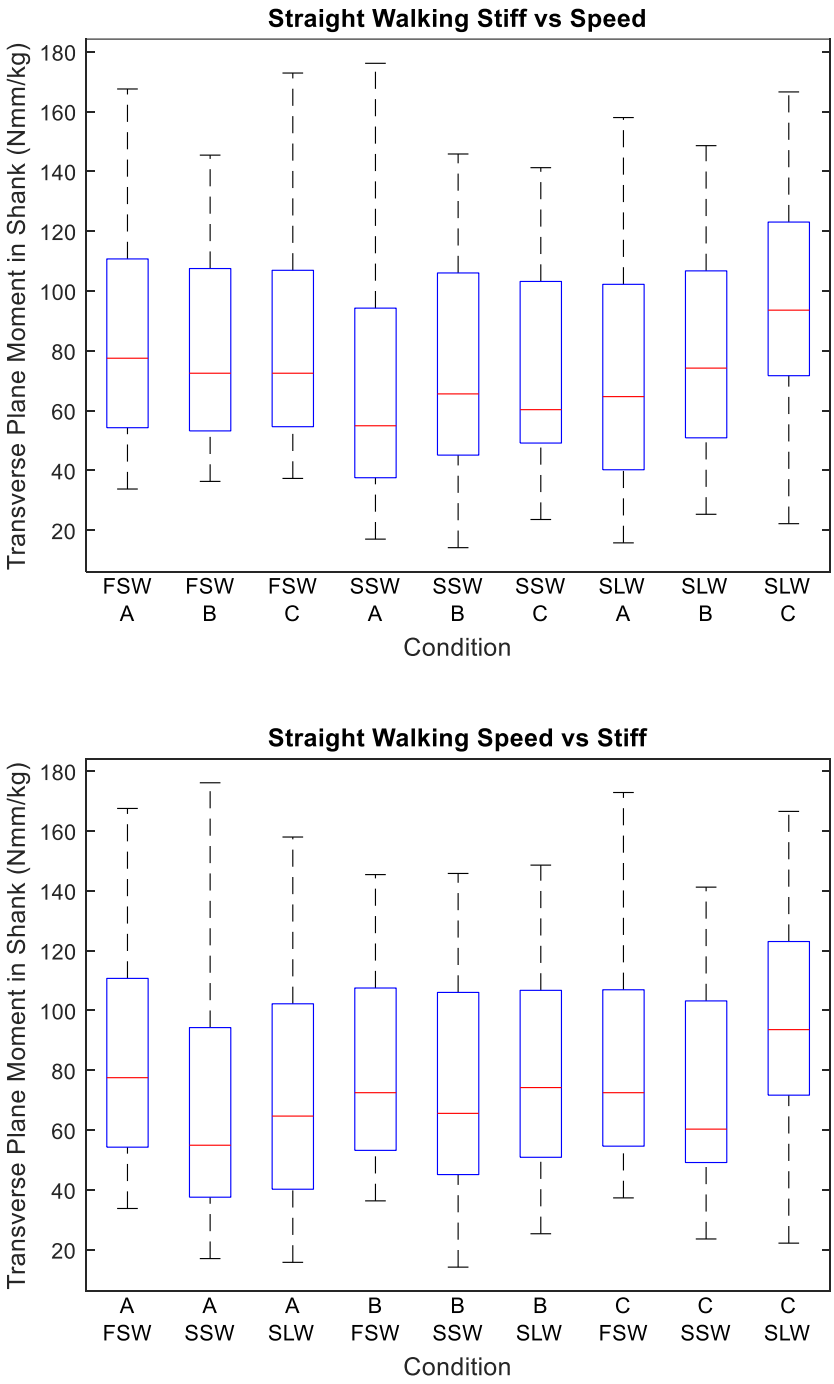

Figure 63: Straight walking box plots. Both plots have the same information arranged in different order to show differences between stiffness and speed. The top plot (Stiff vs Speed) shows the data grouped by walking speed. The bottom plot (Speed vs Stiff) shows the data grouped by stiffness setting. Compliant setting: A (0.31 Nm/deg), Moderate setting: B (0.83 Nm/deg), Stiff setting: C (1.29 Nm/deg). Fast Walking (FSW), Self-Selected Walking (SSW), Slow Walking (SLW).

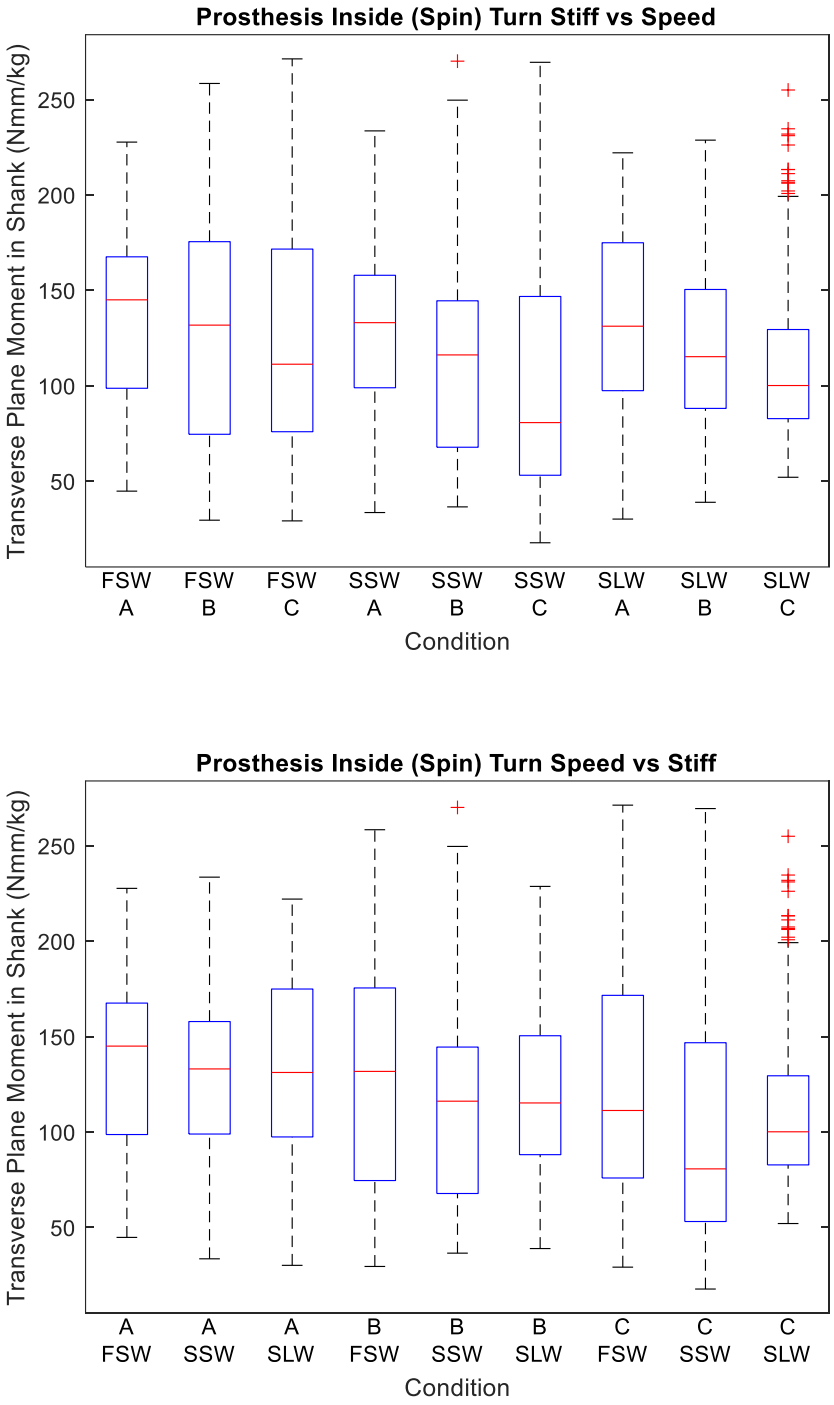

Figure 64: Prosthesis inside turn box plots. Both plots have the same information arranged in different order to show differences between stiffness and speed. The top plot (Stiff vs Speed) shows the data grouped by walking speed. The bottom plot (Speed vs Stiff) shows the data grouped by stiffness setting. Compliant setting: A (0.31 Nm/deg), Moderate setting: B (0.83 Nm/deg), Stiff setting: C (1.29 Nm/deg). Fast Walking (FSW), Self-Selected Walking (SSW), Slow Walking (SLW).

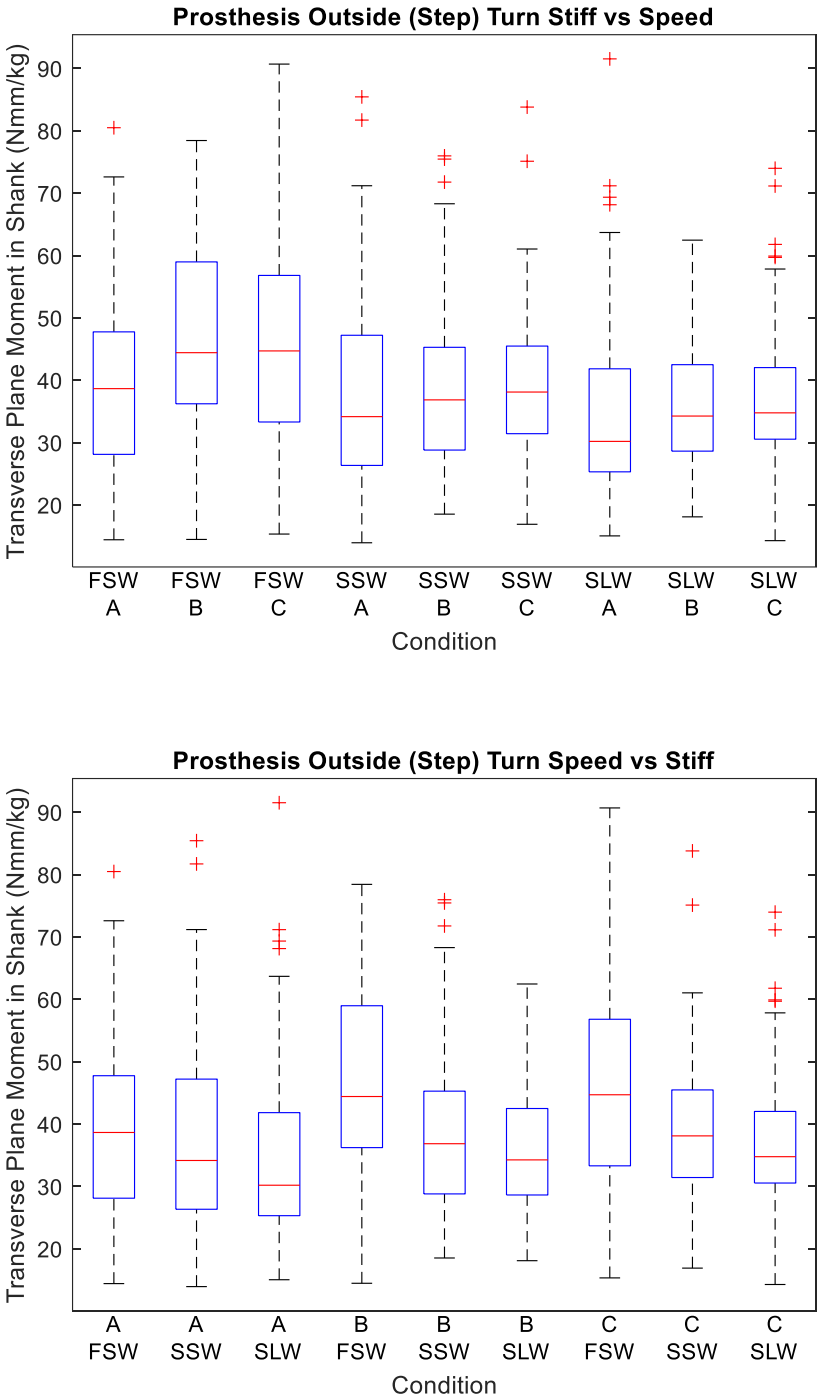

Figure 65: Prosthesis outside turn box plots. Both plots have the same information arranged in different order to show differences between stiffness and speed. The top plot (Stiff vs Speed) shows the data grouped by walking speed. The bottom plot (Speed vs Stiff) shows the data grouped by stiffness setting. Compliant setting: A (0.31 Nm/deg), Moderate setting: B (0.83 Nm/deg), Stiff setting: C (1.29 Nm/deg). Fast Walking (FSW), Self-Selected Walking (SSW), Slow Walking (SLW).

Finally, stiffness preference for each activity and speed combination are shown in Table 19. None of the preference distributions produced a significant result. Turning does qualitatively have less preference for the stiffer, C, setting however, a chi squared test between pooled results within each activity showed no significant difference between straight walking and either of the turning activities.

Table 19: Preference testing results for each activity and speed combination. Each box shows the number of times the stiffness was selected for the given speed within each activity. Each column shows a p-value to indicate if the distribution of preferences deviates significantly from a normal distribution.

Overall Stiffness Preference												
	Straight Walking				Prosthesis Inside Turn				Prosthesis Outside Turn			
Stiffness	Slow	SSW	Fast	All	Slow	SSW	Fast	All	Slow	SSW	Fast	All
A	1	1	1	3	2	1	1	4	1	3	1	5
B	1	2	2	5	1	4	2	7	4	1	3	8
C	3	2	2	7	2	0	2	7	0	1	1	2
p-value	0.63	1	1	0.502	1	0.136	1	0.684	0.136	1	0.63	0.181

8.3 VSTA II Human Subject: Discussion

Testing involved human subject trials performed using the second-generation variable stiffness torsion adapter (VSTA II) in a lower limb prosthesis during different activities and walking speeds. The addition of a transverse rotation adapter may help reduce transverse shear loading of the residual limb leading to soft tissue breakdown [5], [7], [8]. Additionally, testing of the VSTA I indicated that reductions in transverse plane stiffness during a turn as compared to straight walking might further improve that benefit, however, little has been quantified regarding the relationship between ideal transverse plane stiffness, walking speed, and activity. Specifically, it was hypothesized that: 1) peak transverse plane moments related to skin breakdown and

discomfort when ambulating will increase with increased walking speed; 2) reductions in transverse plane stiffness will produce the greatest reductions in peak transverse plane moment when turning vs. walking straight; 3) user preference for stiffness will vary based on walking speed and activity.

Results indicated that walking speed could be a significant factor effecting peak transverse plane moments.

Table *17* indicated that during straight walking there was a difference between self-selected and slow walking, and self-selected and fast walking but with a negative trend between slow and self-selected walking, indicating a non-linear relationship between increasing walking speed and transverse plane moment. During both turning activities, slow walking produced a significantly lower peak transverse plane moment when compared to fast walking as did self-selected as compared to fast. Prosthesis inside turns showed no variation between slow and self-selected speeds, but a linear relationship exists for increasing walking speed and increased transverse plane moment with slow and self-selected speeds being alike and both different than fast walking. Prosthesis outside turns additionally showed a significant difference between slow and self-selected speeds with a linear relationship between all three speed conditions. The results for turning generally support the first hypothesis, however, given the non-linear relationship between speeds, the conclusion does not extend to straight walking.

Consistent with the second hypothesis and previous testing, turning exhibited significant differences in stiffness settings for peak transverse plane moments while straight walking did not. Overall results are comparable to that from the VSTA I pilot testing (Table 10) in magnitude and show trends of increasing magnitude for increasing peak transverse plane moment. However, when compared to the previous VSTA I data, the overall magnitude and percent differences (Table 18)

in peak transverse plane moment are considerably less than those found during the pilot testing. This may indicate that walking a 1 meter radius circle at constant pace is different and less demanding than a single step 90° or 180° turn maneuver, but still a turn type that could benefit from variable transverse plane stiffness when compared to straight walking.

Lastly, no significant difference was found between preferences for stiffness settings. While the total number of high stiffness, C, choices is greater for straight walking than for turning (seven for straight walking versus four for prosthesis inside and two for prosthesis outside turn types) no definitive trend can be declared. Qualitatively all participants commented that they liked the lower stiffness settings when turning as it allowed more flexibility in their lower limb. However, many subjects also commented that lower stiffness when walking slowly felt unstable and created the basis for not choosing the lowest setting. Feedback indicated that at slower speeds the individual spent more time on the limb which at lower stiffness had more motion and less feedback. At higher speeds force was applied quickly and the VSTA II reached its final deflection more in a shorter time alleviating the sense of instability. The lack of a trend may indicate that an ideal stiffness setting may be set on an individual basis, but overall more subjects would be needed to determine a preferred stiffness setting for a given walking speed or activity.

This study is in a preliminary stage and as such results are limited. Testing was performed only on male transtibial amputees in a limited mass range. While results were normalized by subject mass, more factors such as height, width, and arm swing that effect an individual's moment of inertia about the transverse axis may alter how a user interacts with the VSTA II. Next, testing was only performed at three static settings of the VSTA II. More than one subject commented that they liked lowered stiffness settings, but that the most compliant setting, A, was too compliant and chose setting B as a compromise. As there was no consensus for preferred stiffness setting the

ideal setting for a certain individual may have to be customized to that person's kinetic and kinematic peculiarities. While no significant trend was identified, all subjects commented that they liked decreased stiffness during turning for its increased flexibility and ability to unload their residual limb while twisting. As before, regardless of the large mass reduction, all subjects commented on the mass of the VSTA II comparable to comments with the VSTA I. However, after a short acclimation period users were comfortable with mass of the testing setup. Acclimation period was also a limitation of this study. Participants were generally unfamiliar with walking on a transverse rotation adapter and their ability to use the device effectively while maintaining comfortable stability while walking straight and turning may change with increased exposure. Previous studies have suggested a minimum of three weeks and up to three months of acclimation might be required for a device of this nature [70], [71].

8.4 VSTA II Human Subject: Conclusion

Testing was performed to help determine the ideal stiffness settings for individuals given different activities and walking speeds. Subjects performed walking trials for three separate activities (straight walking, prosthesis inside turning, prosthesis outside turning), at their self-selected walking speed and at speeds 20% faster and slower than self-selected. Results indicated correlation between increased peak transverse plane moment with increasing walking speed when turning, but not when walking straight. Similarly, a significant relation was found between increasing peak transverse plane moment and increasing stiffness of the VSTA II. Lastly, results indicated no significant trend for stiffness preference between speeds or activities, while subjects did qualitatively prefer lower stiffness when turning vs straight walking. Findings may indicate that no global ideal stiffness settings may be available given activity and speeds variations, but that VSTA II settings may have to be tailored to individual users.

9 Future Work

This research represents just the beginning of the work needed to help improve a lower limb amputee's quality of life with the addition of variable transverse plane stiffness. While testing has quantitatively shown that peak transverse plane loading on the limb can be reduced by lowering the transverse plane stiffness, there is still no clear trend to indicate optimal settings of the VSTA during actual use. Initial power analysis of VSTA I data indicated at least seven subjects would be required to properly populate the VSTA II study. To better understand how subject preference correlates with stiffness setting and walking speed more subject data is required. Additional subjects should specifically include individuals in a wider mass range such that an extended analysis could be completed to better understand how to identify ideal stiffness settings given an individual's kinetic and kinematic needs.

Continued VSTA studies should also strive to test turning out of the lab. As it was found that 90° and 180° turning varied from the circle walking it might be concluded that turning outside the lab will vary from the previously tested conditions and should be evaluated. As previously stated acclimation time could have been a limiting factor for the in-lab studies. Future work should strive to give a VSTA-like device that could be used for an extended period in-home to determine if users could optimize their performance with the VSTA and consequently alter their stiffness preferences.

Lastly, given the range of testing suggested above, an optimized VSTA device should be conceived out of lab testing and eventual mass production. The VSTA I and VSTA II prototypes strived to give the widest range of stiffness options possible to facilitate preliminary testing, but that range may not be necessary. Given the preliminary data and qualitative reports from the individual subjects, a device like the VSTA may only require one or two settings that could be

packaged into a lighter and more compact device. Ideally, a device like the VSTA could be integrated into an already existing foot, or coupled with other active prosthesis components, such as those that provide variable stiffness in the coronal plane or power in the sagittal plane [72], [73], to deliver the best performance possible for the lower limb amputee.

10 Bibliography

[1] K. Ziegler-Graham, E. J. MacKenzie, P. L. Ephraim, T. G. Travison, and R. Brookmeyer, "Estimating the prevalence of limb loss in the United States: 2005 to 2050," *Arch. Phys. Med. Rehabil.*, vol. 89, no. 3, pp. 422–429, Mar. 2008.

[2] M. F. Owings and L. J. Kozak, "Ambulatory and inpatient procedures in the United States, 1996.," *Vital Health Stat. 13.*, no. 139, pp. 1–119, 1998.

[3] B. J. Hafner, J. E. Sanders, J. M. Czerniecki, and J. Fergason, "Transtibial energy-storage-and-return prosthetic devices: A review of energy concepts and a proposed nomenclature," *J. Rehabil. Res. Dev.*, vol. 39, no. 1, pp. 1–11, 2002.

[4] J. S. Rietman, K. Postema, and J. H. B. Geertzen, "Gait analysis in prosthetics: Opinions, ideas and conclusions," *Prosthet. Orthot. Int.*, vol. 26, no. 1, pp. 50–57, Jan. 2002.

[5] L. W. Lamoureux and C. W. Radcliffe, "Functional analysis of the UC-BL shank axial rotation device," *Prosthet. Orthot. Int.*, vol. 1, no. 2, pp. 114–118, Aug. 1977.

[6] S. W. Levy, "Amputees: Skin problems and prosthesis," *Cutis*, vol. 55, no. 5, pp. 297–302, 1995.

[7] M. L. van der Linden, N. Twiste, and S. V. S. Rithalia, "The biomechanical effects of the inclusion of a torque absorber on trans-femoral amputee gait, a pilot study," *Prosthet. Orthot. Int.*, vol. 26, no. 1, pp. 35–43, Jan. 2002.

[8] A. D. Segal, M. S. Orendurff, J. M. Czerniecki, J. B. Shofer, and G. K. Klute, "Transtibial amputee joint rotation moments during straight-line walking and a common turning task with and without a torsion adapter," *J. Rehabil. Res. Dev.*, vol. 46, no. 3, pp. 375–383, 2009.

[9] B. C. Glaister, G. C. Bernatz, G. K. Klute, and M. S. Orendurff, "Video task analysis of turning during activities of daily living," *Gait Posture*, vol. 25, no. 2, pp. 289–294, Feb. 2007.

[10] P.-F. Su, S. A. Gard, R. D. Lipshutz, and T. A. Kuiken, "The Effects of Increased Prosthetic Ankle Motions on the Gait of Persons with Bilateral Transtibial Amputations," *Am. J. Phys. Med. Rehabil.*, vol. 89, no. 1, pp. 34–47, 2010.

[11] J. M. Donelan, D. W. Shipman, R. Kram, and A. D. Kuo, "Mechanical and metabolic requirements for active lateral stabilization in human walking," *J. Biomech.*, vol. 37, no. 6, pp. 827–835, 2004.

[12] J. G. Buckley, S. F. Jones, and K. M. Birch, "Oxygen consumption during ambulation: Comparison of using a prosthesis fitted with and without a tele-torsion device," *Arch. Phys. Med. Rehabil.*, vol. 83, no. 4, pp. 576–581, Apr. 2002.

[13] A. D. Segal, R. Kracht, and G. K. Klute, "Does a Torsion Adapter Improve Functional Mobility, Pain, and Fatigue in Patients with Transtibial Amputation?," *Clin. Orthop. Relat. Res.*, pp. 3085–3092, 2014.

[14] K. C. Flick, M. S. Orendurff, J. S. Berge, A. D. Segal, and G. K. Klute, “Comparison of human turning gait with the mechanical performance of lower limb prosthetic transverse rotation adapters,” *Prosthet. Orthot. Int.*, vol. 29, no. 1, pp. 73–81, Jan. 2005.

[15] A. H. Hansen, D. S. Childress, S. C. Miff, S. a Gard, and K. P. Mesplay, “The human ankle during walking: implications for design of biomimetic ankle prostheses,” *J. Biomech.*, vol. 37, no. 10, pp. 1467–1474, Oct. 2004.

[16] B. C. Glaister, J. A. Schoen, M. S. Orendurff, and G. K. Klute, “Mechanical behavior of the human ankle in the transverse plane while turning,” *IEEE Trans. Neural Syst. Rehabil. Eng.*, vol. 15, no. 4, pp. 552–559, Dec. 2007.

[17] C. Pew and G. K. Klute, “Design of Lower Limb Prosthesis Transverse Plane Adaptor With Variable Stiffness,” *J. Med. Device.*, vol. 9, no. 3, p. 35001, 2015.

[18] A. Deathe and W. Miller, “The L Test of Functional Mobility: Measurement Properties of a Modified Version of the Timed‘ Up & Go’ Test Designed for People With Lower-Limb Amputations,” *Phys. Ther.*, vol. 85, pp. 626–635, 2005.

[19] C. Pew, “Design and Testing of a Variable Stiffness Transverse Plane Adaptor for Use in a Lower Limb Prosthesis,” University of Washington, 2014.

[20] ISO, “10328:2006 Structural Testing of Lower-Limb Prostheses - Requirements and Test Methods,” 2006.

[21] B. C. Glaister, J. a Schoen, M. S. Orendurff, and G. K. Klute, “A mechanical model of the human ankle in the transverse plane during straight walking: implications for prosthetic design,” *J. Biomech. Eng.*, vol. 131, no. 3, p. 34501, Mar. 2009.

[22] R. W. Selles, J. B. Bussmann, R. C. Wagenaar, and H. J. Stam, “Effects of prosthetic mass and mass distribution on kinematics and energetics of prosthetic gait: a systematic review,” *Arch. Phys. Med. Rehabil.*, vol. 80, no. 12, pp. 1593–9, Dec. 1999.

[23] E. Oberg, F. D. Jones, H. L. Horton, and H. H. Ryffel, *Machinery’s Handbook*, 29th ed. New York: Industrial Press, 2012.

[24] R. C. Juvinall and K. M. Marshek, *Fundamentals of Machine Component Design*, 5th ed. New York: John Wiley & Sons, 2000.

[25] D. A. Winter, *The Biomechanics and Motor Control of Human Gait: Normal, Elderly and Pathological*, 2nd ed. Waterloo: University of Waterloo Press, 1991.

[26] Maxon, “Data Sheet for Maxon EC 45 Motor,” 2014. [Online]. Available: http://www.maxonmotorusa.com/maxon/view/product/motor/ecmotor/ecflat/ecflat45/397172.

[27] K. Hase and R. B. Stein, “Turning Strategies During Human Walking,” *J. Neurophysiol.*, vol. 81, no. 6, pp. 2914–2922, 1999.

[28] M. J. D. Taylor, S. C. Strike, and P. Dabnichki, “Strategies used for unconstrained direction change during walking.,” *Percept. Mot. Skills*, vol. 102, no. 2, pp. 576–88, Apr. 2006.

[29] E. S. Neumann, J. Brink, K. Yalamanchili, and J. S. Lee, “Use of a load cell and force-moment curves to compare transverse plane moment loads on transtibial residual limbs: A preliminary investigation.,” *Prosthet. Orthot. Int.*, vol. 38, no. 3, pp. 253–262, 2013.

[30] M. J. D. Taylor, P. Dabnichki, and S. C. Strike, “A three-dimensional biomechanical comparison between turning strategies during the stance phase of walking,” *Hum. Mov. Sci.*, vol. 24, no. 4, pp. 558–73, Aug. 2005.

[31] J. F. Lehmann, R. Price, R. Okumura, K. Questad, B. J. De Lateur, and A. Negretot, “Mass and mass distribution of below-knee prostheses: Effect on gait efficacy and self-selected walking speed,” *Arch. Phys. Med. Rehabil.*, vol. 79, no. 2, pp. 162–168, 1998.

[32] S. C. Hillery, E. S. Wallace, R. Mcilhagger, and P. Watson, “The effect of changing the inertia of a trans-tibial dynamic elastic response prosthesis on the kinematics and ground reaction force patterns,” *Prosthet. Orthot. Int.*, vol. 21, pp. 114–123, 1997.

[33] J. L. Lelas, G. J. Merriman, P. O. Riley, and D. C. Kerrigan, “Predicting peak kinematic and kinetic parameters from gait speed,” *Gait Posture*, vol. 17, no. 2, pp. 106–112, Apr. 2003.

[34] R. C. Coddington, “Shear Flow in Beams,” *University of Agriculture and Biological Engineering*, 2015. [Online]. Available: http://abe-research.illinois.edu/faculty/dickc/Engineering/beamshear3a.htm. [Accessed: 04-Jul-2016].

[35] J. Shintake, S. Rosset, B. Schubert, D. Floreano, and H. Shea, “Versatile Soft Grippers with Intrinsic Electroadhesion Based on Multifunctional Polymer Actuators,” pp. 1–8, 2015.

[36] MITCalc, “Leaf Springs,” *Mechanical, Industiral, and Technical Calculations*, 2016. [Online]. Available: http://www.mitcalc.com/doc/springs/help/en/springs.htm. [Accessed: 04-Jul-2016].

[37] W.M.Berg, “Gear Reference Guide,” *Berg Technical Data*, 2016. [Online]. Available: http://www.wmberg.com/catalog/pdf/b00k2-16.pdf. [Accessed: 01-Jan-2016].

[38] M. S. Kuster, G. A. Wood, G. W. Stachowiak, and A. Gächter, “Joint load considerations in total knee replacement,” *J. Bone Joint Surg. Br.*, vol. 79–B, no. 1, pp. 109–113, 1997.

[39] P. R. Cavanagh and M. A. Lafortune, “Ground reaction forces in distance running,” *J. Biomech.*, vol. 13, pp. 397–406, 1980.

[40] J. B. Dingwell and L. C. Marin, “Kinematic variability and local dynamic stability of upper body motions when walking at different speeds.,” *J. Biomech.*, vol. 39, no. 3, pp. 444–52, Jan. 2006.

[41] C. Kirtley, M. W. Whittle, and R. J. Jefferson, “Influence of walking speed on gait parameters,” *J. Biomed. Eng.*, vol. 7, no. 4, pp. 282–288, 1985.

[42] S. J. Lin-Chan, D. H. Nielsen, H. J. Yack, M. J. Hsu, and D. G. Shurr, “The Effects of Added Prosthetic Mass on Physiologic Responses and Stride Frequency during Multiple Speeds of Walking in Persons with Transtibial Amputation,” *Arch. Phys. Med. Rehabil.*,

vol. 84, pp. 1865–1871, 2003.

[43] C. Pew and G. K. Klute, “Pilot Testing of a Variable Stiffness Transverse Plane Adapter for Lower Limb Amputees,” *Gait Posture*, vol. 51, pp. 104–108, 2017.

[44] R. Jiménez-Fabián and O. Verlinden, “Review of control algorithms for robotic ankle systems in lower-limb orthoses, prostheses, and exoskeletons,” *Med. Eng. Phys.*, vol. 34, no. 4, pp. 397–408, 2012.

[45] A. J. Young, T. a Kuiken, and L. J. Hargrove, “Analysis of using EMG and mechanical sensors to enhance intent recognition in powered lower limb prostheses.,” *J. Neural Eng.*, vol. 11, no. 5, p. 56021, 2014.

[46] B. Chen, E. Zheng, X. Fan, T. Liang, Q. Wang, K. Wei, and L. Wang, “Locomotion mode classification using a wearable capacitive sensing system,” *IEEE Trans. Neural Syst. Rehabil. Eng.*, vol. 21, no. 5, pp. 744–755, 2013.

[47] H. Huang, T. A. Kuiken, and R. D. Lipschutz, “A Strategy for Identifying Locomotion Modes Using Surface Electromyography,” *IEEE Trans. Biomed. Eng.*, vol. 56, no. 1, pp. 65–73, 2009.

[48] A. J. Young, A. M. Simon, and L. J. Hargrove, “A training method for locomotion mode prediction using powered lower limb prostheses,” *IEEE Trans. Neural Syst. Rehabil. Eng.*, vol. 22, no. 3, pp. 671–677, 2014.

[49] P. R. Golyski and B. D. Hendershot, “A computational algorithm for classifying step and spin turns using pelvic center of mass trajectory and foot position,” *J. Biomech.*, 2017.

[50] D. Novak, M. Goršič, J. Podobnik, and M. Munih, “Toward Real-Time Automated Detection of Turns during Gait Using Wearable Inertial Measurement Units,” *Sensors*, vol. 14, no. 10, pp. 18800–18822, 2014.

[51] Y. Saeys, I. Inza, and P. Larranaga, “A review of feature selection techniques in bioinformatics,” *Bioinformatics*, vol. 23, no. 19, pp. 2507–2517, 2007.

[52] T. W. Way, B. Sahiner, L. M. Hadjiiski, and H.-P. Chan, “Effect of finite sample size on feature selection and classification: a simulation study.,” *Med. Phys.*, vol. 37, no. 2, pp. 907–920, 2010.

[53] M. R. Feldesman, “Classification trees as an alternative to linear discriminant analysis,” *Am. J. Phys. Anthropol.*, vol. 119, no. 3, pp. 257–275, 2002.

[54] H. Huang, F. Zhang, L. J. Hargrove, Z. Dou, D. R. Rogers, and K. B. Englehart, “Continuous locomotion-mode identification for prosthetic legs based on neuromuscular - Mechanical fusion,” *IEEE Trans. Biomed. Eng.*, vol. 58, no. 10 PART 1, pp. 2867–2875, 2011.

[55] A. Mai and S. Commuri, “Intelligent control of a prosthetic ankle joint,” *Control Eng. Pract.*, vol. 49, pp. 17–25, 2016.

[56] C. Sima and E. R. Dougherty, “What should be expected from feature selection in small-sample settings,” *Bioinformatics*, vol. 22, no. 19, pp. 2430–2436, 2006.

[57] J. D. Miller, M. S. Beazer, and M. E. Hahn, “Myoelectric walking mode classification for transtibial amputees,” *IEEE Trans. Biomed. Eng.*, vol. 60, no. 10, pp. 2745–2750, 2013.

[58] M. Liu, D. Wang, and H. Helen Huang, “Development of an Environment-Aware Locomotion Mode Recognition System for Powered Lower Limb Prostheses,” *IEEE Trans. Neural Syst. Rehabil. Eng.*, vol. 24, no. 4, pp. 434–443, 2016.

[59] D. Joshi, B. H. Nakamura, and M. E. Hahn, “High energy spectrogram with integrated prior knowledge for EMG-based locomotion classification,” *Med. Eng. Phys.*, vol. 37, no. 5, pp. 518–524, 2015.

[60] F. Zhang and H. Huang, “Source selection for real-time user intent recognition toward volitional control of artificial legs,” *IEEE J. Biomed. Heal. Informatics*, vol. 17, no. 5, pp. 907–914, 2013.

[61] G. M. Hefferman, F. Zhang, M. J. Nunnery, and H. Huang, “Integration of surface electromyographic sensors with the transfemoral amputee socket: A comparison of four differing configurations,” *Prosthet. Orthot. Int.*, vol. 39, no. 2, pp. 166–173, 2015.

[62] C. Campbell and Y. Ying, *Learning with Support Vector Machines*. Morgan & Claypool, 2011.

[63] G. James, D. Witten, T. Hastie, and R. Tibshirani, *An Introduction to Statistical Learning*. New York: Springer, 2013.

[64] J. H. Freidman, J. L. Bentley, and R. A. Finkel, “An Algorithm for Finding Best Matches in Logarithmic Expected Time,” *ACM Trans. Math. Softw.*, vol. 3, no. 3, pp. 209–226, 1977.

[65] L. Breiman, “Bagging Predictors,” *Mach. Learn.*, vol. 24, no. 421, pp. 123–140, 1996.

[66] A. J. Young, A. M. Simon, N. P. Fey, and L. J. Hargrove, “Classifying the Intent of Novel Users During Human Locomotion Using Powered Lower Limb Prostheses,” in *6th Annual International IEEE EMBS Conference on Neural Engineering*, 2013, pp. 311–314.

[67] E. Schaffalitzky, S. NiMhurchadha, P. Gallagher, S. Hofkamp, M. MacLachlan, and S. T. Wegener, “Identifying the values and preferences of prosthetic users: a case study series using the repertory grid technique.,” *Prosthet. Orthot. Int.*, vol. 33, no. 2, pp. 157–166, 2009.

[68] ASTM, “Standard Test Method for Paired Preference Test,” 2013.

[69] P. Stratford, C. Gill, M. Westaway, and J. M. Binkley, “Assessing disability and change on individual patients: A report of a patient specific measure,” *Physiotherapy Canada*, vol. 47, no. 4. pp. 258–263, 1995.

[70] R. D. English, W. a Hubbard, and G. K. McElroy, “Establishment of consistent gait after fitting of new components.,” *J. Rehabil. Res. Dev.*, vol. 32, no. February, pp. 32–35, 1995.

[71] A. D. Segal, M. S. Orendurff, G. K. Klute, M. L. McDowell, J. a. Pecoraro, J. Shofer, and J. M. Czerniecki, “Kinematic and kinetic comparisons of transfemoral amputee gait using C-Leg and Mauch SNS prosthetic knees,” *J. Rehabil. Res. Dev.*, vol. 43, no. 7, p. 857,

2006.

[72] G. K. Klute, J. Gorges, K. Yeates, and A. Segal, “Variable Stiffness Prosthesis to Improve Amputee Coronal Plane Balance American Academy of Orthotists & Prosthetists,” in *41st Meeting of the American Academy of Orthotists & Prosthetists*, 2015, vol. 2, p. FPTH14.

[73] J. Realmuto, G. Klute, and S. Devasia, “Nonlinear Passive Cam-Based Springs for Powered Ankle Prostheses,” *J. Med. Device.*, vol. 9, no. 1, p. 11007, 2014.